THE
PHYSICAL REVIEW

A journal of experimental and theoretical physics established by E. L. Nichols in 1893

SECOND SERIES, VOL. 74, NO. 6 SEPTEMBER 15, 1948

Ranges in Air and Mass Identification of Plutonium Fission Fragments

SEYMOUR KATCOFF, JOHN A. MISKEL,* AND CHARLES W. STANLEY
University of California, Los Alamos Scientific Laboratory, Los Alamos, New Mexico

(Received May 28, 1948)

Determinations were made of the mean and extrapolated ranges in air of plutonium fission fragments for twenty individual masses between 83 and 157. Collimated fission fragments passing through air at 120 or 140 mm pressure were deposited, after being stopped by the air, on a series of fourteen thin lacquer films. These were analyzed radio-chemically for individual fission products. The corrected activities were plotted against distance traversed by the fragments, yielding differential range curves whose widths at half-maximum were 11.7±1.3 percent, independent of fragment mass. The activities found beyond each distance were plotted against distance giving integral range curves. Mean and extrapolated ranges were derived from these. In the light group the extrapolated ranges decrease from 2.90 cm (15°C and 760 mm) for mass 83, to 2.25 cm for mass 117; in the heavy group they decrease from 2.25 cm for mass 127, to 1.95 cm for mass 157. From the range-mass curve drawn for well-known masses, definite assignments of 92, 93, and 132 were given to 3.5-hr. Y, 10-hr. Y, and 77-hr. Te, respectively. Highly probable assignments of 94 and 134 were given to 20-min. Y and 54-min. I, respectively.

I. INTRODUCTION

SINCE the discovery of the process of nuclear fission, several measurements have been made of the range of the fission recoil fragments. Corson and Thornton[1] observed in a cloud chamber that the maximum range was about 3 cm standard air. Booth, Dunning, and Slack[2] used a shallow ionization chamber to measure the number of fission fragments as a function of air pressure in the system. Two groups appeared with maximum ranges of 1.5 cm and 2.2 cm. E. McMillan[3] irradiated a plate of U_3O_8 covered with a series of aluminum foils. By plotting the gross recoil radioactivity in each foil against thickness of aluminum, a maximum range of 2.2 cm air equivalent was obtained.

Segrè and Wiegand,[4] using two methods, measured the relative stopping power for fission fragments of collodion, aluminum, copper, silver, and gold. In one method, the gross radioactivity that penetrated various thicknesses of foil was collected on a celluloid plate and counted. The maximum range in aluminum was found to be 3.7 mg/cm² or about 2.5 cm normal air equivalent. In the other method, fission pulses which penetrated various thicknesses of foil were counted in a shallow ionization chamber. It was found that the relative stopping powers for fission fragments of the above materials are roughly the same as for 4.6-Mev alpha-particles.

* Now at Washington University, St. Louis, Missouri.

[1] D. R. Corson and R. L. Thornton, Phys. Rev. **55**, 509 (1939).

[2] E. T. Booth, J. R. Dunning, and F. Slack, Phys. Rev. **55**, 982 (1939).

[3] E. McMillan, Phys. Rev. **55**, 510 (1939).

[4] E. Segrè and C. Wiegand, Phys. Rev. **70**, 808 (1946).

Bøggild, Brostrøm, and Lauritsen,[5] and Bøggild, Arrøe, and Sigurgeirsson[6] have made extensive cloud-chamber studies of the stopping of fission fragments from uranium in xenon, argon, helium, hydrogen, and deuterium. The heavy fragment tracks usually show some curvature caused by many collisions with gas atoms that are not close enough to give observable recoil tracks. Numerous collisions, however, do give rise to definite branches, and a tuft of several short branches frequently appears at the end of the range of a fission fragment. By a study of the distribution of branches along the tracks and also by direct measurements of the angles and lengths of individual large branches, velocity-range curves were constructed for the light and heavy groups of fission fragments. These curves show that first the fragments are slowed down mostly by electronic interactions but that during the last portion of the path most of the stopping results from nuclear collisions. The greatest variation in range reduced to normal air was from a mean total range for both fragments of 5.2 cm in helium to 3.9 cm in hydrogen.

Experiments to determine the range of fission fragments of a single mass were performed by Freedman, Metcalf, and Sugarman.[7] Their apparatus consisted of a small ground quartz joint containing a thin enriched uranium source at one end, and a Cellophane disk at the other end for collecting the fission fragments. An aluminum foil, 1.4 mg/cm^2 thick, was placed just in front of the Cellophane to prevent diffusion of stopped fission fragments to the Cellophane. The chamber was given a series of irradiations for various pressures of air. After each bombardment the Cellophane collecting disk was analyzed radio-chemically for 85-min. Ba^{139} and 9.7-hr. Sr^{91}. Then by plotting activity against air pressure, absorption curves were obtained for fission recoils of the given mass numbers. The maximum ranges were 2.58 cm and 2.05 cm of normal air for masses 91 and 139, respectively. Since the absorption curves that were obtained were not horizontal, as expected, over the first portion of the range, the experiments were repeated by Finkle, Hoagland, Katcoff, and Sugarman.[8] A very thin zapon film ($\sim$15 μg/cm^2) was substituted for the aluminum foil and measurements were made for plutonium as well as for U^{235}. This time the absorption curves were nearly horizontal over the initial portion and resembled corresponding curves for alpha-particles. The maximum ranges were 2.58 cm and 1.85 cm normal air for masses 91 and 139, respectively, from U^{235}; 2.69 cm and 1.95 cm, respectively, for these masses from plutonium.

In continuing a series of experiments initiated by F. Joliot,[9] Suzor[10] irradiated with thermal neutrons a stack of aluminum foils placed over a thin layer of uranium oxide. Half of the fission recoils of a given range leaving any point in the source would thus be deposited in the aluminum on a hemisphere whose radius is equal to the range. It follows from geometrical considerations that the activity of a fission product deposited in any foil is proportional to the thickness of that foil up to a distance from the uranium equal to the range. Three isotopes were separated radiochemically from each of the foils and the activity per unit thickness plotted against distance from the uranium. The curves were horizontal over the initial portion and then dropped gradually to zero. The average ranges for 17-hr. Zr^{97}, 67-hr. Mo^{99}, and 77-hr. Te^{132} were found to be 3.78, 3.78, and 3.11 mg/cm^2, respectively. The corresponding maximum ranges were 4.50, 4.40, and 3.85 mg/cm^2.

A similar series of experiments was performed by Finkle, Hoagland, Katcoff, and Sugarman.[11] In this case eight fission products from uranium were investigated and the total activity of each isotope which passed through each foil was plotted against the thickness of aluminum. Straight lines were obtained over most of the range, and these were extrapolated to zero activity to give values of 3.74, 3.64, 3.57, 3.34, 3.16, 2.75, 2.69, and 2.54 mg/cm^2 for masses 89,

[5] J. K. Bøggild, K. J. Brostrøm, and T. Lauritsen, Kgl. Danske Vid. Sels. Math-Fys. Medd. (Math-Phys. Comm., Acad. Sci. Copenhagen) **18**, 4 (1940).

[6] J. K. Bøggild, O. H. Arrøe, and T. Sigurgeirsson, Phys. Rev. **71**, 281 (1947).

[7] M. S. Freedman, R. P. Metcalf, and N. Sugarman, Manhattan Project Report CC-1559 (April 8, 1944); Plutonium Project Record IXB, 6.6.1 (1946).

[8] B. J. Finkle, E. Hoagland, S. Katcoff, and N. Sugarman, Manhattan Project Report CK-1806 (June 30, 1944); Plutonium Project Record IXB, 6.6.2 (1946).

[9] F. Joliot, Comptes Rendus **218**, 488 (1944).

[10] F. Suzor, Comptes Rendus **224**, 1155 (1947); J. de phys. et rad. **8**, 39 (1947).

[11] B. J. Finkle, E. Hoagland, S. Katcoff, and N. Sugarman, Manhattan Project Report CC-2076 (August 25, 1944); Plutonium Project Record IXB, 6.6.3 (1946).

95, 103, 129, 131, 140, 141, and 144, respectively. These results are not accurate because it was discovered later that the method used to determine the thickness of the aluminum foils was unreliable.

N. Sugarman[12] measured the approximate ranges of the delayed neutron-emitting isotopes from uranium fission by means of a slightly modified aluminum foil technique. From fission yield considerations and from a comparison of the ranges of the 4.51-second and 1.52-second isotopes with the ranges of the better-known 55.6-second and 22.0-second isotopes, the former were assigned possible mass numbers of 87 to 90 and 129 to 135, respectively.

During the investigation reported here the ranges in air of plutonium fission fragments were measured for twenty mass numbers between 83 and 157. Both differential and integral range curves (Figs. 2 and 3) were obtained directly from the data for each mass. Then from a range *vs.* mass curve (Fig. 4) it was possible to make definite assignments of mass to three decay chains whose assignments were doubtful previously, and to give strong support for mass assignments to two other chains. Some conclusions were made as to the dependence of range on the mass and energy of the fragments, and data were obtained on the distribution in range of fragments of uniform mass.

II. EXPERIMENTAL METHOD AND RESULTS

The apparatus consisted of a beryllium tube about eight inches long and one inch in diameter. At one end was a thin foil of plutonium ($\sim$0.1 mg/cm^2) perpendicular to the axis of the tube (Fig. 1). Starting at about four inches from this foil there were mounted on beryllium spacer rings at intervals of one-eighth inch a series of about fourteen zapon lacquer films (8 μg/cm^2 thick). The spacer rings were measured accurately with micrometer calipers. The apparatus was usually filled with dry air to a pressure of 120 or 140 mm mercury at a known temperature. It was then irradiated with neutrons in the Los Alamos homogeneous pile for times varying from 30 minutes to 14 hours. The zapon films were so situated that nearly all fission fragments in the mass range being studied (which did not strike the walls of the tube) were stopped in the region of the films. Practically all of the stopping was by the air, the zapon contributing at most only about five percent. It was assumed as a first approximation that the stopped fission fragments would deposit on the nearest zapon film, i.e., fragments stopped within $\frac{1}{16}$ inch on either side of a film belong to that film.

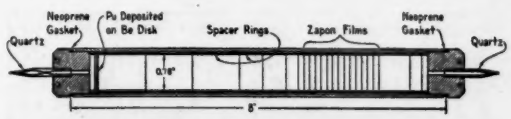

FIG. 1. Sectional view of fission recoil range apparatus. All parts are of Be except where otherwise indicated. The chamber is attached to a vacuum line by means of the quartz tube on the right for filling to the proper pressure. After an irradiation the tip of the left-hand quartz tube is broken so that air leaks through the capillary to bring the pressure to atmospheric without rupturing the zapon films. The spacer rings contain small notches to permit rapid equalization of pressure.

After irradiation, each film, except the first and last, was dissolved in acetone or concentrated HNO_3 and analyzed radio-chemically for a few fission products. The procedures were modified from those reported in Chapter 8, Volume IXB, of the Plutonium Project Record. Some modification was usually needed because two or more elements were isolated from all of each solution. Ordinarily, a solution is divided into aliquots, one for each of the elements analyzed for. In this work the activities were too low for such a procedure. Radio-chemical exchange among the various chemical states of each element was always effected before any precipitations were made. In the case of the yttrium analyses no chemical separations from the rare earths were necessary because of the great difference in fragment range. Element 61 was not isolated from any of the other rare earths except cerium and samarium. La^{140} activity ($T_{\frac{1}{2}}$=40 hr.) was kept down to about two percent of the 47 hr. 61^{149} activity by removing the 12.8-day Ba^{140} parent immediately after 2- to 3-hour irradiations. The 47-hr. Sm^{153} was partially extracted from the element 61 by means of sodium amalgam. The Sm^{153} fission yield is only one-third of the 61^{149} yield; furthermore, a small 47-hr. Sm^{153} contamination would hardly affect the range of mass 149 because the range of the former is shorter than that of the latter. The effect of all other contaminating rare earth

[12] N. Sugarman, J. Chem. Phys. **15**, 544 (1947).

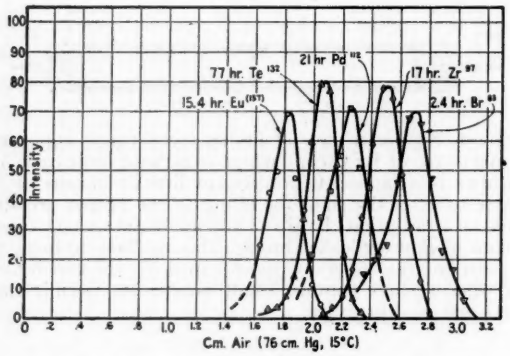

FIG. 2. Five typical differential range curves. The ordinates for each curve are entirely arbitrary.

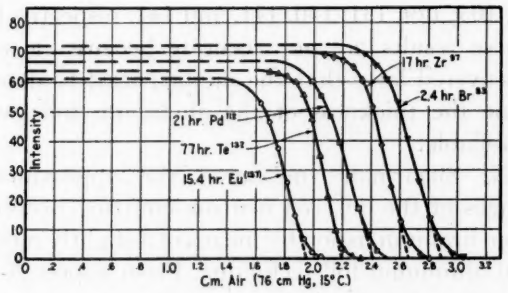

FIG. 3. Five typical integral range curves. The ordinates for each curve are entirely arbitrary.

isotopes was removed by a resolution of the decay curves.

The activity of each sample was followed with a G-M tube for one or two half-lives. In some cases it was necessary to analyze the decay curves into two components. The duration of the bombardment and the time allowed for decay before analysis were chosen so as to emphasize the component under investigation. The activity at a specified time of a given isotope from each film was corrected to 100 percent chemical yield and to the same solid angle, and then plotted against distance of air traversed by the fragments. Figure 2 shows five representative differential range curves (these are really smoothed-out histograms). The vertical scale for each of the curves is entirely arbitrary. The distance, plotted as abscissae, was corrected to air at 15°C and 760 mm mercury pressure (normal temperature and pressure). The zapon thickness was taken into account by relating its stopping power for fission fragments to that of aluminum[13] and then relating the stopping power of aluminum for alpha-particles to that of air.[14] One-half the thickness of the plutonium foil was also included in the distance, taking one mg/cm² of the foil equivalent to 0.36 mg/cm² of air.[4] By plotting the total activity of a given isotope *stopped* beyond each film against the distance of the film from the source, integral range curves were obtained. Figure 3 shows five such curves corresponding to the differential curves of Fig. 2; again the vertical scale for each mass is entirely arbitrary. The dashed horizontal portions were drawn in by extrapolation. The steepest slopes of all the curves were extended to zero activity to give *extrapolated ranges*.

In Table I the individual runs are separated into blocks enclosed by lines. The upper figures within each block (roman type) give the measured values of extrapolated ranges, while the lower figures (italics) give normalized extrapolated ranges. Nearly all of the runs overlapped each other: in each successive run the range of at least one mass that was measured in an earlier run was redetermined. Relative values of the range as a function of mass number could be obtained accurately only in this way. As a first approximation, each range value was normalized in as direct a manner as possible to the average value (2.504 cm) of the extrapolated range of mass 109. For example, each measured range of mass 157 was corrected by normalizing to the average normalized value of mass 143; each normalized value of mass 143 was obtained from its corresponding measured value by normalizing to the average normalized value of mass 132; the latter was obtained from two runs in which the ranges of both mass 132 and mass 109 were measured simultaneously. In general, there were small differences between the average measured values and the corresponding average normalized values. The algebraic sum of these differences, weighted according to the number of runs for each mass, showed that the average normalized value was 0.17 percent smaller than the corresponding measured value. This resulted from the arbitrary choice of the standard for normalization. Therefore this standard was increased by 0.17 percent (from 2.504 cm to 2.508 cm for mass

[13] E. Segrè and C. Wiegand, see reference 4. Zapon was taken to be the same as collodion since the atomic compositions are nearly identical.

[14] M. S. Livingston and H. A. Bethe, Rev. Mod. Phys. 9, 272 (1937).

109) and the measured ranges were then renormalized to this new and final value. In Table I the figures in italics give these final normalized extrapolated ranges and the average value for each mass is plotted in Fig. 4 as a function of mass number.

Table II gives both the average values of the normalized extrapolated ranges and the average values of the normalized mean ranges. The latter were calculated from the measured data in the same manner as were the former. However, the mean ranges could not be measured as precisely as the extrapolated ranges. The last column of Table II gives the average values of the width at half-maximum of the differential range curves for the various mass numbers. The indicated limits of error are merely the standard deviations from the mean of the individual determinations. Parentheses indicate that only two individual measurements were made. The widths are all the same within experimental error and the over-all average is 11.7 ± 1.3 percent of the mean range.

Radio-chemical analyses were not performed directly for some of the isotopes listed in Table I. Instead, their radioactive daughters were first extracted quantitatively from the gross fission product activity, discarded, and then allowed to grow in again from the parents. This method was used for 60-min. Te^{133}, whose daughter is 22-hr. I^{133}, because a direct measurement is made very difficult by other tellurium isotopes and their decay products. A direct isolation of the iodine is also troublesome because 6.7-hr. I^{135} and its 9.2-hr. Xe daughter interefere seriously. Since the tellurium parent of 6.7-hr. I^{135} is very short-lived (<2 min.), an initial iodine separation removes the 6.7-hr. I permanently, but more 22-hr. I^{133} can be formed from its 60-min. Te parent. This regenerated 22-hr. I was then isolated together with the 54-min. $I^{(134)}$ that was formed from its 43-min. $Te^{(134)}$ parent. The decay curves were easily resolved into 54-minute and 22-hour components. By suitably adjusting the times of bombardment, decay, and growth, and by counting the beta-rays from the 22-hr. I through 71 mg/cm² of aluminum absorber, all other components were made negligibly small. The measurements with 21-hr. Pd^{112} were made without the interference of 13.4-hr. Pd^{109} by utilizing the 3.2-hr. Ag daughter of 21-hr. Pd^{112} in a manner similar to that described for the iodine daughters. The range for mass 92 was measured once by

TABLE I. Extrapolated ranges in air of plutonium fission fragments. The values are given in centimeters at 760 mm Hg and 15°C. The individual runs are indicated by the enclosing lines. The upper values in each block are the actually measured ones; the lower italicized values were obtained by normalizing to a value of 2.508 cm for mass 109.

ISOTOPE	Br^{93} 24h	Sr^{91} 9.7h	Y^{92} 3.5h	Y^{93} 10h	$Y^{(94)}$ 20m	Zr^{97} 17h	Mo^{99} 67h	Rh^{105} 36.5h	Pd^{109} 13.4h	Pd^{112} 21h	In^{117} 1.95h	Sb^{127} 93h	Sb^{129} 4.2h	Te^{132} 77h	Te^{133} 60m	$Te^{(134)}$ 43m	Ba^{140} 12.8d	Ce^{143} 33h	61^{149} 47h	$Eu^{(157)}$ 15.4h
	2.976 *2.967*	2.746				2.736			2.512			2.256 *2.242*	2.250 *2.236*	2.212				2.002	1.958 *1.995*	
	2.860 *2.893*	2.707			2.758			2.580 *2.586*	2.502	2.421 *2.427*		2.269 *2.254*	2.266 *2.251*	2.213				1.947	1.879 *1.969*	
	2.848 *2.815*	2.770		2.754	2.749 *2.692*			2.598 *2.589*	2.517		2.195 *2.232*		2.206	2.192	2.184 *2.190*	2.182 *2.188*		2.011	1.940 *1.968*	
	2.910 *2.921*	2.728		2.738 *2.702*		2.683 *2.648*	2.657 *2.623*	2.621	2.540	2.436 *2.405*	2.204 *2.272*		2.176	2.178	2.157 *2.177*	2.163 *2.183*		2.017 *2.036*		
	2.840 *2.878*	2.702		2.720 *2.701*		2.665 *2.647*	2.661 *2.643*	2.605	2.506		2.266 *2.268*			2.223	2.198 *2.173*	2.193 *2.168*		2.068 *2.045*		
		2.802 *2.743*	2.783 *2.724*	2.755		2.747 *2.689*			2.478		2.188 *2.214*						2.029 *2.078*	1.992		1.904 *1.950*
		2.762 *2.732*	2.740 *2.710*	2.727			2.669 *2.640*		2.485		2.222 *2.243*						2.026 *2.088*	1.979		1.885 *1.943*
				2.794	(2.815) *(2.717)*				2.488		2.138 *(2.155)*						(1.921) *2.083*	(1.881)		(1.802) *1.954*
				2.774	2.761 *2.684*				2.451					2.141 *2.191*			2.112 *2.071*	2.080		
				2.797	2.783 *2.694*				2.481					2.181 *2.205*				2.038		
				2.742 *2.688*					2.558											
				2.720 *2.698*					2.528											
MEASURED AVERAGE	2.887	2.745	2.762	2.752	2.763	2.708	2.662	2.601	2.504	2.429	2.202	2.263	2.225	2.191	2.180	2.179	2.056	2.015	1.926	1.894
NORMALIZED AVERAGE	*2.895*	*2.738*	*2.717*	*2.697*	*2.687*	*2.661*	*2.635*	*2.587*	*2.508*	*2.416*	*2.246*	*2.248*	*2.243*	*2.198*	*2.180*	*2.180*	*2.080*	*2.040*	*1.977*	*1.949*

TABLE II. Extrapolated and mean ranges of plutonium fission fragments in normal air, and the straggling as indicated by the widths at half-height of the differential range curves.

Mass number	Isotope	Normalized extrapolated range (cm)	Normalized mean range (cm)	Average width at half-maximum (percent)
83	2.4-hr. Br	2.895	2.65	13.4±1.5
91	9.7-hr. Sr	2.738	2.55	11.4±0.7
92	3.5-hr. Y	2.717	2.55	10.5±(0.6)
93	10-hr. Y	2.697	2.53	10.1±0.7
(94)	20-min. Y	2.687	2.52	10.5±0.7
97	17-hr. Zr	2.661	2.50	10.7±1.1
99	67-hr. Mo	2.635	2.48	10.8±0.5
105	36.5-hr. Rh	2.587	2.42	11.4±0.6
109	13.4-hr. Pd	2.508	2.35	10.7±0.9
112	21-hr. Pd	2.416	2.24	13.4±(0.2)
117	1.95-hr. In	2.246	2.08	10.1±1.7
127	93-hr. Sb	2.248	2.09	11.9±(1.3)
129	4.2-hr. Sb	2.243	2.09	12.5±0.5
132	77-hr. Te	2.198	2.05	11.5±0.6
133	60-min. Te	2.180	2.04	11.8±0.8
(134)	43-min. Te	2.180	2.04	11.4±1.3
140	12.8-day Ba	2.080	1.92	12.6±1.3
143	33-hr. Ce	2.040	1.89	11.8±0.6
149	47-hr. 61	1.977	1.82	13.1±1.2
(157)	15.4-hr. Eu	1.949	1.79	15.1±1.3

isolating 3.5-hr. Y^{92} directly and once by isolating that 3.5-hr. Y which grew from its 2.7-hr. Sr^{92} parent during an interval after the irradiation. The two values are in close agreement, within 0.5 percent.

When attempts were made to measure the range of the fission fragments of mass 139 by analyzing for 85-min. Ba^{139}, differential range curves were obtained that were considerably distorted. This is attributed to appreciable migration in the apparatus of the 41-sec. Xe^{139} grandparent. The differential curves obtained from 12.8-day Ba^{140} were normal, although its xenon ancestor has a half-life of sixteen seconds. Therefore, it appears that this method of range determination does not apply to those mass numbers which contain in the early part of their decay chains a gaseous isotope with a half-life greater than 20–30 seconds. The differential range curves obtained from 2.4-hr. Br^{83} looked normal, although bromine may exist in volatile chemical forms. However, bromine in such volatile states might react rapidly with the beryllium and zapon, thus preventing the undesirable migration.

By measuring the range of fission fragments of uncertain mass an assignment can be made in many cases by reference to the range-mass curve of Fig. 4. This was done for five decay chains. In three separate experiments the range of fragments that result in 77-hr. Te was found to be greater than the range of those whose mass is known to be 133. This places an upper limit of 132 on the mass of 77-hr. Te, its 5-min. Sb parent, and its 2.4-hr. I daughter. Masses lower than 132 are ruled out because they are assigned to other well-known isotopes. These facts combined with some secondary considerations (e.g., fission yield) establish the mass assignment at 132. The same three experiments showed that fragments resulting in 43-min. Te have, within experimental error, very nearly the same range as those of mass 133. For the same reasons that were presented above, the mass of 43-min. Te and its 54-min. I daughter must be greater than 133. Since mass 135 is definitely assigned to other isotopes, 134 is very probably the correct mass number. Assignment to a greater mass would require serious distortion of the range-mass curve.

The mass numbers of 3.5-hr. Y, 10-hr. Y, and 20-min. Y have all been uncertain. The present range studies (Fig. 4 and Tables I and II) demonstrate that all three masses are in the interval 92–96 inclusive, and that the mass increases in the order just given. This immediately locates 3.5-hr. Y at mass 92 because assignment to 94 would put 10-hr. Y at 95 which has been previously excluded;[15] assignment to 93 is impossible because 3.5-hr. Y has been prepared by a (n, p) reaction,[15] and zirconium does not have a stable isotope there. The 10-hr. Y almost certainly belongs at mass 93. An assignment to mass 94 is highly improbable because 10-hr. Y could not be prepared from zirconium by a (n, p) reaction under conditions which did produce[16] 3.5-hr. Y and 20-min. Y; moveover, 20-min. Y would then have to be assigned to mass 96 which is also unlikely since this would require considerable distortion of the mass *vs.* range curve. Assignment of the 20-min. Y to 95 is impossible because then it could not have been produced by (n, p) from natural zirconium which is not stable there. Thus assignment of 20-min. Y to a mass of 94 is very probably correct.

[15] "Nuclei formed in fission," J. Am. Chem. Soc. **68**, 2411 (1946); Rev. Mod. Phys. **18**, 441 (1946).
[16] W. Seelmann-Eggebert, Naturwiss. **31**, 510 (1943).

The foregoing discussion of mass determination assumes that there are no radical changes in slope of the mass-range curve in the regions considered. In Fig. 4 the crossed points indicate mass numbers whose assignments have been facilitated by these range measurements.

III. DISCUSSION OF RESULTS

The uncertainty in the absolute values of the normalized extrapolated ranges which are listed in Table II is about 1.5 percent. Much of this may be attributed to variations in the thickness of the zapon films. These were not measured individually; instead, several large films of known area were weighed. The mean thickness value obtained in this way was applied to all films which were made in as reproducible a fashion as possible from the same batch of zapon lacquer. If any air leaked into the apparatus before or during an irradiation, the measured ranges would be low. However, a leak was suspected in only one or two of the runs. Small systematic errors may have been introduced by inaccurate reduction of range in zapon and in the plutonium foil to range in air. A few duplicate runs were made with a different plutonium foil, and the results are indistinguishable from those obtained with the main foil. All of the preceding errors can have only a small effect on the ratio of the ranges of different fission fragment masses that are measured in a single run.

The scattering of points in the differential curves may be produced by several factors. Although the zapon films were stretched tightly across the spacer rings when inserted into the tube, they may have buckled occasionally during the irradiations. The films have been observed to expand under certain conditions. The radiochemical analyses were subject to the usual errors. No corrections were applied for the differences in self-absorption of the beta-rays from samples of different weight because the radiation was generally hard.

The graphical method used to obtain the extrapolated fission fragment ranges is subject to some inaccuracy; individual authors were able to arrive independently at virtually the same results. However, there is an uncertainty in the absolute range values of about one percent caused by the arbitrary assumption that the stopped fragments deposit on the nearest zapon film.

Many of the above errors become more important in the measurements of the straggling. The observed spread in range of fragments of a single mass arises from three fundamental sources: (1) the variation in initial charge and kinetic energy of the fragments; (2) the statistical variation in the number of collisions, electronic and nuclear, that are encountered by the fragments; and (3) limitations introduced by the experimental arrangement. The latter were small and consisted of approximately a 1.4 percent total spread in range caused by the thickness of the plutonium source and roughly a 1.5 percent total spread caused by the difference between a perpendicular path from the source to zapon and an extreme diagonal path. These experimental factors were slightly more important for the heavy group than for the light group; therefore this may account for the slightly greater spread that seems to occur in the heavy group. None of the differential curves (Fig. 2) is Gaussian in form; all are steeper on the side distant from the source. Unfortunately, the work performed so far does not reveal whether this form of the range distribution is inherent in the fission process or in the experimental arrangement. If the plutonium fission source were thick over a small fraction of its area or if a small portion of it were covered with foreign matter, then an originally Gaussian distribution would be distorted to the observed shape. Small angle scattering of fission fragments from the walls of the tube might also lead to the same results.

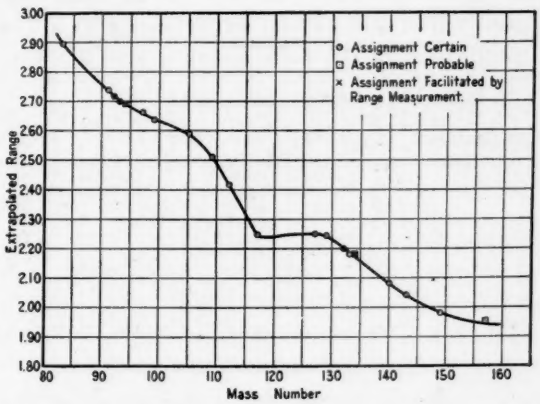

FIG. 4. Extrapolated range (76 cm pressure, 15°C) of plutonium fission fragments in air as a function of mass.

According to a relation derived by Bohr,[17] the range R of a fission fragment should be approximately proportional to the square root of its energy E, and inversely proportional to the sixth root of its mass M. This assumes the charge Z proportional to M. Deutsch and Ramsey[18] have investigated the energy release of plutonium fission fragments in a double ionization chamber. By combining values for the maximum energy derived from their paper with the range values found here, calculations were made of $RM^{1/6}/E^{1/2}$ for both the light and heavy fragments for mass ratios between 1.3 and 1.8. The ionization chamber data are most reliable in this region. The value of $RM^{1/6}/E^{1/2}$ was roughly constant, in approximate agreement with Bohr's calculations; it decreased monotonically from 0.584 to 0.548 for both the light and heavy fragment as the mass ratio was varied from 1.8 to 1.3. Below a mass ratio of 1.2 there is a sharp change in slope of the range *vs.* mass curve for both the light and heavy fragments. This seems to indicate that the kinetic energy release in the fission of plutonium reaches a maximum at a mass ratio of about 1.2 instead of at symmetric fission as calculated by Jentschke.[19] The data of Deutsch and Ramsey on energy release do not extend below a mass ratio of 1.2. However, Jentschke[19] does give data down to a ratio of about 1.1 for U^{235} and U^{238} fission. There is also some indication from his curves that the kinetic energy decreases as symmetric fission is approached. It would be interesting to refine and extend the ionization experiments so that this point could be settled.

Comparison of the ranges reported here with those reported in previous work is difficult. One reason is that the various experiments were not all performed in the same manner and the data are plotted in different ways. Most previous work was on the fission of U^{235} instead of Pu^{239}, and many of the experiments measured the ranges in aluminum instead of in air. The only directly comparable experiment was by Finkle, Hoagland, Katcoff, and Sugarman.[8] The *extrapolated* ranges given there for masses 91 and 139 are 2.66 cm and 1.92 cm (at normal temperature and pressure) instead of 2.74 cm and 2.09 cm as reported here. The cause of this discrepancy is probably that the earlier plutonium foil was far from uniform in thickness, as was pointed out in the original paper. There was only one previous investigation[11] in which the ranges of a sufficient number of fragment masses were measured to obtain a range-mass curve. This was for U^{235} fission fragments in aluminum. Only a limited region was covered, but the shape of the curve was considerably different from the corresponding curve plotted in Fig. 4 for Pu^{239} fission fragments in air. This may be due to the difference between the stopping by aluminum and by air. The older work was based on only a single experiment which should be repeated and extended to include more fragment masses and also plutonium fission.

The apparatus described here (Fig. 1) can be applied to the study of the shorter-lived fission products. Complete or partial separations of certain fission products from certain others can be effected during the bombardment because of the differences in range (see Fig. 2). This makes feasible simplified chemical procedures, so that more rapid isolations could be carried out.

This paper is based on work performed at Los Alamos Scientific Laboratory of the University of California under Government Contract W-7405-eng-36 and the information contained therein will appear in Division V of the National Nuclear Energy Series (Manhattan Project Technical Section) as part of the contribution of the Los Alamos Laboratory.

[17] N. Bohr, Phys. Rev. **59**, 270 (1941).
[18] M. Deutsch and M. Ramsey, Manhattan Project Report LA-510 (Jan. 31, 1946).
[19] W. Jentschke, Zeits. f. Physik **120**, 165 (1943).

Theory of Strain Interaction of Solute Atoms*

C. ZENER
Institute for the Study of Metals, University of Chicago, Chicago, Illinois

(Received May 18, 1948)

A general method is developed for evaluating the strain-energy interaction of solute atoms in body-centered and in face-centered cubic lattices. The method has many features in common with that used in the evaluation of the interaction of electric or magnetic dipoles, a surface distribution of forces replacing a surface distribution of electric charge or of magnetic poles. Particular emphasis is given to the interaction of interstitial solute atoms in b.c.c. lattices, where the possibility exists of a self-induced preferential distribution of solute atoms in one of the three types of tetragonal interstitial positions.

I. INTRODUCTION

THE present study was undertaken for the purpose of understanding the strain interaction of interstitial solute atoms in body-centered cubic (b.c.c.) metals. Many of the problems encountered were found to be common to substitutional as well as to interstitial solutions, and not to be confined to b.c.c. lattices. In this paper primary emphasis is therefore placed upon the general theory.

The particular interest of interstitial solutions in b.c.c. lattices lies in the tetragonal symmetry of the interstitial positions in these lattices. As was first demonstrated by Snoek[1] in his anelastic studies of alpha-iron containing carbon and nitrogen, studies which have been recently extended by Kê[2] to tantalum, the positions occupied by interstitial solute atoms in b.c.c. lattices are of the type $(0, \frac{1}{2}, \frac{1}{2})$, or $(\frac{1}{2}, 0, \frac{1}{2})$ or $(\frac{1}{2}, \frac{1}{2}, 0)$. These three positions have tetragonal symmetry with their tetragonal axes along the x, y, or z principal axes, respectively. They will be designated as the x, y and z type positions. In the absence of an externally applied stress, and of strain interaction, the interstitial atoms will be distributed at random among the three types of positions. When a tensile stress is applied along, say, the z axis, the equilibrium distribution of solute atoms will be one in which more atoms are in the z type position than in the other two. The continual striving of the solute atoms to maintain the equilibrium distribution during cyclic vibration gives rise to the anelastic effects observed, and interpreted in this manner, by Snoek. On the other hand, even in the absence of an externally applied stress the existence of a strain-energy interaction between the solute atoms gives rise to the possibility of a self-induced preferential distribution. The author[3] has previously suggested, without, however, a detailed analysis, that it is just such a self-induced preferential distribution which gives rise to the tetragonality of martensite, alpha-iron supersaturated with atomically dispersed carbon. Such a self-induced preferential distribution would, of course, have a critical temperature above which, in the absence of applied stresses, the distribution would be random. Nevertheless, the effect of the ordering tendency should be detectable above the critical temperature in the magnitude of the preferred distribution induced by an externally applied stress, just as coupling in ferromagnetic materials influences the magnetic susceptibility above the Curie temperature. Such an effect has been sought by Kê,[2] with negative results. The magnitude of this effect above the critical temperature will, of course, depend upon the magnitude of the strain-energy coupling between the solute atoms. The calculation of this coupling is one of the objectives of this paper.

When solid solutions are quenched considerably below their solubility limits it has frequently been observed,[4] through x-ray diffraction studies, that the solute atoms segregate along certain crystallographic planes prior to

* This research has been partially supported by the Office of Naval Research, U.S.N. (Contract No. N-6ori-20-IV, Contract NR 015 018).

[1] J. Snoek, Physics 6, 591 (1939); 8, 711 (1941); 9, 862 (1942); and Chemisch Weekblod, 39, 454 (1942).

[2] T. S. Kê, Phys. Rev. 74, 9, 16 (1948).

[3] C. Zener, Trans. A.I.M.E. 167, 550 (1946).

[4] C. S. Barrett, *Structure of Metals* (McGraw-Hill Book Company, Inc., New York, 1943) p. 470.

precipitation of the stable phase. The driving force for such segregation may of course reside in the difference between the bonds linking like and unlike atoms, the strain energy playing only a minor role in determining the shape of the segregate region. On the other hand it is possible that in some cases the driving force for segregation arises entirely from strain-energy interaction. A second purpose of this paper is to examine this possibility.

II. GENERAL THEORY

One can enumerate many ways in which solute atoms may interact, as for example by electrostatic forces if they carry a net charge. In this paper we are considering only that interaction which arises from a coupling of their strain energies.

The essential features of strain interaction can best be obtained by an analysis of an auxiliary problem. Suppose two atoms of a lattice, designated by subscripts 1 and 2, are acted upon by external forces F_1 and F_2. These forces are then linear functions of the components of the resulting displacements along the direction of the applied forces. Thus if h_1 and h_2 are these displacement components, then

$$\begin{aligned} F_1&=a_{11}h_1+a_{12}h_2,\\ F_2&=a_{12}h_1+a_{22}h_2. \end{aligned} \tag{1}$$

The strain energy of the lattice is a quadratic function of h_1 and h_2, and hence may be written as

$$E=\tfrac{1}{2}(F_1h_1+F_2h_2). \tag{2}$$

In view of Eq. (1), this strain energy may also be written in the form

$$\begin{aligned} E=&\tfrac{1}{2}(F_{11}h_1+F_{22}h_2)\\ &+\tfrac{1}{2}(F_{21}h_1+F_{12}h_2), \end{aligned} \tag{3}$$

where the force coefficients are defined as

$$F_{ij}=a_{ij}h_i. \tag{4}$$

The first term in Eq. (3) would alone give the strain energy if the two atoms were so far apart that the coupling term a_{12} were negligible. This first term is not, however, itself independent of the coupling. Thus, if we regard a_{12} as a first-order small quantity, F_2 will give rise to a first-order small change in h_1, and hence to a first-order small change in the first term of Eq. (3). If, however, the force F_1 has a potential $V_1(h_1)$, the value of h_1 in the absence of interaction is such as to minimize the sum

$$\tfrac{1}{2}F_{11}h_1+V_1(h_1).$$

The first order changes in this sum, due to the coupling between the two atoms, vanishes. If we therefore neglect second-order small quantities, the change in the total energy introduced by the coupling between the two atoms is given by the second term in Eq. (3), namely by

$$E_{\text{Int}}=\tfrac{1}{2}(F_{21}h_1+F_{12}h_2). \tag{5}$$

The force coefficient F_{21} may be interpreted as the external force which must act upon atom 1 in order to maintain its displacement component h_1 zero in the presence of the force F_2 acting upon atom 2. This force coefficient may also be interpreted as the negative of the force $f_{2,1}$ with which the rest of the lattice acts upon atom 1 when the two displacement components have the values $(0, h_2)$ respectively. The strain energy interaction may thus be written in terms of these lattice forces as

$$E_{\text{Int}}=-\tfrac{1}{2}(f_{2,1}h_1+f_{1,2}h_2). \tag{6}$$

It is to be particularly noted that the sign of the interaction energy is negative if the lattice coupling forces $f_{i,j}$ are in the same direction as the displacements h_j. At first sight this conclusion seems erroneous, since under these conditions strain energy is increased by the coupling. This apparent contradiction is removed when we recall that the total energy includes the potential of the applied forces, and that in the case under consideration the lowering of these potentials more than compensates for the rise in strain energy.

One further simplification will be introduced before passing to our original problem of solute atoms. We have already considered the coupling a_{12} as a small-order correction, and have neglected second-order small changes in the quantities $\tfrac{1}{2}F_{11}h_1+V(h_1)$ and $\tfrac{1}{2}F_{22}h_2+V(h_2)$. In order to take into account these second-order small changes we would have to know more precisely the form of the potentials $V_1(h_1)$ and $V_2(h_2)$. We are therefore not justified in retaining second-order small quantities in the right side of Eq. (6). Since the lattice forces $f_{2,1}$ and $f_{1,2}$ are already first-order small quantities, the displacement components h_1 and h_2 will be regarded as having

those values which minimize $\frac{1}{2}F_{11}h_1+V_1(h_1)$ and $\frac{1}{2}F_{22}h_{22}+V_2(h_2)$, respectively, i.e., h_i will be regarded as the solution of the elastic problem in which only the force potential $V_i(h_i)$ is different from zero.

The characteristic feature of the forces exerted by a solute atom upon a lattice is that the resultant of all the forces is precisely zero. In b.c.c. and f.c.c. lattices these forces occur in pairs, the two forces of each pair being equal in magnitude but opposite in direction, their line of action passing through the solute atom position, and acting on two atoms symmetrically placed on either side of the solute atom. Thus a substitutional solute atom in a b.c.c. lattice is associated with four pairs of forces, each pair acting along one of the four cube diagonals. An interstitial solute atom is associated with three pairs of forces. If it is occupying a z type position, one pair acts along the z principal axis, the other two along the [110] and [$\bar{1}$10] axes. The pairs of forces will be called force dipoles. We shall denote each corresponding pair of solvent atoms by the subscript σ; the relative radial displacement of each atom of the pair with respect to the other, referred to their equilibrium displacement, we shall denote by $h_{j\sigma}$, j denoting the associated solute atom. Each system of force dipoles will then have a potential which is a function of the corresponding displacements $h_{j\sigma}$. The interaction energy may then be generalized from the form of Eq. (6) to

$$E_{\text{Int}}=-\tfrac{1}{2}\sum_\sigma\{f_{2,1\sigma}h_1+f_{1,2\sigma}h_2\}. \qquad (7)$$

In our former equation for the interaction energy the force coefficient $f_{2,1}$ was the force exerted by the lattice upon lattice atom 1. In the present equation the coefficient $f_{2,1\sigma}$ is the radial force dipole exerted by the lattice upon the pair σ of solvent atoms associated with solute atom 1 while the relative separation of all pairs of lattice atoms surrounding solute atom 1 are held fixed when solute atom 2 is introduced.

III. LONG RANGE FORCES

In estimating the strain energy interaction of solute atoms, we shall adopt the conventional procedure used in estimating the interaction of magnetic or electric dipoles. Thus, in estimating the strain energy interaction of a particular solute atom 1 with all other solute atoms, we imagine this solute atom enclosed by a small sphere, and that all the other solute atoms are outside this sphere. In the first approximation we consider that the positions of the solute atoms outside the sphere are completely independent of the presence of the single solute atom within the sphere. The interaction computed in this manner will be called the long-range interaction. In the second approximation we take partially into account the effect of the presence of the single solute atom inside the sphere upon the positions of the solute atoms outside the sphere. The change in the interaction energy introduced in this approximation will be called the short-range interaction.

From Eq. (7) we note that the effect of solute atom 2 upon the strain energy of solute atom 1 may be expressed in terms of that stress pattern at the site of solute atom 1 which is induced by the presence of solute atom 2. In the evaluation of the long-range interaction it is therefore sufficient to compute the stress within the sphere arising from the presence of all the solute atoms outside the sphere. In the evaluation of this stress we continue to follow the conventional method used with magnetic and electric dipoles. For interstitial solutions, in place of considering a discrete number of sets of dipole forces, one set for each solute atom, we shall consider that a set of dipole forces is associated with each potential interstitial position, the magnitude of the forces in each set being equal to the actual magnitude for a solute atom times the atomic concentration of solute atoms referred to the number of potential lattice sites. A very similar procedure may be adopted in the case of substitutional solute atoms in a b.c.c. or f.c.c. lattice. Here the dipole forces specifically associated with each solute atom are defined as the difference between the actual dipole forces exerted by the solute atoms and the dipole forces which would be exerted if the solute atom were replaced by a solvent atom. The net force acting upon each lattice atom is thus precisely zero provided this lattice atom is not near a surface, either the exterior or the interior surface. The problem of long-range interaction has thus been reduced to finding the stress produced by a system of surface forces.

In the case of a substitutional solution in a b.c.c. or a f.c.c. lattice the net force acting on any element of surface is directed normal to the surface, and is in the direction away from the uniform distribution of force dipoles provided the solute atoms are larger than the solvent atoms. For our present purpose we are not interested in the magnitude of the surface density of this force, but only in the fact that this surface density is uniform and is independent of crystallographic orientation, being the same on the interior surface as on the exterior surface. The forces acting on the exterior surface will give rise to a hydrostatic tensile stress throughout the specimen, including the interior of the sphere. The magnitude of this hydrostatic tensile stress will simply be the bulk modulus K, times the observed dilation of the lattice, Θ. On the other hand, the forces acting upon the interior spherical surface will give rise to a compressive stress which tends to counteract the stress produced by the forces acting on the external surface. However, the inner surface forces must not only compress the inner sphere, they must also compress the whole of the surrounding lattice, i.e., the surrounding lattice must be deformed so as to maintain contact with the compressed sphere. Now the elastic modulus for the compression of a sphere is K, while the elastic modulus for the compression of a spherical cavity[5] is $(4/3)\mu$, where μ is the rigidity modulus. That fraction of the surface force which is available for compressing the sphere is therefore the ratio $K/(K+4\mu/3)$. The net hydrostatic stress σ within the sphere is therefore given by

$$\sigma=\alpha K\Theta, \tag{8}$$

with

$$\alpha=\frac{(4/3)\mu}{K+(4/3)\mu}. \tag{9}$$

Upon taking as an example the typical case of a Poisson ratio of 1/3, we find that α itself has a typical value of 1/3. It is of interest to note that the present treatment gives the correct value of zero strain interaction in the limiting case of a fluid, for in a fluid the rigidity modulus μ, and hence α, is precisely zero.

Our next step is to evaluate the effect of the hydrostatic stress σ upon the strain energy of our solute atom. Towards this end we consider a unit volume to which we apply a hydrostatic tensile stress σ. The number of solute atoms will be denoted by n, the total energy of the system by E. If we now denote by U the energy required to introduce a new solute atom under conditions of constant stress, exclusive of the work done by the applied forces, then

$$dE-\sigma dv=Udn. \tag{10}$$

This equation may be written in the form of a perfect differential, namely as

$$d(E-\sigma v)=-vd\sigma+Udn, \tag{11}$$

from which we deduce

$$(\partial U/\partial\sigma)_n=-(\partial v/\partial n)_\sigma. \tag{12}$$

In our actual problem the stress σ is produced by the forces of the solute atoms within the lattice itself. These forces have of course a potential, and the dilation of the lattice is just such as to minimize the sum of these potentials and of the strain energy. In evaluating the change in energy associated with the introduction of a solute atom into our spherical region, we must therefore neglect the change in strain energy σdv, as this is compensated by the change in the potentials of the solute atoms. We may therefore apply Eq. (12) for the variation of the energy of a solute atom due to the long-range interaction of the other solute atoms. We may thus write for the long-range strain interaction

$$E_{\text{Int}}=-(\partial\Theta/\partial n)_\sigma\cdot\sigma, \tag{13}$$

where n is the number of solute atoms per unit volume. Upon combining Eqs. (8) and (13) we thereby obtain for the long-range interaction energy

$$E_{\text{Int}}=-\alpha K(\partial\Theta/\partial n)\cdot\Theta. \tag{14}$$

Since, at least for small concentrations, Θ is a linear function of n,, this equation may be rewritten as

$$E_{\text{Int}}=-\alpha nK(\partial\Theta/\partial n)^2. \tag{15}$$

It is to be noted that E_{Int} in this equation is the increment in energy, due to the other solute atoms, when one additional solute atom is introduced. Since this is proportional to n, the interaction energy per solute atom is just half as great as given in Eq. (15).

[5] A. E. H. Love, *Mathematical Theory of Elasticity* (Cambridge University Press, Cambridge, 4th ed., 1934) p. 187.

We shall now consider the interaction of interstitial solute atoms in a b.c.c. lattice, where the stress pattern surrounding each solute atom has tetragonal symmetry. So far we have emphasized the similarities in the interaction of solute atoms and of magnetic and electric dipoles. A consideration of interstitial solute atoms in a b.c.c. lattice provides us with the opportunity of pointing out some striking dissimilarities in the two types of interaction. Suppose, for example, that we have a single crystal in which only the z type positions are occupied, and further that the solute atoms in these positions are associated with only a single force dipole, acting parallel to the z axis. The long-range influence of all the other solute atoms upon one particular solute atom may then be represented as the effect of two sets of surface forces, one acting on the external surface, and one acting over the surface of a sphere surrounding the given solute atom. The external surface force will give rise to a pure tensile stress Z_z whose magnitude is independent of the shape of the specimen. The magnitude of Z_z is identical in the case of a thin slab normal to the z axis as in the case of a long rod along the z axis. The shape invariancy of the effect of the surface forces is of course in marked contrast to the corresponding cases with magnetic or electric dipoles. The physical interpretation of this difference lies in the fact that the stress field produced by the mechanical forces is confined to the specimen itself, while the magnetic and electric fields produced by a surface distribution of poles are not so confined.

In the case of actual interstitial solute atoms in b.c.c. lattices, we cannot consider each solute atom as equivalent to a single force dipole. If such were the case, then when all the solute atoms were in the same type of position, e.g., the z type, the observed contraction along the x and y axes would be related to the extension along the z axis by the appropriate Poisson ratio. Thus in the case of carbon dissolved in iron this ratio would be 0.37. Its observed[6] value in martensite is 0.15, indicating that at least in this system the solute atoms exert radial forces upon the neighboring four atoms lying in a plane normal to the z axis.

[6] S. Epstein, *The Alloys of Iron and Carbon*, I. (McGraw-Hill Book Company, Inc., New York, 1936) p. 212.

The stress in the interior of our sphere due to a preferred distribution of sets of dipole forces not having cubic symmetry is difficult to evaluate. The author has not been able to evaluate the constant α in the relation corresponding to Eq. (8). It is anticipated, however, that only a slight error will be made by assuming this constant to have the same value as in the case of a hydrostatic tensile stress. We shall therefore set

$$\begin{pmatrix} X_x \\ Y_y \\ Z_z \end{pmatrix} = \alpha \begin{Vmatrix} c_{11} & c_{12} & c_{12} \\ c_{12} & c_{11} & c_{12} \\ c_{12} & c_{12} & c_{11} \end{Vmatrix} \begin{pmatrix} e_{xx} \\ e_{yy} \\ e_{zz} \end{pmatrix} \tag{8a}$$

as the relation between the stress in the interior of the sphere due to long-range interaction and the over-all strain produced by the solute atoms. The interaction energy associated with this stress may be found by an analysis identical to that used in the case of a hydrostatic tensile stress. We find that the effect of the stress upon the energy required to introduce a solute atom into a given type of interstitial position is

$$E_{\text{Int}} = -\sum_i \delta\epsilon_i \sigma_i, \tag{13a}$$

where $\delta\epsilon_i$ is the ith principal strain attending the introduction of one solute atom per unit volume into the given type of interstitial position, and σ_i is the ith principal stress.

Equations (8a) and (13a) will now be used to evaluate the influence of long range strain interaction upon the relaxation associated with a stress-induced preferential distribution of interstitial solute atoms in one of the three types of interstitial positions. We suppose a tensile stress σ is applied along one principal axis, hereafter called the preferred axis. We shall denote by N_p and N_n the number of solute atoms per unit volume, in the preferred and non-preferred type of interstitial positions, respectively, and by $\delta\epsilon_p$, $\delta\epsilon_n$ the increments in principal strains along the preferred and along one of the non-preferred principal axes, respectively, introduced by one atom per unit volume into a p position. Upon denoting the preferred axes by the subscript 1, the principal strain components associated with the solute atoms become

$$\begin{aligned}(\epsilon_1, \epsilon_2, \epsilon_3) = \{ & N_p\delta\epsilon_p + N_n\delta\epsilon_n, \\ & \tfrac{1}{2}N_n\delta\epsilon_p + (N_p + \tfrac{1}{2}N_n)\delta\epsilon_n, \\ & \tfrac{1}{2}N_n\delta\epsilon_p + (N_p + \tfrac{1}{2}N_n)\delta\epsilon_n\},\end{aligned} \tag{16}$$

and the change in long-range strain energy inter-

action associated with the transfer of one solute atom from an n to a p interstitial position becomes, according to Eq. (13a)

$$\delta U = -(\delta\epsilon_p - \delta\epsilon_n)(\sigma_p - \sigma_n). \quad (17)$$

When we now utilize Eqs. (8a) and (16) to compute σ_p and σ_n, we find

$$\delta U = -\alpha(N_p - \tfrac{1}{2}N_n)(c_{11} - c_{12})(\delta\epsilon_p - \delta\epsilon_n)^2. \quad (18)$$

We now utilize this explicit expression for the change in long-range strain interaction energy to compute the equilibrium value of $N_p - \frac{1}{2}N_n$, as was first carried out by Polder[7] for an arbitrary δU, and compute the relaxation strength

$$\Delta_E \equiv (E_U - E_R)/E_R, \quad (19)$$

where E_U is the elastic modulus E_{100} as measured under conditions in which N_p remains constant, and E_R is the same modulus measured under conditions in which N_p has its equilibrium value. We find

$$\Delta_E = T_0/(T - \gamma T_0), \quad (20)$$

where

$$T_0 = (2/9)nE_{100}(\delta\epsilon_p - \delta\epsilon_n)^2, \quad (21)$$

in agreement with Polder, and where the constant γ has the explicit form

$$\gamma = (3/2)[(c_{11} + c_{12})/(c_{11} + 2c_{12})]\alpha. \quad (22)$$

In the author's[3] original derivation of Eq. (20) the constant γ was undetermined, and was assumed to be of the order of magnitude of unity. The recent measurements of Kê[2] upon the relaxation strength associated with interstitial solute atoms in a b.c.c. lattice showed definite disagreement with Eq. (20) when γ was taken as unity. Upon taking our previously estimated value of α, namely 1/3, and upon observing that C_{12} is always less than C_{11}, we find that γ varies between 1/3 and 1/2, being 0.38 for iron. The data of Kê are not sufficiently extensive to distinguish between the above lower theoretical limit of 1/3 and his assumed value of zero.

The change in the constant γ from unity to 0.38 for the case of iron has important theoretical consequences. As was shown by Polder,[7] the data on the variation of the lattice parameters of martensite with carbon concentration may be used in conjunction with Eq. (21) to obtain an explicit expression for T_0 for iron containing carbon, namely

$$T_0 = 1190X_c \quad (23)$$

where X_c is the weight percent concentration of carbon. Now the critical temperature for ordering by long-range interaction is very close to γT_0, namely[8]

$$T_c = 1.05\gamma T. \quad (24)$$

One should therefore anticipate that for iron the critical temperature would be igven by

$$T_c = 470X_c. \quad (25)$$

According to this equation, the carbon concentration would have to be above 0.64 wt. percent for the critical temperature to lie above room temperature. The self-ordered structure of martensite has been observed at carbon concentrations as low as 0.4 wt. percent. We are therefore led to believe that the long-range strain interaction between the carbon atoms is not sufficient alone to cause the observed self-induced ordering. One possibility is that the strain-interaction between close pairs of carbon atoms is of such a sign and magnitude as to aid the long-range strain interactions in establishing an ordered distribution. This possibility is investigated in the following section.

IV. SHORT RANGE STRAIN INTERACTION AND SEGREGATION

Interesting qualitative conclusions may be reached merely by considering the general form of the strain interaction as developed in Section II. We there saw that the strain energy interaction of two solute atoms 1 and 2 is negative if the force resulting from solute atom 2 upon the nearest neighbors of solute atom 1 is in the same direction as that exerted by solute atom 1 itself. In applying this rule it would appear unprofitable to consider cases where the solute atoms are themselves nearest neighbors, since in such cases the interaction will usually be dominated by types of interaction other than strain.

The first example to be considered will be substitutional solutions in b.c.c. lattices. If two solute atoms are neighbors along a principal axis, as in a of Fig. 1, having four common lattice atoms as nearest neighbors, the strain inter-

[7] D. Polder, Philips Research Reports, 1, 5 (1945).

[8] C. Zener, *Elasticity and Anelasticity of Metals* (University of Chicago Press, Chicago, Illinois, 1948) p. 125.

action will be negative. Thus in this case the cosine of the angle between the vectors from each solute atom to a common nearest neighbor is positive, namely $3^{-\frac{1}{2}}$. On the other hand, if the two solute atoms are situated as in *b* of Fig. 1, having two neighbors in common, the corresponding cosine is negative, namely $-3^{-\frac{1}{2}}$, and hence the two solute atoms repel one another. A still less favorable situation is illustrated in *c* of Fig. 1, where the two solute atoms tend to displace a common nearest neighbor in opposite directions. We conclude that the strain energy interaction of substitutional solute atoms in b.c.c. lattices is highly dependent upon relative crystallographic orientation, a common ⟨100⟩ axis being preferred, while a common ⟨110⟩ or ⟨111⟩ axis tends to be avoided. By examining in a similar manner the interaction between solute atoms spaced further along a ⟨100⟩ axis than one lattice constant, we conclude that they likewise have a negative interaction strain energy. A linear array of solute atoms along a ⟨100⟩ axis thus has a lower strain energy than if the solute atoms were in pairs, which paired system in turn has a lower strain energy than if the solute atoms were atomically dispersed. We next inquire as to whether a planar array, formed by placing linear arrays side by side, would have a still lower strain interaction. At first sight it would appear that the energy would not be lowered since, when two linear arrays are placed next to each other so as to have a common face, the attraction of each solute atom by its nearest neighbor in the other linear array is exactly counteracted by the repulsion of the two next nearest neighbors. However, in a plane array of solute atoms in a plane containing two crystallographic axes, the strain will be confined essentially to the unit cubes containing the solute atoms, the strain outside these unit cubes decreasing exponentially as we go away from the plane of solute atoms. Such a planar array must therefore have a lower strain energy than an assembly of isolated linear arrays.

If we exclude from our discussion the case of nearest neighbor solute atoms, as discussed above, the case of substitutional solution in f.c.c. lattices appears less interesting. It seems that no strong strain-energy attraction between two substitutional solute atoms can be obtained

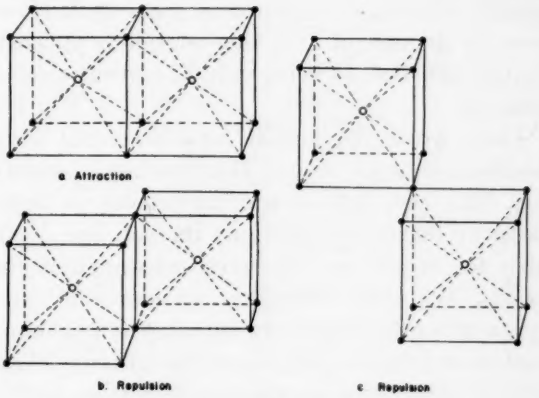

FIG. 1. Examples of strain interaction.
○ Solute atom; ● solvent atom.

for any positions. Thus if two solute atoms are one lattice constant apart along a ⟨100⟩ axis, the common nearest lattice neighbors are displaced by the two solute atoms in directions normal to one another. If the two solute atoms are on opposite corners of the face of a unit cell, the displacements of their common lattice nearest neighbor due to the two solute atoms are in opposite directions, and hence the solute atoms repel one another. A similar situation of no strong strain energy attraction exists in the case of interstitial solutions in f.c.c. lattices. In order that substitutional solute atoms may form a stable planar array in a f.c.c. lattice, it appears as if they must themselves be nearest neighbors, and hence interactions other than strain energy must be operative.

Since considerable data are available regarding the interstitial solution of carbon in the b.c.c. lattice of alpha-iron, this case will be treated in considerable detail. The energy of the iron lattice will be considered as expressible in terms of central force bond energies, i.e., bond energies which are a function only of the distance between the two atoms under consideration. As is well known,[9] such a representation of the lattice energy cannot be exact, since it would require that the Cauchy relations between the elastic coefficients be satisfied. For a cubic metal these relations reduce to the single equation

$$c_{12}=c_{44}. \tag{26}$$

In most cubic metals this relation is far from being even approximately satisfied, c_{12} being

[9] A. E. H. Love, reference 5, pp. 616–627.

greater than c_{44} by a factor as great as 3. However, in the case of iron, this relation is approximately satisfied, c_{12} being only 22 percent greater than c_{44}.

Once we have decided to use central force bonds, and hence require that the lattice satisfy Eq. (26), only two elastic coefficients, or independent linear combinations thereof, are available for specifying the force constants of the bonds. We shall therefore consider only two types of bonds, those between nearest neighbors, and those between next nearest neighbors. These will be designated as the α and β type bonds, respectively. In the unstrained lattice the α bonds are along the $\langle 111\rangle$ axes, the β bonds along the $\langle 100\rangle$ axes. The two shear coefficients c_{44} and $(c_{11}-c_{12})/2$ will be chosen to determine the force constants of the α and β bonds, corresponding to the fact that the local distortions surrounding solute atoms are primarily shear distortions. We denote by A and B the force constants of the α and β bonds, respectively, i.e.,

$$A=d^2U_\alpha/dr^2$$
$$B=d^2U_\beta/dr^2,$$

where U_α and U_β are the corresponding bond energies, and where the second derivatives are to be taken at the value of r corresponding to an unstrained lattice, namely

$$r=\begin{cases}(\sqrt{3}/2)a, & \alpha \text{ bond}\\ a, & \beta \text{ bond},\end{cases}$$

where a is the lattice constant. One then finds that

$$a^2A=(3a^3/2)c_{44},$$
$$a^2B=a^3(c_{11}-c_{12})/2. \tag{27}$$

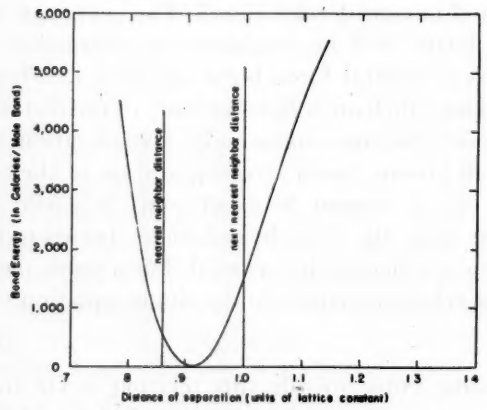

FIG. 2. Bond energy of iron atoms in b.c.c. lattice, computed from elastic constants.

Upon taking the known values of the two shear coefficients[10] for iron,

$$c_{44}=1.16\times10^{12} \text{ dynes/cm}^2,$$
$$(c_{11}-c_{12})/2=0.48\times10^{12}, \tag{28}$$

we find

$$a^2A=\begin{cases}4.1\times10^{-11} \text{ ergs}\\ 595{,}000 \text{ cal/mole bond},\end{cases} \tag{29}$$

and

$$B=0.276\text{A}. \tag{30}$$

One could interpret the force constants A and B as being the second derivatives of a single bond energy $V(r)$ taken at the distance of separation corresponding to nearest and next nearest neighbors. An estimate of $V(r)$ has been obtained by expanding in a Taylor series about $r=a$ up to the cubic term, and determining the three coefficients by the condition of stability with respect to a cubical expansion and by the condition that the second derivation at $(\sqrt{3}/2)a$ and at a reduce to A and B, respectively. An estimate of V obtained in this manner is reproduced in Fig. 2.

We are now in a position to compute the distortion surrounding an interstitial carbon atom. Suppose a carbon atom is at a z type position, as in Fig. 3. It then acts downwards upon iron atom 1, upwards on atom 2, and horizontally upon atoms 3–6. In the preceding section we saw how the over-all distortion may be computed in terms of these forces. In the present case the computation will be reversed, since the over-all distortion is known from the data upon the variation of the lattice parameters of martensite with carbon content. Upon letting C be the atomic concentration of carbon, the over-all tetragonal strain in martensite induced by the addition of carbon is given by[6]

$$e_{zz}=0.90\text{C},$$
$$e_{xx}=e_{yy}=-0.14\text{C}. \tag{31}$$

As discussed in the last section, the carbon atoms may be thought of as giving rise to these strains by means of a distribution of surface forces. The dependence upon carbon concentration of the stress system arising from this surface distribution of forces is

$$Z_z=c_{11}e_{zz}+2c_{12}e_{xx},$$
$$X_x=c_{11}e_{xx}+c_{12}(e_{xx}+e_{zz}). \tag{32}$$

[10] E. Goens and E. Schmid, Naturwiss. 19, 520 (1931).

The vertical force F_V acting upwards on atom 2 and downwards upon atom 1, and the horizontal force F_H acting upon each of atoms 3–6, are given by

$$CF_V=(a^2/2)Z_z,$$
$$CF_H=(a^2/2^{\frac{1}{2}})X_x. \tag{33}$$

We now solve for these two forces from Eqs. (31)–(33), and express the results in terms of A through Eq. (27), obtaining

$$F_V=0.50aA,$$
$$F_H=0.30aA. \tag{34}$$

An approximate description of the distortion of the lattice in the vicinity of the carbon atom is now obtained by allowing all the atoms shown in Fig. 3 to attain those positions which minimize the strain energy, all other atoms of the lattice being held constant. We find that atoms 1 and 2 are displaced along the vertical axis by the amount

$$\delta_{100}=0.13a;$$

atoms 3–6 are displaced in the horizontal plane radially away from the carbon atom by the amount

$$\delta_{100}=0.052a;$$

and finally, atoms 7–14 are displaced along the corresponding ⟨111⟩ axes by the amount

$$\delta_{111}=0.022a.$$

With these distortions, and the general theory developed in Section II, some conclusions may be drawn regarding short-range strain energy interaction of carbon atoms in iron. We shall, somewhat arbitrarily, take the radius of the sphere surrounding a carbon atom as equal to one lattice constant, a. Interstitial positions lying on or outside of this sphere will then be regarded as potential sites for other carbon atoms. We shall consider the given carbon atom as being in a z type position, as in Fig. 3. Of the six nearest potential z type positions, the two on the same z axis have a strong positive interaction, the four lying on the same x–y plane have fairly strong negative strain interaction, namely -2000 calories/mole. If p is the probability of any given potential interstitial position being occupied in the absence of interaction, the above

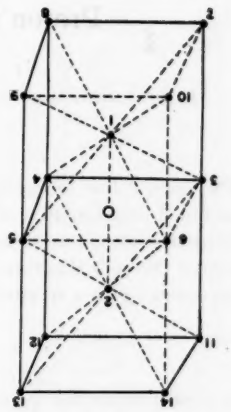

FIG. 3. Vicinity of carbon atom in iron lattice. ○ Carbon; ● iron.

mentioned interaction reduces the probability of occupancy of two of the neighboring z type positions from p to essentially 0, at the same time increasing the probability of occupancy of four of the neighboring z type positions from p to $28p$, the factor 28 being the value of $\exp(2000/RT)$ at room temperature. The short-range interaction thus greatly increases the average number of carbon atoms in a neighboring z type position. On the other hand, the nearest potential x and y type positions correspond to a positive interaction, and hence to a reduction in the probability of occupancy. We therefore conclude that in the case of carbon in iron, the short-range interaction aids the long-range interaction in giving rise to a self-induced preferential distribution.

While the conclusions regarding long-range interaction have been expressed in terms applicable to any solute atoms in any b.c.c. or f.c.c. lattice, the above conclusions regarding the short-range interaction of carbon atoms in iron cannot be extended to the general case of interstitial solute atoms in b.c.c. lattices. Each case will have to be examined separately. Thus we anticipate carbon will introduce considerably less distortion in the b.c.c. lattice of tantalum, which has a larger lattice constant than iron. If the strains are half that in iron, the interaction energy will be reduced by approximately a factor of four, resulting in an increase in the probability of occupancy of a neighboring interstitial position of like type by a factor of only 2.3, rather than of 28 as in the case of iron.

Proton Stopping Power of Solid Beryllium

C. B. MADSEN* AND P. VENKATESWARLU
Institute for Theoretical Physics, University of Copenhagen, Copenhagen, Denmark

(Received May 17, 1948)

The energy loss of protons penetrating beryllium foils of different thicknesses has been determined as a function of the proton energy by measuring the shift of those potentials at which a thin aluminum target gives resonance radiation. The experimental points fit within ±2 percent a theoretical curve corresponding to an average ionization energy of 64±5 ev, which is in agreement with a recent theory for the stopping power of metals.

THE sharp resonances for proton capture by light nuclei offer a convenient means for analyzing the energy distribution of a beam of protons, and the phenomenon may thus be used to make accurate measurements of the energy loss suffered by protons passing through matter by inserting thin foils in a homogeneous proton beam before it reaches the target.

The theory of the stopping power of metals has recently been discussed,[1,2] and therefore, it appeared of interest to apply the method of determining the specific stopping power of protons in beryllium, because of the high relative number of conduction electrons in this metal and because it is well suited for the preparation of thin foils.

Aluminum was chosen as target material, because its spectrum was well known from an earlier investigation at this institute.[3] The technique and apparatus for the production of the proton beam and for the detection of the gamma-radiation were those described in the work mentioned.

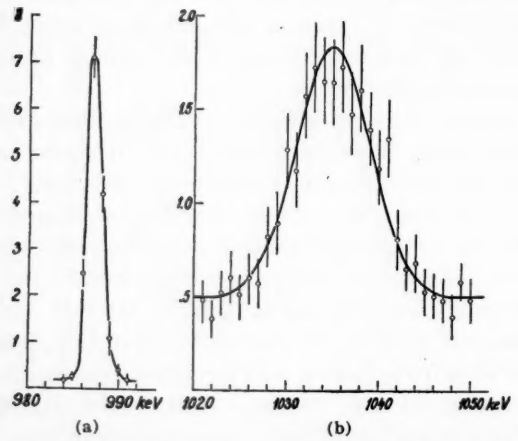

FIG. 1. The 986 kev Al resonance measured (a) without foil, and (b) with a 0.22 mg per cm² Be foil inserted in the proton beam. The ordinates give the γ-ray yield in the same arbitrary unit.

A small disk with six circular openings, three of which were covered by beryllium foils, was mounted in the acceleration tube at a height of 35 cm above the aluminum target. By the help of a small magnet the different openings of the disk could be brought into the path of the protons.

The proton current used was of the order of 0.2 microamp and the width of the beam was 3 mm. Counting was only allowed by means of an electronic switch,[3] when the fluctuations of the acceleration voltage were smaller than ±2 kv. The different aluminum targets used had stopping powers of 1 to 10 kev.

The foils had been prepared by evaporation and the total contamination of other metals was found by a spectral analysis to be less than 0.1 percent.[4] A possible oxidation of the surface of the foils would be insignificant for the present purpose, since the stopping power of oxygen per weight is very nearly equal to that of beryllium.

The areas of the foils were calculated from measurements with a traveling microscope and their weights were determined with a microbalance. The thicknesses obtained in this way are supposed to be correct within ±1 percent. After the measurements of the stopping power, the thicknesses of the foils were checked and found to be unchanged within this limit.

* On leave from the University of Aarhus, Denmark.
[1] H. A. Kramers, Physica 13, 401 (1947).
[2] Aage Bohr, Kgl. Danske Vid. Selsk. Mat.-fys. Medd. (in press).
[3] K. J. Broström, T. Huus, and R. Tangen, Phys. Rev. 71, 661 (1947).
[4] We are most indebted to civil engineer Mr. Kühnel-Hagen for carrying out this analysis.

As an example of the measurements of the stopping power, Fig. 1 shows the aluminum resonance at 986 kev measured without foil, and with a foil of thickness 0.222 mg per cm² inserted in the proton beam. The difference between the mean energies for the two curves has been taken as the energy loss of the protons.

The standard deviation is seen to be 4 to 5 kev and 1 to 2 kev with and without foil, respectively. It is of interest that this broadening effect just corresponds to the theoretical estimate of the straggling.[5] The same is the case with the other foils, and it is likely, therefore, that inhomogenities in the foils do not contribute essentially to the broadening. The precision should thus approach the limit given by the straggling.

In Fig. 2 are plotted the experimental values of the specific stopping power 's' obtained with three foils of thicknesses 0.609 (crosses), 0.245 (circles) and 0.222 (dots) mg per cm² as a function of the average energy of the protons in the foil.

The theoretical curves are drawn according to the formula:[6]

$$s=\frac{2\pi e^4}{E\mu}\frac{Z}{A}\left(\log\frac{4E}{I_{av}}\frac{\mu}{M}-\frac{C_k(E)}{Z}\right)$$

with the average ionization energy I_{av} of the electrons in the beryllium atoms as a parameter. E is the energy, and M the mass of the protons, e, the charge, and μ the mass of an electron, and Z the atomic number and A the mass number of beryllium. C_k is a correction, which is due to the strong binding of the K electrons.[6]

It is seen that the experimental points fit with a curve corresponding to I_{av} equal to 64 ± 5 ev. The theoretical value of I_{av} for the metallic state of beryllium has been estimated

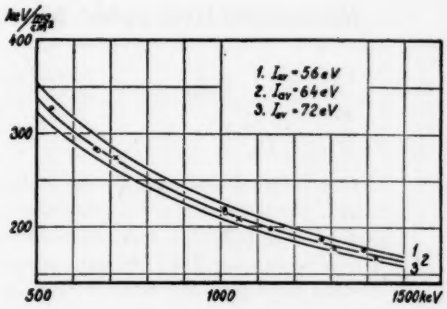

FIG. 2. The specific stopping power for protons on metallic Be measured with foils of thicknesses 0.222 (dots), 0.245 (circles) and 0.609 (crosses) mg per cm².

to be about 60 ev,[2] whereas the value of I_{av} for separated beryllium atoms would be only about 45 ev. The measurements thus confirm the predicted increase in I_{av} for the metallic state, which is to be ascribed to the mutual interaction of the electrons in the substance. This effect, which is especially pronounced in beryllium with its high electron density, implies, in fact, a screening of the field of the moving particle and thus gives rise to a decrease in the stopping power.

It may be added, that the earlier theory of v. Weizsäcker[7] of the stopping power of metals, in which the conductivity was assumed to play a decisive role, gives a value for I_{av} of the order of 10 ev.

In conclusion we wish to thank Professor Niels Bohr for his continuous interest in this work, and mag. scient. Aage Bohr for suggesting the investigation. Our thanks are also due to cand. mag. K. J. Broström and mag. scient. Torben Huus for their advice in experimental questions.

One of us (CBM) is indebted to the Carlsberg Foundation and to Landsforeningen til Kræftens Bekæmpelse, and another (PV) to the Rask-Ørsted Foundation for grants enabling us to take part in the work in Copenhagen.

[5] See N. Bohr, Kgl. Danske Vid. Selsk. Mat.-fys. Medd. 18, 8 (1948).

[6] M. S. Livingston and H. A. Bethe, Rev. Mod. Phys. 9, 264 (1937).

[7] C. F. v. Weizsäcker, Ann. d. Physik 5, 17, 869 (1933).

Mass Spectrographic Mass Assignment of Radioactive Isotopes

RICHARD J. HAYDEN*
Metallurgical Laboratory, University of Chicago, Chicago, Illinois
(Received June 3, 1948)

Characteristics of positive ion emission for various compounds on a tungsten filament are noted. Methods of analysis of mixtures of radioactive isotopes by mass spectrograph are described. The following mass assignments are made: 108-day yttrium, 88; 57-day yttrium, 91; 1-year ruthenium, 106; 300-day cerium, 144; 3.7-year element 61, 147; 55-day strontium, 89; 25-year strontium, 90; 60-hour yttrium, 90; 12.6-day barium, 140; 40-hour lanthanum, 140.

1. INTRODUCTION

THE phenomenon of fission gave rise to a great number of new radioactive isotopes that had not been previously observed. Many could be identified from the fact that most occurred in "chains," a sequence of beta-emitting isotopes of the same mass leading to a stable isotope. However, among the one hundred and fifty new radioactive isotopes many could not be so identified, and the question arose whether the masses of these new isotopes could be determined by the mass spectrograph.

In early experiments, a 4-mg sample of uranium with a quarter of a millicurie activity due to the fission products formed in it by the Clinton pile was analyzed with a spark source and a double focusing mass spectrograph, and gave a radioactive deposit on a photographic plate in the fission mass range whose beta-rays could be observed with a counter.[1] However, only one in 10 or 100 million of the active isotopes was collected, and attempts were made to find more efficient ion sources. Blewett and Jones[2] in 1936 had observed ion emission from the heated oxides of Sr, Ba, Y, and Cs, elements in the fission product range, and experiments by Lewis, Hayden, King, and Garrison[3] confirmed these results and extended the list to include the oxides of columbium, lanthanum, praseodymium, and neodymium. In the case of lanthanum it was found that 16 percent of the molecules that are evaporated from a tungsten filament appear as positively charged oxide ions, and since about one in fifty of the ions formed appear in the analyzed deposit, we obtained in the analyzed deposit one out of 300 of the original radioactive isotopes. That many rare earth oxides are good ion emitters was a welcome discovery, as the opposite was suggested by Dr. Aston's experience with hot anodes made from the bromides of these elements. He obtained very weak rays and was able to photograph only the stronger stable isotopes. If the yield is as much as one atom deposited for 1000 atoms evaporated from the source, a source with only one microcurie of radioactivity will give a deposit with 2000 counts/minute, which is ample for detecting the active isotopes, and even identifying their half-lives. However, if the yield is only 1 in 10^8, as with the spark source, 20 counts/minute from the deposit would require a millicurie of activity in the source and this amount requires special shielding and precautions in handling.

The instrument used for the analyses reported in the paper will be described in detail elsewhere.[4] The ions were produced by heating the oxides of the active fission products on a tungsten filament and analyzing by a magnetic field. The ions were collected on photographic plates, and after identifying the active isotopes as explained below, the plates were developed to provide the mass scale. Thus the position of the active lines could be obtained by comparison with the normal spectrum. Measurements for fission activities were simpler than for isotopes made by (n,γ) reactions because the former could be obtained carrier-free and in high concentration, whereas the (n,γ) active atoms were usually

* Now at University of Chicago.
[1] A. J. Dempster, CP-1507, p. 25, March, 1944.
[2] J. P. Blewett and E. J. Jones, Phys. Rev. **50**, 464 (1936).
[3] Lewis, Garrison, King, and Hayden, CP-2122, August 5, 1944.
[4] Lloyd G. Lewis and Richard J. Hayden, Rev. Sci. Inst. (to be published).

only a very small fraction of the total sample. Measurements for various fission products are described below.

2. ION SOURCE CHARACTERISTICS

The ion source in the spectrograph was a 0.001-in. by 0.030-in. tungsten ribbon, about ½-in. long. This filament could be removed for loading through a ground glass joint. Samples contained in solutions were placed on the filament from calibrated micropipettes and then were evaporated to dryness in air. To produce the ions the filament was heated by a 6.3-volt transformer. Many of the materials tested emitted ions other than those of the metallic element. In general, the emission from nitrates or oxides of elements of normal valence one or two was, when emission occurred, of the form R^+. Emission from nitrates or oxides of elements of normal valence three or four was of the form RO^+. No multiply charged ions were observed. Table I gives the types of ions emitted by various compounds. Care must be taken to avoid confusing compound ions with atomic ions. For example, the compound ion $NaKCl^+$ gives masses at 97 and 99 which may easily be misinterpreted.

A tungsten filament was chosen as the ion source for this radioactive work because, although it does not give ions of all elements, it is usually more efficient (i.e., gave a larger ratio of ions given off to molecules given off) for the elements with which it could be used than were other ion sources. Thus smaller samples could be used. A list of ionization efficiencies for various compounds is given in Table II. Of every 50 ions formed by the filament one reached the photographic plate. Thus the percentages given in Table I must be multiplied by 0.02 to give the over-all efficiency of the spectrograph for the compound in question.

The data which gave these ionization efficiencies were observed by placing a metallic ion collector, connected to a Dershem electrometer, in place of the photographic plate. Then, when ions of a single mass were being emitted from the filament, the ratio of the current to a grounded diaphragm which defined the ion beam to the current to the electrometer was the factor of fifty previously mentioned. Thus,

TABLE I. Types of ionic emission.

Compound	Types of Ions
NaCl	Na^+, Na_2Cl^+
KCl	K^+, K_2Cl^+
NaCl+KCl	Na^+, K^+, Na_2Cl^+, K_2Cl^+, $NaKCl^+$
$Ba(NO_3)_2$	Ba^+
$Sr(NO_3)_2$	Sr^+
$Ca(NO_3)_2$	Ca^+
$Y(NO_3)_3$	YO^+
ZrO_2	ZrO^+
$RuCl_3$, $Ru(NO_3)_3$	Ru^+
$RhCl_3$	Rh^+
$La(NO_3)_3$	LaO^+
$Ce(NO_3)_3$	CeO^+
$Pr(NO_3)_3$	PrO^+
$Nd(NO_3)_3$	Nd^+(~1%); NdO^+(~99%)
$61(NO_3)_3$	61^+(~5%); $61O^+$(~95%)
$Sm(NO_3)_3$	Sm^+(~60%); SmO^+(~40%)
$Eu(NO_3)_3$	Eu^+
$Gd(NO_3)_3$	Gd^+(~40%); GdO^+(~60%)
U_3O_8	U^+, UO^+, UO_2^+

when a known number of molecules was placed on the filament, and when, after heating the filament, the voltage across the capacity in parallel with the electrometer was observed, the over-all efficiency of the spectrograph was calculated. Two successive runs with the same filament and the same size samples which were heated in the same manner always gave over-all efficiencies which were within 20 percent of each other. Measurements of memory in the filament indicated that in every case less than 5 percent of the sample remained on the filament after heating. With use a given filament became more efficient in the formation of ions. For example, one filament, which was used for more than fifty samples began by giving 0.5 percent ionization efficiency for $Nd(NO_3)_3$ and ended by giving 1 percent ionization efficiency. The ionization efficiencies in Table I were measured with frequent checking of the $Nd(NO_3)_3$ efficiency. Only values obtained when the $Nd(NO_3)_3$ efficiency was 1 percent were used. The ionization efficiency seemed independent of the size of the sample so long as the amount of material on the filament was small (roughly, less than 100 micrograms). This was checked with the electrometer method for $Nd(NO_3)_3$ by using different size samples, and was verified for many other compounds by counting plates after a known activity was placed on the filament. The efficiency of $61(NO_3)_3$ was obtained only in this manner. It was found that heating the filament

TABLE II. Ionization efficiencies.

Compound	Ionization Efficiency (%)
$Ba(NO_3)_2$	0.02
$Sr(NO_3)_2$	0.08
$Y(NO_3)_3$	0.025
$La(NO_3)_3$	16.
$Ce(NO_3)_3$	0.12
$Pr(NO_3)_3$	12.
$Nd(NO_3)_3$	1.
$61(NO_3)_3$	0.5
$Sm(NO_3)_3$	0.16
$Eu(NO_3)_3$	0.16
$Gd(NO_3)_3$	0.05
U_3O_8	0.008
$RuCl_3$, $Ru(NO_3)_3$	0.01
$RhCl_3$	0.005

rapidly so as to obtain a short, intense burst of ions was, by as much as a factor of four, less efficient than slowly raising the filament temperature. The above measurements were made by adjusting the filament current so as to keep the positive ion current constant at 0.05 microampere.

3. METHODS OF ANALYSIS

Two general methods were used to determine the mass of an active isotope after its ions had been deposited on the photographic plate. In the first method the radioactive material and also an inactive compound which would give a mass spectrum in the mass range of the active isotope were placed on the filament. After the spectrograph was run, the plate was removed and, before being developed, was placed under a Geiger counter tube which, except for an adjustable slit, was shielded from the plate by $\frac{1}{8}$ in. of lead. By observing the counting rate with different portions of the plate next to the slit, the activity was plotted as a function of the distance from the end of the plate. Thus the position of the radioactive line was determined. After this was done the plate was developed to give the standard mass spectrum. Knowing the position of the active isotope, the position of known masses, and the dispersion, the mass of the active isotope was calculated. The standard mass spectrum was necessary because, due to the hysteresis in the magnetic circuit, the same current through the magnet coils did not always give the same magnetic induction in the gap. Thus a knowledge of the position of a line on the plate, the accelerating voltage, and the current through the magnet coils was not sufficient to determine the mass number corresponding to that line.

In the second method the loading of the sample and exposure of the plate were made as in the first. When the plate was removed from the spectrograph, it was placed face to face with an unexposed plate and left in this position for a time calculated to be long enough for the beta- or gamma-rays from the deposit to give developable lines on both plates. The plates were then developed. The lines on the transfer plate showed that corresponding lines on the original plate were due, at least in part, to a radioactive deposit. This, together with the known mass spectrum, determined the mass numbers at which the active isotopes were located. The photographic plates used were Eastman III-O spectroscopic plates. To produce a developable line (about 0.2 mm by 1 cm) on one of these plates roughly 10^{10} mass 100 to 150, 8000 volt positive ions or 10^6 1-Mev gamma-rays or 10^5 beta-rays were needed. Dependence of blackening on energy and mass of particles was not studied. The counter method was more sensitive if the half-life of the isotope was less than twelve hours; the plate method was more sensitive if the half-life was greater than twelve hours.

In cases where two or more activities which could not be separated were present in the original sample, a half-life determination of the activity on each line of the plate was desirable. In cases where high activity was deposited on the plate, this was accomplished by watching the decay of a given line. In addition, relative half-lives (i.e., which of two activities had the longer half-life) were obtained by taking successive transfer plates from a given plate and observing the change in the relative darkening of the lines in question.

4. MASS DETERMINATIONS

108-Day Yttrium

A 108-day isotope of yttrium was first produced by Dubridge and Marshall[5] by a (p,n)

[5] L. A. Dubridge and J. Marshall, Phys. Rev. **57**, 348 (1940).

reaction on strontium. Later[6] it was produced by $(n,2n)$ on yttrium. This isotope decays by K capture and accompanying emission to stable Sr. Gamma-rays of 0.908 Mev and 1.89 Mev have been observed.[7] Formation of this isotope by (p,n)(or $d,2n$ as was later done) reaction on strontium states only that its mass must be 84, 86, 87, or 88. Formation by fast neutron bombardment establishes the mass at 88 only if the production of two neutrons is assumed. Thus, though the previous assignment of the isotope to mass 88 seemed well founded a direct measurement was made.

About 10 mC of 108-day yttrium, obtained from Paul Tompkins at Clinton Laboratory, and 3 micrograms of normal Y_2O_3, both in nitric acid solution, were placed on the filament. After the run the plate transfer technique was used and a twelve-hour transfer was made. Upon development the original plate showed two lines one mass number apart, and the transfer plate showed one line which corresponded to the lower mass line on the original plate. Therefore the higher mass line was the normal $Y^{89}O^+$, and the active line one mass unit lighter was $Y^{88}O^+$. Thus the mass of the 108-day yttrium isotope is 88.

57-Day Yttrium

A 57-day yttrium activity was first observed by Hahn and Strassman[8] who observed this activity among uranium fission products and made chemical identification of the element. Later work on the Manhattan Project[9] showed the emitted beta-particles to have a maximum energy of 1.53 Mev. No accompanying gamma-radiation was observed.[10] Since this activity had been observed only in fission, determination of the mass by formation by known reactions was never accomplished. The fact that the fission yield of this isotope was near the top of the lower fission yield maximum made this type of mass assignment unreliable.

About 8 microcuries of 57-day yttrium, separated from other fission products by Waldo Cohn at the Clinton Laboratories, 3 micrograms of normal Y_2O_3, and 1 microgram of normal SrO, all in nitric acid solution, were placed on the filament. After the run an activity of 33 counts/minute above background at about 50 percent geometry was found on the plate. The position of this activity was located with the counter-slit technique and a scratch was made on the edge of the plate to indicate the position of the activity. After fifty-six hours the plate was developed. It showed lines of masses 86, 87, and 88 (the Sr^+ lines), a line at 105 (the $Y^{89}O^+$ line), and a line at 107. The line at 107 corresponded in position to the scratch on the edge of the plate. It, therefore, was the radioactive line $Y^{91}O^+$. Thus the mass of the 57-day yttrium isotope is 91.

1-Year Ruthenium

One-year ruthenium from fission was first observed by Glendenin.[11] It emits only a very weak beta, decaying to 30-sec. rhodium. This rhodium daughter emits 2.8-Mev and 3.9-Mev betas and 0.3-Mev and 0.8-Mev gamma-rays. It is by this daughter that the ruthenium is usually detected. Steinberg[12] found the fission yield for this isotope to be 0.48 percent and on this basis placed one-year ruthenium at mass 106. Direct measurement by the mass spectrograph has led to the same result.

About 5 microcuries of 1-year ruthenium, separated from a two-year-old fission product mixture by Mr. Robert Schumann of the Metallurgical Laboratory, and 50 micrograms of normal ruthenium, both in hydrochloric acid solution, were placed on the filament. After the run, the plate transfer technique was used and a six-day transfer made. Upon development the original plate showed the normal ruthenium spectrum and also a line at mass 106, two mass numbers above the heaviest normal isotope. The transfer plate showed one line, corresponding to the line at 106. Thus the mass of the 1-year ruthenium isotope is 106.

300-Day Cerium

In a separation of cerium from a fission product mixture which is made a few days after

[6] A. C. Helmholz, Phys. Rev. **62**, 301 (1942).
[7] Downing, Deutsch, and Roberts, Phys. Rev. **60**, 470 (1941).
[8] O. Hahn and F. Strassman, Naturwiss. **28**, 543 (1940).
[9] P. W. Levy, MonP-104, p. 13, April, 1946.
[10] N. E. Ballou, CC-298-D, p. 3, October, 1942.
[11] L. E. Glendenin, Plutonium Project Report, Vol. 9B, 7.18.3.
[12] E. P. Steinberg, CC-2310, p. 106, January, 1945.

irradiation, only two active cerium isotopes should be present in appreciable quantity. These are the 28-day cerium discovered by Pool and Kurbatov,[13] and investigated in fission by Burgus;[14] and the 300-day cerium activity.[15] The 28-day isotope emits a 0.65-Mev beta and a 0.2-Mev gamma,[13] and was known to decay to stable praseodymium. Since praseodymium has only one known stable isotope at mass 141, this was very strong evidence for the assignment of 48-day cerium to mass 141. The 300-day cerium isotope emits a 3.07-Mev beta and a 0.135-Mev gamma.[16] It has been formed only in fission. On the basis of a fission yield of 5.3 percent measured by Rubinson[17] it was assigned to mass 144. Direct measurement gave masses 141 and 144 for these isotopes.

Two hundred and fifty microcuries of fission product cerium, separated from a fission product mixture by Waldo Cohn at Clinton Laboratories, together with 0.3 microgram of normal Nd_2O_3, both in nitric acid solution, were placed on the filament. After the run a transfer plate was made and both transfer and original plate were developed. This showed that there were activities on the plate at masses 157, 159, 160, and 163. Another run was then made, this time using an exposed x-ray film as an ion collector. Five minutes after the run the film was counted and a counting rate of 15,000 counts/minute was observed. The film was then placed against an unexposed photographic plate for twenty minutes. This plate was then developed and showed one line; this served to locate the major activity on the film. Two cuts were then made across the film, each 0.5 mm from the position corresponding to the line. The 1-mm wide center section was counted and the decay observed. The half-life for the short-lived activity was 17.5 ± 0.5 min. Thus the short-lived activity on the plate, the activity which produced the blackening on the twenty-minute transfer plate, was seen to be due to the previously observed 17-minute praseodymium[7] which was known to be a beta-decay daughter of the 300-day cerium. After the praseodymium and the cerium came to equilibrium on the film, the three sections of the film were placed together in their original position and a two-day transfer made. Again the four lines appeared, and the 1-mm strip, with the 300-day cerium, corresponded to the second heaviest of the masses, the one which was identified in the first exposure as 160. Since both praseodymium and cerium ionize with oxygen atoms attached, the mass of 300-day cerium and of 17-minute praseodymium is 144. After the last transfer was taken, the film was cut so that one active line was on each piece of the film. An attempt was made to determine the half-life of each of the activities; but, due to the instability with time of the counter used and due to the scattering of $Ce^{144}O^+$ over the plate, only rough limits could be set. These results were: 157 (40d); 159 (30d); 160 (300 ± 50d); 163 (−). These half-life limits are consistent with an assignment of the mass 157 line to 28-day Ce^{141} with oxygen attached and the mass 159 line to 14-day Pr^{143} with oxygen attached.[18] This sample told nothing of the mass 163 activity except that there was a relatively long-lived fission activity of mass 147. The nature of this activity is described below.

3.7-Year Element 61

A long-lived isotope of element 61 was discovered in fission by Ballou.[19] Seiler and Winsberg[20] give its half-life as 3.7 yr. Marinsky and Glendenin[21] observed its radiation and by aluminum absorption curves gave the maximum energy as 0.20 Mev. They observed no accompanying gamma-radiation. Because this isotope was so long-lived and because of the known masses of the shielding neodymium isotopes, the mass of this isotope was very certainly either 147 or 149. Direct measurement decided in favor of 147.

About 2 microcuries of 3.7-year element 61, separated by resinous column from other fission activities by Glendenin and Marinsky at Clinton

[13] M. L. Pool and J. D. Kurbatov, Phys. Rev. **63**, 463 (1943).
[14] W. H. Burgus, CC-465B, p. 13, February, 1943.
[15] W. H. Burgus, CC-2310, p. 210, January, 1945.
[16] V. A. Nedzel, CC-2283, October, 1944.
[17] W. Rubinson, Plutonium Project Report, Vol. 9B, 7.52.1.
[18] N. E. Ballou, CC-298-D, p. 3, October, 1942.
[19] N. E. Ballou, CC-680, p. 22, May, 1943.
[20] J. A. Seiler and L. Winsberg, Plutonium Project Report, Vol. 9B, 7.54.2.
[21] J. A. Marinsky and L. E. Glendenin, Plutonium Project Report, Vol. 9B, 7.54.1.

Laboratories, together with a 0.3 microgram sample of normal Nd_2O_3, both in nitric acid solution, were placed on the filament. After the run a transfer was made; and, after eighteen hours, both plates were developed. The original plate showed the NdO^+ spectrum (158, 159, 160, 161, 162, 164, and 166), and also a line at 163. This last line corresponded to the single line on the transfer plate. Thus this blackening was due to the $61^{147}O^+$, and the mass of 3.7-year element 61 is 147. Evidently this was the 147 activity observed in the cerium sample.

55-Day Strontium[22]

Four microcuries of 55-day strontium separated from fission products by Mr. Waldo Cohn of the Clinton Laboratories in the form $SrCl_2$, together with 5×10^{-4} ml of $16N$ HNO_3 and 5×10^{-4} ml of $0.1N$ inactive $Sr(NO_3)_2$ solution, were placed on the filament. After running the spectrograph, the plate was placed in a slit counter and moved until a maximum count was obtained. A scratch was made on the plate at the position of maximum activity. Development of the plate showed this scratch to be located one mass unit above the Sr^{88} line, heaviest of the normal strontium isotopes. Thus the mass of 55-day strontium is 89.

25-Year Strontium[23]

A strontium sample was allowed to stand for approximately a year after separation from a fission product mixture. After this length of time the activity in the sample was primarily that of the 25-year strontium and its 60-hr yttrium daughter. Twenty microcuries of this activity in nitrate solution were placed on the filament. After running the spectrograph approximately 250 counts/minute were observed on the plate. After a two-day transfer, lines were observed at masses 89, 90, and 106. The first of these was attributed to the previously discussed Sr^{89} which had not completely decayed from the sample. The other two lines can be attributed to Sr^{90+} and $Y^{90}O^+$, respectively. Three other successive transfers were made and showed the activity at mass 106 to decay at a rate consistent with the known 60-hr. half-life of yttrium. This shows that the 25-year strontium and the 60-hr. yttrium both have mass 90.

40-Hr. Lanthanum and 12.8-Day Barium[24]

Normal barium and about 20 microcuries of barium-lanthanum activity were placed on the filament of the spectrograph. After the run 1500 counts/minute were observed on the photographic plate. This activity was shown by the slit counter to be all at one position on the plate. The decay of this activity with time was observed through the slit counter. The activity observed was the 40-hr. lanthanum and not the 12.5-day barium. This is an expected result because La_2O_3 is ionized much more efficiently by the filament than is BaO. After the decay of the 40-hr. activity had been observed for a period long enough to establish the half-life, the plate was placed against a transfer plate to check the position of the activity. Development of the original plate showed the normal Ba^+ spectrum at masses 134, 135, 136, 137, and 138, and also another line at 156. This 156 line corresponded to the activity as located both by the slit counter and the photographic plate. Since lanthanum oxide is known to emit only ions of the form LaO^+, this line at mass 156 must be due to $La^{140}O^+$ and thus the mass of 40-hr. lanthanum and hence, also, of the daughter 12.8-day barium is 140.

The author wishes to acknowledge his indebtedness to Dr. A. J. Dempster for encouragement and helpful suggestions throughout the work and to Dr. L. G. Lewis, with whom the author was associated in the performance of certain of the mass analyses and with whom he worked on the design and construction of the mass spectrograph.

[22] Stewart, Lawson, and Cork, Phys. Rev. **52**, 901 (1937).
[23] Hahn, Strassman, and Gotte, Abhandl. Preuss. Akad. Wiss., Math.-Naturw. Klasse No. 3 (1942).
[24] O. Hahn and F. Strassman, Naturwiss. **28**, 543 (1940).

PHYSICAL REVIEW VOLUME 74, NUMBER 6 SEPTEMBER 15, 1948

Some Effects of the Intrinsic Magnetic Moment of the Electron

G. BREIT
Yale University, New Haven, Connecticut*
(Received June 3, 1948)

Effects of the magnetic moment of the electron of the six-vector type are calculated. According to the hypothesis followed here, the electron's behavior in the field of a nucleus is described only approximately as that of a point charge. More accurately, it behaves as a particle having mainly the properties of a point charge which are corrected by the addition of a small "intrinsic" magnetic moment. In the present note the purely empirical point of view of an intrinsic magnetic moment is followed without any attempt at a justification from the point of view of quantum electrodynamics which has been given by Schwinger. Formulas are worked out for the effect on hyperfine structure, on the Landé g factor and the contribution to the Lamb-Retherford line shift. The arrangement of the calculations is such as to have the same system for the ordinary hyperfine structure and the other effects. The finite rather than zero size of the nuclear current system is explicitly included in the formulas.

I. INTRODUCTION

THE measurements of the hyperfine structure of hydrogen and deuterium in its ground state made by Nafe, Nelson, and Rabi[1] disagreed with theoretical prediction.[2] The observed energy difference of hyperfine structure levels $h\nu$ appeared to be too large for both isotopes, and the ratio of the energy difference of the lighter to that of the heavier isotope also appeared to be too large in comparison with theory. Part of the latter effect has disappeared as a result of refinements in experimental precision. The remainder of this effect has been explained by A. Bohr[3] as a result of the centering of the electron's wave function on the proton within the deuteron. Unpublished attempts by the writer to explain the factor ~ 1.0024 by which both ν_H and ν_D exceed theoretical prediction were made during the summer of 1947 on the basis of the distortion of electronic wave functions by the magnetic field of nuclear moments. These were not successful and suggested that any explanation having to do with nuclear properties would be likely to be a forced one because it could not reproduce in a simple way the close equality of fractional discrepancy for H and D. It was natural to look for an explanation in an incomplete understanding of the nature of the electron. This point of view makes the discrepancy between theory and experiment automatically the same for H and D. Since the magnetic moment of the electron in Dirac's theory is the result of the Schroedinger vibratory motion of a point charge and since there are reasons for doubting the exact validity of ordinary space-time concepts, it appeared reasonable to question the exact relationship between the effective magnetic moment and the fundamental constants. It appeared, on the other hand, that it would be safest to make the modification in the theory so as to have a relativistically covariant answer. Pauli's investigation[4] of covariant forms pointed to the interaction energy having the form of Eq. (1) of the next section and it was proposed[5] to consider the possibility of the addition to the Hamiltonian of an interaction energy of the Pauli type. The order of magnitude of the intrinsic Pauli type moment μ_e required by experiment appeared to be a reasonable one because μ_e/μ_0 turned out to be of the order α where μ_0 is the Bohr magneton. In a reference system moving with a velocity close to the velocity of light c the Bohr magneton μ_0 appears as an electric moment equivalent to displacing a charge e through a distance $\hbar/2mc$. A limitation in the validity of space time concepts of the order e^2/mc^2 could conceivably result in a modification of the length $h/2mc$ by the amount e^2/mc^2 and introduce a relative uncer-

* Assisted by Contract N6ori-44, Task Order XVI of the Office of Naval Research.
[1] J. E. Nafe, E. B. Nelson, and I. I. Rabi, Phys. Rev. **71**, 914 (1947).
[2] E. Fermi, Zeits. f. Physik **60**, 320 (1930); G. Breit, Phys. Rev. **35**, 1447 (1930). The relativistic corrections of the latter paper are too small to account for the observed discrepancy.
[3] A. Bohr, Phys. Rev. **73**, 1109 (1948). The writer would like to thank to Dr. Bohr for letting him see the manuscript of this paper before publication.
[4] W. Pauli, *Handbuck der Physik* (Verlag Julius Springer, Berlin, 1933), Vol. 24/1, p. 211.
[5] G. Breit, Phys. Rev. **72**, 984 (1947).

tainty of the order $(e^2/mc^2)/(\hbar/mc)=\alpha$ into the value of the moment.

The writer's first publication contained an error[6] in the evaluation of the expected contribution to the hyperfine splitting of s terms which exaggerated the other expected effects. Among the effects of the moment μ_e which were listed[5] there was mentioned the possibility of finding a characteristic deviation from the Landé g formula. It was noticed by Rabi that this possibility was especially suitable for experimental test and as a result the effect of μ_e was found by Kusch and Foley.[7] Soon after the writer became aware of the development by Schwinger of an improved quantum electrodynamics which predicts $\mu_e/\mu_0=-\alpha/2\pi$ and a more detailed publication appeared to be unwarranted at the time.

In reviewing the calculations which led to the first publication it appeared that there might be considerable work involved in reproducing them or in developing abridged methods. The present note has been, therefore, prepared even though the more vital physical questions involved have in the meanwhile been treated more deeply by others and especially by Schwinger. It contains formulas for the effects of μ_e and compares the effects with those of ordinary hyperfine structure allowing for some of the effects of finite nuclear dimensions. A brief comparison with experimental results is also included.

II. THE INTERACTION ENERGY

The Hamiltonian is taken to be

$$H=-eA_0-c\boldsymbol{\alpha}(\mathbf{p}+e\mathbf{A}/c)-\beta mc^2 +\mu_e[\rho_3(\mathcal{H}\boldsymbol{\sigma})-\rho_2(\mathcal{E}\boldsymbol{\sigma})] \quad (1)$$

in the original Dirac notation, with β standing for Dirac's α_4. The matrices σ_x, σ_y, σ_z are the four-row square matrices. The externally applied electric and magnetic fields are $\mathcal{E}$, $\mathcal{H}$. The Pauli part of the electron's moment is μ_e. The nucleus is considered to be fixed in position. Its magnetic field is taken to be produced by a current system distributed through a volume which is supposed to give rise to a magnetic field

$$\mathcal{H}=[\nabla(\boldsymbol{\mu}_N\nabla)-\boldsymbol{\mu}_N\Delta]u=\operatorname{curl}[\nabla u\times\boldsymbol{\mu}_N], \quad (1.1)$$

where

$$u\sim 1/r. \quad (1.2)$$

Here r is the distance from the center and the asymptotic form for u is supposed to apply for large r. The nuclear magnetic moment is μ_N. The vector potential due to the nucleus is

$$\mathbf{A}_N=[\nabla u\times\boldsymbol{\mu}_N], \quad (1.3)$$

as is seen from Eq. (1.1). According to Eqs. (1.2), (1.3), this vector potential approaches asymptotically that of a magnetic dipole μ_N for any function u which has asymptotically the same gradient as $1/r$. For such u

$$\mathbf{A}_N\sim[\boldsymbol{\mu}_N\times\mathbf{r}]/r^3, \quad (1.3')$$

which is the vector potential of a dipole μ_N. The same is clear from the first expression for $\mathcal{H}$ in Eq. (1.1) according to which

$$\mathcal{H}\sim\nabla(\boldsymbol{\mu}_N\nabla)(1/r), \quad (1.3'')$$

which is directly related to the picture of a dipole as two coincident poles. The validity of this representation does not depend on whether u is assumed to be spherically symmetric or not. It will be assumed that Δu is finite and differentiable as well as continuous everywhere. In this representation the nuclear current density is

$$\mathbf{J}=(c/4\pi)[\boldsymbol{\mu}_N\times\nabla(\Delta u)], \quad (1.3''')$$

and is finite everywhere. For this type of current density one has

$$\operatorname{div}\mathbf{J}=0.$$

If instead of ∇u one had an arbitrary vector in Eq. (1.3) the divergence of the current would not necessarily be zero.

In the special case of

$$u=-r^2/2a^3+3/2a \quad (r<a)$$
$$=1/r \quad (r>a)$$

the current distribution becomes a spherical current sheet on a sphere of radius a and the magnetic field inside the sphere is then $2\boldsymbol{\mu}_N/a^3$. In this case $-\boldsymbol{\mu}_N\Delta u=3\boldsymbol{\mu}_N/a^3$ for $r<a$ and 0 for $r>a$. It has a discontinuity at $r=a$. On the surface of the sphere the current density integrated through the thickness of the sphere is $(3c/4\pi)[\boldsymbol{\mu}_N\times\mathbf{r}]/a^4$. This corresponds to the change of $\Delta u=-3/a^3$ inside the sphere to $\Delta u=0$ outside which gives in the integration of Eq. (1.3'') through the sphere

[6] Julian Schwinger, Phys. Rev. **73**, 415 (1948); G. Breit, Phys. Rev. **73**, 1410, (1948).
[7] P. Kusch and H. M. Foley, Phys. Rev. **72**, 1256 (1947).

thickness the value $3\mathbf{r}/a^4$ for the second factor of the vector product. In this special case Δu has a discontinuity at $r=a$. This case can be considered as the limit of a continuous u and discontinuous $\mathcal{K}$. It is mentioned so as to add concreteness to the meaning of u. In particular, Δu, when integrated through the volume inside the sphere, gives -4π and Δu has a constant value inside the sphere. On account of Eq. (1.2) and Gauss' theorem the integral over-all space is -4π also in the general case.

The interaction energy arising from effects other than the electrostatic energy will be broken up into a sum of three parts.

$$H'=-e(\boldsymbol{\alpha}\mathbf{A}),\quad H''=\mu_e\rho_3(\mathcal{K}\boldsymbol{\sigma}),\quad H'''=-\mu_e\rho_2(\mathcal{E}\boldsymbol{\sigma}). \tag{1.4}$$

The energy H' enters standard discussions of hyperfine structure. For H'' one has

$$H''=\mu_e\rho_3[(\boldsymbol{\sigma}\nabla)(\boldsymbol{\mu}_N\nabla)-(\boldsymbol{\sigma}\boldsymbol{\mu}_N)\Delta]u. \tag{1.5}$$

Denoting the nuclear spin by $\mathbf{I}$, the nuclear spin quantum number by I and the absolute value of $\boldsymbol{\mu}_N$ by μ_N one has

$$\boldsymbol{\mu}_N=\mu_N\mathbf{I}/I \tag{1.51}$$

and

$$H''=(\mathbf{B}''\mathbf{I}), \tag{1.52}$$

where

$$\mathbf{B}''=(\mu_e\mu_N/I)\rho_3[(\boldsymbol{\sigma}\nabla)\nabla-\boldsymbol{\sigma}\Delta]u. \tag{1.53}$$

For a spherically symmetric u

$$\mathbf{B}''=\frac{\mu_e\mu_N}{I}\left\{\left[-\boldsymbol{\sigma}+\frac{\mathbf{r}}{r}\left(\frac{\mathbf{r}}{r}\boldsymbol{\sigma}\right)\right]\Delta u+\left[\boldsymbol{\sigma}-3\frac{\mathbf{r}}{r}\left(\frac{\mathbf{r}}{r}\boldsymbol{\sigma}\right)\right]\frac{u'}{r}\right\}\rho_3. \tag{1.54}$$

The diagonal matrix elements of H'' for hyperfine structure levels of quantum number F are obtained as

$$\Delta E''=\tfrac{1}{2}[F(F+1)-J(J+1)-I(I+1)]\times(\mathbf{B}''\mathbf{J})_J/J(J+1), \tag{1.55}$$

where $\mathbf{J}$ is the operator representing the electronic angular momentum and J is the inner quantum number so that $J(J+1)$ are the characteristic values of $\mathbf{J}^2$. The quantity $(\mathbf{B}''\mathbf{J})_J$ is the diagonal element of $\mathbf{B}''\mathbf{J}$ in the J representation. In the evaluation of this matrix element one needs to know the matrix elements of products of $\mathbf{J}$ with $U\mathbf{r}(\mathbf{r}\boldsymbol{\sigma})r^{-2}\rho_3$ where U can be either Δu or u'/r. For its evaluation as well as that of other quantities it is convenient to use the radial functions f, g for which the radial equations are

$$\begin{cases}(p_0+mc)f-\hbar[dg/dr+(1+k)g/r]=0\\(p_0-mc)g+\hbar[df/dr+(1-k)f/r]=0.\end{cases} \tag{1.6}$$

The Dirac matrix

$$\epsilon=(\boldsymbol{\alpha}\mathbf{r})/r \tag{1.61}$$

corresponds in terms of these wave functions to the multiplication rule

$$\epsilon\begin{pmatrix}f\\g\end{pmatrix}=\begin{pmatrix}0&-i\\i&0\end{pmatrix}\begin{pmatrix}f\\g\end{pmatrix}=\begin{pmatrix}-i&g\\i&f\end{pmatrix} \tag{1.62}$$

as has been shown by Dirac.[8] This rule means that $\epsilon\psi$ is obtained from ψ by changing the f into $-ig$ and the g into if. In the representation which corresponds to Eq. (1.6) the matrix ρ_3 is diagonal and has diagonal elements 1, 1, -1, -1 in ascending order of μ in ψ_μ. When operating on the two-row-column matrix having f, g as its elements the operator ρ_3 leaves f unchanged and changes g into $-g$. Its effect amounts to a change of sign of g^2 in the final expression. For the calculation of matrix elements of

$$U(\mathbf{Jr})(\mathbf{r}\boldsymbol{\sigma})r^{-2}\rho_3, \tag{1.63}$$

one has

$$(\mathbf{r}\boldsymbol{\sigma})/r=\rho_1\epsilon, \tag{1.64}$$

and hence

$$(\mathbf{Jr})(\mathbf{r}\boldsymbol{\sigma})r^{-2}=(\mathbf{Lr})(\mathbf{r}\boldsymbol{\sigma})r^{-2}+\tfrac{1}{2}(\mathbf{r}\boldsymbol{\sigma})^2r^{-2}=\tfrac{1}{2}(\rho_1\epsilon)^2=\tfrac{1}{2}. \tag{1.65}$$

It follows that

$$(\psi,\ U(\mathbf{Jr})(\mathbf{r}\boldsymbol{\sigma})r^{-2}\rho_3\psi)=\tfrac{1}{2}\int_0^\infty(f^2-g^2)\,Ur^2dr, \tag{1.66}$$

where the normalization is such that

$$\int_0^\infty(f^2+g^2)r^2dr=1. \tag{1.67}$$

In the result of substituting Eq. (1.54) into Eq. (1.55) there occur, besides, terms of the type

$$U(\boldsymbol{\sigma}\mathbf{J})\rho_3. \tag{1.7}$$

Their evaluation brings in Dirac's quantum num-

[8] P. A. M. Dirac, Proc. Roy. Soc. **A118**, 351 (1928). In accordance with later custom the symbol j of Dirac's article is called k in the present paper.

ber k which is an eigenvalue of the operator

$$k=\rho_3[(\mathbf{L}\boldsymbol{\sigma})+1]. \tag{1.71}$$

One has

$$(\boldsymbol{\sigma}\mathbf{J})=\boldsymbol{\sigma}\mathbf{L}+\tfrac{3}{2} \tag{1.72}$$

and hence according to Eq. (1.71)

$$(\boldsymbol{\sigma}\mathbf{J})\rho_3=\tfrac{3}{2}\rho_3+k-\rho_3=k+\tfrac{1}{2}\rho_3, \tag{1.73}$$

so that

$$(\psi,\ U(\boldsymbol{\sigma}\mathbf{J})\rho_3\psi)$$

$$=\int_0^\infty[(k+\tfrac{1}{2})f^2+(k-\tfrac{1}{2})g^2]r^2dr. \tag{1.74}$$

Combining Eqs. (1.54), (1.66), (1.74) one obtains

$$(\mathbf{B}''\mathbf{J})_J=\frac{\mu_e\mu_N}{I}\int_0^\infty\left\{-k(f^2+g^2)\left(\Delta u-\frac{u'}{r}\right)\right.$$

$$\left.+(g^2-f^2)\frac{u'}{r}\right\}r^2dr, \tag{1.75}$$

where $'$ denotes differentiation with respect to r. The terms in u' in this expression arose from corresponding terms in Eq. (1.54). For $u=1/r$ the part of H'' arising from these terms has the same form as the interaction energy between magnetic doublets $\boldsymbol{\mu}_N$, $\mu_e\boldsymbol{\sigma}$. There is present in addition a contribution in Δu. According to Eq. (1.3''') this quantity is confined to nuclear dimensions. For the current sheet considered right after Eq. (1.3'') the value of Δu was seen to be finite everywhere. There are clearly many types of volume distributions of current density for which Δu is finite. The example of the current sheet shows that at $r=0$ the quantity Δu is of the order $-3\langle a^{-3}\rangle$ where the average is taken over the nucleus and a is the radius of the elementary spherical current sheet into which the volume distribution is broken down. The value of Δu at $r=0$ is, therefore, not necessarily much larger than for the spherical current sheet. The functions f and g become infinite at $r=0$ for s terms. The integral of $(f^2+g^2)r^2dr$ converges. In view of the finiteness of Δu the integral of the term involving Δu in Eq. (1.75) converges also.

The results will be considered next for *light nuclei*, i.e., for the limit $Z=0$ where Z is the atomic number. For these nuclei the radial functions f, g differ from their non-relativistic approximations which are finite only in a narrow range of values close to $r=0$. In this case the term in Δu matters only for s terms. It contributes to the right side of Eq. (1.75) the amount

$$-(\mu_e\mu_N/I)g^2(0). \tag{1.8}$$

The function g is related to the non-relativistic Schroedinger function by

$$g^2=4\pi\psi_S^2,\quad (Z=0) \tag{1.81}$$

where subscript S stands for Schroedinger.

The quantity u'/r is $-1/r^3$ outside the nucleus. Inside the spherical current sheet it is $-1/a^3$ which is of the same order as Δu. The integral over the nuclear interior arising from $(u'/r)g^2$ is therefore comparable with that originating from $g^2\Delta u$. Neither of these is important except for s terms. For these, however, the combination $(1+k)g^2$ which occurs with u' vanishes because $k=-1$ for s terms. The integral of $-(1+k)f^2ru'dr$ does not vanish but since f/g is of order αZ it is much smaller than the corresponding contribution of Δu. The terms in u'/r are important, therefore, only for non-s terms. Neglecting the contribution of f^2 to these terms one obtains for their contribution

$$-(\mu_e\mu_N/I)(1+k)\langle r^{-3}\rangle. \tag{1.82}$$

Combining Eqs. (1.75), (1.8), (1.81), (1.82) one obtains the approximation

$$(\mathbf{B}''\mathbf{J})_J\cong(\mu_e\mu_N/I)\{-4\pi\psi_S^2(0)\delta_{L,0}$$

$$-(1+k)\langle r^{-3}\rangle\delta'_{L,0}\}, \tag{1.83}$$

where $\delta_{L,0}$ is the Kronecker δ and

$$\delta'_{L,0}=1-\delta_{L,0}. \tag{1.84}$$

The term H''' of Eq. (1.4) brings in the interaction which is expected in classical anology on account of the motion of $\boldsymbol{\mu}_e$ in the electric field of the nucleus. This field is

$$\mathcal{E}=Ze\mathbf{r}/r^3, \tag{1.9}$$

and one can express H''' as

$$H'''=-Ze\mu_e\rho_2(\mathbf{r}\boldsymbol{\sigma})/r^3=i\mu_eZe\rho_3\epsilon/r^2. \tag{1.91}$$

In accordance with Eq. (1.62) ϵ operates on f, g and

$$i\rho_3\epsilon=\begin{pmatrix}0 & 1\\ 1 & 0\end{pmatrix}. \tag{1.92}$$

One has thus

$$\langle H'''\rangle=(\psi,H'''\psi)=2\mu_eZe\int_0^\infty fgdr. \tag{1.93}$$

The interaction energy H' occurs in the ordinary theory of hyperfine structure. Since the current distribution is not ordinarily taken into account and since the ordinary way of deriving hyperfine structure formulas can be put into a neater form, a brief derivation of the formula for the expectation value of H' will now be sketched. According to Eqs. (1.3), (1.4) and similarly to Eq. (1.55), one has for the first-order perturbation effect of H'

$$E'=\tfrac{1}{2}[F(F+1)-J(J+1)-I(I+1)] \times(\mathbf{B}'\mathbf{J})_J/J(J+1), \quad (2)$$

where

$$\mathbf{B}'=(e\mu_N/I)u'[(\mathbf{r}/r)\times\boldsymbol{\alpha}], \quad (2.1)$$

and only the case of spherically symmetric u is under consideration. The quantity $(\mathbf{B}'\mathbf{J})_J$ is analogous to $(\mathbf{B}''\mathbf{J})_J$ of Eq. (1.55). Its evaluation can be made by noting that

$$\mathbf{J}[\mathbf{r}\times\boldsymbol{\sigma}]=\{(\mathbf{J}\boldsymbol{\sigma})(\boldsymbol{\sigma}\mathbf{r})-(\mathbf{J}\mathbf{r})\}/i, \quad (2.11)$$

as a consequence of multiplication rules for the components of $\boldsymbol{\sigma}$. Multiplying both sides of the above equation on the right by L_1/r one obtains

$$\mathbf{J}[(\mathbf{r}/r)\times\boldsymbol{\alpha}]=(\mathbf{J}\boldsymbol{\sigma})\epsilon/i-(\mathbf{J}\mathbf{r})/ir. \quad (2.12)$$

One also has the following identities

$$(\mathbf{J}\boldsymbol{\sigma})=\rho_3 k+\tfrac{1}{2}, \quad (2.13)$$

$$(\mathbf{J}\mathbf{r})/r=\tfrac{1}{2}\rho_1\epsilon. \quad (2.14)$$

Combining Eqs. (2.12), (2.13), (2.14) there follows

$$\mathbf{J}[(\mathbf{r}/r)\times\boldsymbol{\alpha}]=k\rho_3\epsilon/i. \quad (2.15)$$

The operator k commutes with both ϵ and ρ_3. For a state having a definite eigenvalue k the operator k amounts to multiplication by the c number k. Multiplication of such a state by the right side of Eq. (2.15) amounts, therefore, to multiplication by $\rho_3\epsilon/i$ followed by multiplication by the c number k. For operations on the f, g column matrix of Eq. (1.62)

$$\rho_3\epsilon/i=-\begin{pmatrix}0 & 1\\ 1 & 0\end{pmatrix}, \quad (2.16)$$

and hence, combining Eqs. (2.1), (2.12), (2.15), (2.16),

$$(\mathbf{B}'\mathbf{J})_J=2k(e\mu_N/I)\int_0^\infty fg(-u'r^2)dr. \quad (2.2)$$

For a nuclear current distribution concentrated at very small r the factor $(-u'r^2)$ is unity and one has the usual approximation[9]

$$(\mathbf{B}'\mathbf{J})_J\cong 2k(e\mu_N/I)\int_0^\infty fgdr; \quad (a=0). \quad (2.3)$$

In this limiting case the integral occurring in the expression for the hyperfine structure interval factor is the same as that for the effect of the nuclear electric field which occurs in Eq. (1.93). The latter should really be modified also because Eq. (1.9) does not take into account the finite—rather than zero—nuclear volume. This may be done in the approximation of a spherically symmetric charge distribution for which

$$\mathcal{E}=-Zerv'/r \quad (2.4)$$

corresponding to an electrostatic potential

$$Zev(r), \quad (2.5)$$

and a revised

$$\langle H'''\rangle=2\mu_e Ze\int_0^\infty fg(-v'r^2)dr. \quad (2.6)$$

For very concentrated charge distributions $-v'r^2=1$ and Eq. (1.93) is obtained again.

III. LIMIT OF SMALL Z AND SMALL NUCLEAR RADIUS

For a small nuclear radius and small Z the effect of μ_e on the hyperfine structure is given by Eqs. (1.55), (1.83). The effect of the interaction of $\mathcal{E}$ and μ_e is given by Eq. (1.93) which is the limiting form of Eq. (2.6) for small nuclear radius. The hyperfine structure arising from effects other than μ_e is obtained from Eqs. (2), (2.3). For Eqs. (1.93), (2.3) one must still make the approximations corresponding to small Z. These are obtained by means of the first Eq. (1.6) which gives

$$f\cong(\hbar/2mc)[dg/dr+(1+k)g/r]. \quad (3)$$

This approximation breaks down for small values of r if the Coulomb potential is supposed to be valid everywhere. The radial integrals involved are, however, familiar ones from the theory of hyperfine structure and it is known that they

[9] G. Breit, Phys. Rev. **38**, 463 (1931). The quantity referred to as B′ in the present paper is called A in reference 9.

may be approximated by neglecting the difference between p_0+mc and $2mc$ as is done in Eq. (3) and by identifying g with the Schroedinger radial function at small r where g is infinite. The reason why this procedure works is that the contribution to the radial integral of Eq. (2.3) which arises from the small range of values of r within which the approximations are poor is not significant and also because the two approximations have mutually compensating effects. The approximate value of the radial integral is

$$\int_0^\infty fgdr \cong (\hbar/2mc)\Big[-2\pi\psi_S^2(0) + (1+k)\langle r^{-3}\rangle\delta'_{L,0}\Big], \quad (3.1)$$

so that

$$(\mathbf{B}'\mathbf{J})_J = (2\mu_0\mu_N/I)[2\pi\psi_S^2(0) + k(1+k)\langle r^{-3}\rangle\delta'_{L,0}], \quad (3.2)$$

and

$$\langle H'''\rangle \cong 2Z\mu_0\mu_e[-2\pi\psi_S^2(0) + (1+k)\langle r^{-3}\rangle\delta'_{L,0}]. \quad (3.3)$$

Here the positive number

$$\mu_0 = e\hbar/2mc \quad (3.4)$$

is the Bohr magneton. The ratio of the effect of μ_e on hyperfine structure to the normal effect is

$$(\mathbf{B}''\mathbf{J})_J/(\mathbf{B}'\mathbf{J})_J = -\mu_e/\mu_0 (L=0)$$
$$(\mathbf{B}''\mathbf{J})_J/(\mathbf{B}'\mathbf{J})_J = -(1/2k)(\mu_e/\mu_0) (L\neq 0). \quad (3.5)$$

The values of the ratio for different terms are as in Table I.

The effect of an external magnetic field is to give an addition to the energy

$$(\Delta E)_{|\mathcal{H}|} = -\mu_e(\mathcal{H}\sigma), \quad (4)$$

because for small Z multiplication by ρ_3 amounts to multiplication by -1. This result may be compared with

$$\mu_0(\mathcal{H}\sigma), \quad (4.1)$$

which is the contribution to the energy involving $\mathcal{H}$ and σ in the absence of μ_e. The effect of μ_e is, therefore, to increase the contribution of the electron spin to the Landé g value by the factor

$$1-\mu_e/\mu_0, \quad (4.2)$$

TABLE I. Values of $(\mathbf{B}''\mathbf{J})_J/(\mathbf{B}'\mathbf{J})_J$ for single electron spectra.

Term =	$s_{1/2}$	$p_{1/2}$	$p_{3/2}$	$d_{3/2}$	$d_{5/2}$
Ratio $(\mu_e/\mu_0)=$	-1	$-\frac{1}{3}$	$\frac{1}{4}$	$-\frac{1}{4}$	$\frac{1}{6}$

so that the modified Landé g factor becomes

$$g' = 1+[1-2(\mu_e/\mu_0)] \times \frac{J(J+1)+S(S+1)-L(L+1)}{2J(J+1)}$$
$$= g-2(\mu_e/\mu_0)(g-1), \quad (4.3)$$

which means that

$$g'-1 = [1-2\mu_e/\mu_0](g-1). \quad (4.4)$$

Here g is the ordinary Landé g factor.

The experimental discrepancy[1] between the atomic and molecular beam values of the proton's and deuteron's magnetic moments indicated[5] the probable existence of μ_e. In order to obtain the value of μ_e from these experiments it is essential to note that the molecular beam measurements[10] have been made, making use of a calibration of the magnetic field by means of the deflection produced in virtue of the atomic magnetic moment of a single electron s term. According to Eq. (4.4) this moment is $\mu_0-\mu_e$. The molecular beam experiment thus measures

$$\mu_N/(\mu_0-\mu_e). \quad (4.5)$$

The atomic beam experiments on the hyperfine structure of the ground states of hydrogen are essentially independent of applied magnetic fields since they are concerned with absorption frequencies extrapolated to zero field. The theoretically expected value of hyperfine structure separation is proportional to

$$\mu_N(\mu_0-\mu_e), \quad (4.6)$$

in accordance with Eq. (3.5) and Table I. The theoretically expected ratio of the atomic to the molecular beam values is, therefore,

$$(\mu_0-\mu_e)^2/\mu_0^2 \cong 1-2\mu_e/\mu_0. \quad (4.7)$$

This ratio represents the theoretically expected

[10] S. Millman and P. Kusch, Phys. Rev. 60, 91 (1941). The writer is grateful to Professors I. I. Rabi and N. F. Ramsey for discussions concerning the way in which the Columbia group standardized their measurements by measuring different moments in the same magnetic field.

value of the "measured" to the "calculated" value of the hyperfine structure of the ground state where by "calculated" one means calculated neglecting μ_e. The experimental value of this ratio is believed to be[11] close to 1.00242, which indicates that

$$\mu_e/\mu_0 \cong -0.00121. \tag{4.8}$$

No correction is being made here for the effect of centering of the electron's wave function on the proton within the deuteron which has been brought out by Bohr.[3] The latter effect is an order of magnitude smaller than that of Eq. (4.8). It is absent for the lighter isotope of hydrogen and need not be considered in connection with Eq. (4.8) if only measurements on the lighter isotope are used.

From Eq. (4.3) one obtains for the ratio of two values of g' for two spectroscopic terms I, II

$$\frac{g'_I/g'_{II}}{g_I/g_{II}} \cong 1+\frac{2\mu_e}{\mu_0}\left(\frac{1}{g_I}-\frac{1}{g_{II}}\right) \cong 1+0.00242\left(\frac{1}{g_{II}}-\frac{1}{g_I}\right), \tag{5}$$

which gives

$$g'(p_{3/2})/g'(p_{1/2}) \cong 2\times 1.00182, \tag{5.1}$$

$$g'(s_{1/2})/g'(p_{1/2}) \cong 3\times 1.00242 \tag{5.2}$$

as the expected ratios of measured g values. The first of these may be compared with the experimental value $2(1.00172\pm 0.00006)$ of Kusch and Foley.[7] The disagreement is almost within experimental error. The agreement of the results of Kusch and Foley with expectation is even better if instead of the experimental value -0.00121 of Eq. (4.8) one makes use of Schwinger's[6] value $-\alpha/2\pi = -0.001163$ for this number. The number taking place of 1.00182 on the right side of Eq. (5.1) is then 1.00174(4). The preliminary result of Foley and Kusch[12] for the ratio of the g' for $s_{1/2}$ of Na to the g' for $p_{1/2}$ of Ga is 3.00732 ± 0.00018 which according to Eq. (5) is $1-2\mu_e/\mu_0$ which gives $2\mu_e/\mu_0 = -0.00242\pm 0.00006$ in good agreement with the value in Eq. (4.8). It is understood,[13] however, that there is other experimental evidence which indicates that Na is an exception and that Schwinger's $-\alpha/2\pi$ is favored by experiment.

The expectation value of H''' is expressed in terms of a radial integral by means of Eq. (1.93). Substitution of the Schroedinger function approximation for the radial integral gives Eq. (3.3). The electric field is supposed to be central but not necessarily Coulombian in this formula. For the Coulombian case well-known formulas[14] for $\psi_s^2(0)$ and $\langle r^{-3}\rangle$ give on substitution into Eq. (3.3)

$$\langle H'''\rangle_s = -2(\mu_e/\mu_0)\alpha^2 Z^4 n^{-3} Ry, \tag{6}$$

where n is the principal quantum number and Ry is the value of the Rydberg in ergs. Also for the same n the ratio of $\langle H'''\rangle$ for a term with $L\neq 0$ to that for $L=0$ is

$$\langle H'''\rangle/\langle H'''\rangle_s = -1/[k(2L+1)]. \tag{6.1}$$

In connection with the Lamb-Retherford-Bethe[15] line shift one has substituting numbers into Eq. (6)

$$\langle H'''\rangle_{ns} = -11.64(\mu_e/\mu_0)(Z^4/n^3)\ \text{cm}^{-1} = -3.49\times 10^5(\mu_e/\mu_0)(Z^4/n^3)\ \text{mc/s}, \tag{6.2}$$

$$\langle H'''\rangle_{2s} = -1.455(\mu_e/\mu_0)Z^4\ \text{cm}^{-1} = -4.36\times 10^4(\mu_e/\mu_0)Z^4\ \text{mc/s}. \tag{6.3}$$

For the value of μ_e/μ_0 corresponding to Eq. (4.8) one has for the displacement of $2s$ the value 0.00176 $\text{cm}^{-1}=53$ mc/sec. and for $\mu_e/\mu_0=-\alpha/2\pi$ the displacement is 0.00169(2) $\text{cm}^{-1}=51$ mc/sec. These amounts are small in comparison with the total shift[15] of about 1000 mc/sec. According to Eq. (6.1) the shifts of the $2p_{1/2}$, $2p_{3/2}$ terms are, respectively, $-\frac{1}{3}$ and $+\frac{1}{6}$ of the shift of the $2s$ term. The expected separation between $2s$ and $2p_{1/2}$ produced by H''' is 0.00234 $\text{cm}^{-1}=70$ mc/sec. for Eq. (4.8) and 0.00226 $\text{cm}^{-1}=68$ mc/sec. for $\mu_e/\mu_0=-\alpha/2\pi$.

IV. CONCLUSION

The addition of a six-vector type of interaction between the electromagnetic field and the electron spin variables to the usual four-vector type is in good agreement with experiments on the

[11] I. I. Rabi, private communication.
[12] H. M. Foley and P. Kusch, Phys. Rev. **73**, 271 (1948).
[13] I. I. Rabi and P. Kusch, private communication.
[14] H. A. Bethe, *Handbuch der Physik* (Verlag Julius Springer, Berlin, 1933), Vol. **24/1**, p. 211.
[15] Willis E. Lamb and Robert C. Retherford, Phys. Rev. **72**, 241 (1947).

hyperfine structure of the hydrogen isotopes and on the Zeeman Effect of gallium and other elements.

The writer would like to express his indebtedness to the Pocono Conference of the National Academy of Sciences in connection with the preparation of this paper. His thanks are also due to Professor Schwinger for a helpful discussion.

Note in proof. The results of the present paper which matter most for comparison with experiment are the ratios of contributions to the hyperfine structure interval factors and to the spin part of the Landé g factor contained in Eqs. (3.5), (4.2). It appears desirable to supply an explanation of these results making more use of physical pictures than has been done above. This may be done in the following way. The four-component Dirac equation can be reduced to an approximate two-component form which shows[16] the ordinary hyperfine structure in the absence of μ_e as arising from three effects: (a) an interaction of nuclear spin and electronic orbital angular momentum having an r^{-3} dependence and proportional to the scalar product of the two angular momenta; (b) an interaction of the nuclear spin with the electronic spin having the same mathematical form as the interaction energy between two magnetic doublets; (c) an additional interaction energy of nuclear and electronic spins which matters only for s terms, giving in this case the whole hyperfine structure effect.

[16] G. Breit, Phys. Rev. **37**, 51 (1931).

For $L\neq 0$ only effects (a) and (b) matter. When their sum is projected onto the total electronic angular momentum one finds that the answer depends only on L and J in agreement with the fact that the interval factor is proportional to $L(L+1)$. But it is clear that the scalar product of the interaction energy with $\mathbf{J}$ must contain $(\mathbf{L}+\boldsymbol{\sigma}/2)\mathbf{L}$ for the effect (a) and consequently $-(\boldsymbol{\sigma}\mathbf{L})/2$ for effect (b). The ratio of the contribution coming from interactions with electronic spin to the total is, therefore,

$$\begin{aligned}&-(\boldsymbol{\sigma}\mathbf{L})/2L(L+1)\\&=-[J(J+1)-L(L+1)-S(S+1)]/2L(L+1)\\&=1/2k.\end{aligned}\tag{7}$$

For $L=0$ on the other hand only effect (c) matters and the ratio of the electronic spin contribution to the total is unity. One has thus

$$\begin{aligned}\frac{\text{Spin contribution}}{\text{Total}}&=1/2k \qquad (L\neq 0)\\ \frac{\text{Spin contribution}}{\text{Total}}&=1 \qquad (L=0)\end{aligned}\tag{7.1}$$

which differs from Eq. (3.5) only through the absence of the factor $-\mu_e/\mu_0$. This is as it should be because the contribution of μ_e arises, in the approximation of small Z from a spin current which differs from the current that gives rise to ordinary hyperfine structure in the absence of μ_e the proportionality factor $-\mu_e/\mu_0$. This is seen to fit in with Eq. (4.2) above and in the limit of small Z the effects of μ_e just discussed appear as though the number μ_0 were changed into $\mu_0-\mu_e$ wherever the interaction of the magnetic moment of the electron spin is dealt with.

Theory of Scattering Processes*

EUGENE FEENBERG
Washington University, St. Louis, Missouri
(Received June 8, 1948)

The formal infinite series for the probability amplitudes are transformed by (*i*) a regrouping procedure which separates out "repetitive" terms from all orders beyond the second and combines them to produce a common factor multiplying all orders, (*ii*) a procedure of summation to a closed form (essentially an analytical continuation) replacing the above common factor by a generalized energy denominator, and (*iii*) unlimited repetition of (*i*) and (*ii*). Procedure (*ii*) is based on the generalized energy quantity

$$\mathcal{E}_{gh\cdots np}=E_p+\sum_{q\neq gh\cdots np}\frac{V_{pq}V_{qp}}{(q)}+\sum_{qr\neq gh\cdots np}\frac{V_{pq}V_{qr}V_{rp}}{(q)(r)}+\cdots$$

and the formal identity

$$[E-\mathcal{E}_{gh\cdots np}]^{-1}=\frac{1}{(p)}\left[1+\sum_{q\neq gh\cdots n}\frac{V_{pq}V_{qp}}{(p)(q)}+\sum_{qr\neq gh\cdots n}\frac{V_{pq}V_{qr}V_{rp}}{(p)(q)(r)}+\cdots\right]$$

employing the notation $(x)=E-E_x$.

INTRODUCTION

THE present discussion of scattering theory resembles an earlier treatment of the energy eigenvalue problem.[1] Both utilize a formal transformation to modify the energy denominators and reduce simultaneously the number of intermediate states in all orders beyond the second. In the absence of interaction the scattering system and the incident particle are described by the Hamiltonian operator H and the complete ortho-normal set of eigenfunctions ϕ_x with eigenvalue E_x. These functions are obtained as a discrete set by the imposition of a periodic boundary condition in a large cube of side L. Transitions are produced by an interaction operator V. The calculations are facilitated by including the diagonal matrix elements of the interaction operator in H (as a diagonal matrix) and in E_x. What remains of the interaction operator is then denoted by V.

I seek a solution of the equation

$$(E_a-H-V)\psi=0, \tag{1}$$

subject to the asymptotic boundary condition

$$\psi\rightarrow\phi_a+\text{outgoing spherical waves.} \tag{2}$$

Equation (1) can be expressed in the form

$$\psi'=(E_a-H)^{-1}V\psi'+\phi_a, \tag{3}$$

provided that a suitable interpretation, consistent with the asymptotic boundary condition, is found for the inverse operator $(E_a-H)^{-1}$. It is well known that the analytical device of displacing the singular point from the real axis into the upper half of the complex energy plane produces a solution containing no incoming spherical waves.[2] With $E=E_a+i\gamma$. $(\gamma>0)$, Eq. (3) is replaced by

$$\psi'=(E-H)^{-1}V\psi'+\phi_a \tag{4}$$

and all transition probabilities and cross sections are evaluated in the limit $\gamma\rightarrow 0$. In view of the profound difference between Eqs. (1) and (4) it is not surprising that function ψ' does not always, in the limit $\gamma\rightarrow 0$, include the incident wave ϕ_a with unit amplitude.[3]

Equation (4) possesses the formal solution[4]

* The research described in this paper was supported in part by contract N6ori-117, Office of Naval Research.

[1] E. Feenberg, Phys. Rev. **74**, 206 (1948). Presented at the second Symposium on Applied Mathematics of the American Mathematical Society, July 29–31, 1948.

[2] A. Sommerfeld, *Wellenmechanik* (Frederick Ungar Publishing Company, New York), p. 442; P. A. M. Dirac, *The Principles of Quantum Mechanics* (Oxford University Press, London, 1930), p. 184; J. Schwinger, *The General Theory of Scattering Processes* (unpublished seminar notes).

[3] An alternative equation $\psi=(E-H)^{-1}V\psi-\phi_a(\phi_a^*, (E-H)^{-1}V\psi)+\phi_a=(E-H)^{-1}V\psi-(1/i\gamma)\phi_a(\phi_a^*, V\psi)+\phi_a$ has the desirable property of automatically insuring that the incident wave ϕ_a appears with unit amplitude in the wave function.

[4] The notation $(x)\equiv E-E_x$ is used in Eqs. (6) and (7) and in the remainder of the paper.

$$\psi' = \sum_{v=0}^{\infty} \{(E-H)^{-1}V\}^v \phi_a \qquad (5)$$

$$= \sum_x \phi_x S'_{xa}$$

$$S'_{xa}(x \neq a) = \frac{V_{xa}}{(x)} + \sum_b \frac{V_{xb}V_{ba}}{(x)(b)} + \sum_{bc} \frac{V_{xb}V_{bc}V_{ca}}{(x)(b)(c)} + \cdots \qquad (6)$$

$$S'_{aa} = 1 + \sum_b \frac{V_{ab}V_{ba}}{(a)(b)} + \sum_{bc} \frac{V_{ab}V_{bc}V_{ca}}{(a)(b)(c)} + \cdots . \qquad (7)$$

The unsatisfactory character of this solution is evident in the apparent deviation of S'_{aa} from the initially assumed value of unity. Even more disturbing is the fact that

$$\operatorname*{Limit}_{\gamma \to 0} (E - E_a) S'_{aa}$$

appears not to vanish. However, one should not pass adverse judgment too hurriedly on the solution represented by Eq. (6). The more obvious blemishes are removed in the following section.

The explicit consideration of convergence difficulties may be deferred by introducing a suitable convergence factor in the interaction operator V. The matrix elements are then functions of a cutoff parameter λ. I suppose that V_{bc} approaches the value $V_{bc}{}^0$ of the unmodified theory as $\lambda \to 0$ and decreases rapidly with increasing λ for $E_b \neq E_c$. In this manner it is possible to insure the absolute convergence of Eqs. (6) and (7) excluding a finite region, centered about the origin, in the λ, γ plane. Obviously the extent of the excluded region can be reduced by transformations having the general character of analytical continuation. Such transformations may, however, make extremely difficult the direct verification that ψ' is a solution of Eq. (4).

FACTORIZATION OF THE AMPLITUDES

The transformation of Eqs. (6) and (7) required to overcome the difficulties mentioned in the introduction begins with the algebraic identity

$$\sum_{bc\cdots mn} \frac{V_{xb}V_{bc}\cdots V_{mn}V_{na}}{(b)(c)\cdots(m)(n)} \equiv \sum_{bc\cdots mn \neq a} \frac{V_{xb}V_{bc}\cdots V_{mn}V_{na}}{(b)(c)\cdots(m)(n)} + \frac{V_{xa}}{(a)} \sum_{cd\cdots mn} \frac{V_{ac}V_{cd}\cdots V_{mn}V_{na}}{(c)(d)\cdots(m)(n)} \sum_{b \neq a} \frac{V_{xb}V_{ba}}{(a)(b)} \sum_{d\cdots mn} \frac{V_{ad}\cdots V_{mn}V_{na}}{(d)\cdots(m)(n)} + \cdots + \sum_{bc\cdots l \neq a} \frac{V_{xb}V_{bc}\cdots V_{la}}{(a)(b)(c)\cdots(l)} \sum_n \frac{V_{an}V_{na}}{(n)}. \qquad (8)$$

With the aid of Eq. (8) the infinite series of sums denoted by $S'_{xa}(x \neq a)$ can be rearranged in the factored form

$$S'_{xa}(x \neq a) = \frac{1}{(x)} \left[V_{xa} + \sum_{b \neq a} \frac{V_{xb}V_{ba}}{(b)} + \sum_{bc \neq a} \frac{V_{xb}V_{bc}V_{ca}}{(b)(c)} + \cdots \right] S'_{aa}. \qquad (9)$$

It is immediately clear that a failure of the condition $S'_{aa} = 1$ does not in fact complicate the theory nor does it create difficulties for the physical interpretation. The reduced amplitudes

$$S_{xa} = S'_{xa}/S'_{aa} \qquad (10)$$

yield a solution in which the coefficient of the incident wave has precisely the value required by the asymptotic boundary condition stated in Eq. (2):

$$\psi = \sum_x \phi_x S_{xa},$$

$$S_{aa} = 1,$$

$$S_{xa}(x \neq a) = \frac{1}{(x)} \left[V_{xa} + \sum_{b \neq a} \frac{V_{xb}V_{ba}}{(b)} + \sum^{*}_{bc \neq a} \frac{V_{xb}V_{bc}V_{ca}}{(b)(c)} + \cdots \right]. \qquad (11)$$

The reduced amplitudes are characterized by one significant property: they are all linear functionals of the incident wave ϕ_a. *There are no repetitive terms involving the state a as an inter-*

mediate station on the road from a to x. Eq. (11) establishes the result that such repetitive terms are devoid of physical meaning.

A second algebraic identity is useful in factoring out repetitive terms involving the final state x as an intermediate station on the road from a to x:

$$\sum_{bc\cdots mn\neq a}\frac{V_{xb}V_{bc}\cdots V_{mn}V_{na}}{(b)(c)\cdots(m)(n)}$$
$$\equiv\sum_{bc\cdots mn\neq ax}\frac{V_{xb}V_{bc}\cdots V_{mn}V_{na}}{(b)(c)\cdots(m)(n)}$$
$$+\sum_{bc\cdots lm\neq a}\frac{V_{xb}V_{bc}\cdots V_{mx}}{(b)(c)\cdots(m)}\frac{V_{xa}}{(x)}$$
$$+\sum_{bc\cdots l\neq a}\frac{V_{xb}V_{bc}\cdots V_{lx}}{(b)(c)\cdots(l)}$$
$$\times\sum_{n\neq ax}\frac{V_{xn}V_{na}}{(x)(n)}+\cdots+\sum_{b\neq a}\frac{V_{xb}V_{bx}}{(b)}$$
$$\times\sum_{de\cdots mn\neq ax}\frac{V_{xd}V_{de}\cdots V_{mn}V_{na}}{(x)(d)(e)\cdots(m)(n)}. \quad (12)$$

Proceeding as in the derivation of Eq. (11) one finds that the amplitude S_{xa} factors into

$$(x)S_{xa}=\left[V_{xa}+\sum_{b\neq ax}\frac{V_{xb}V_{ba}}{(b)}\right.$$
$$\left.+\sum_{bc\neq ax}\frac{V_{xb}V_{bc}V_{ca}}{(b)(c)}+\cdots\right]$$
$$\cdot\left[1+\sum_{b\neq a}\frac{V_{xb}V_{bx}}{(x)(b)}\right.$$
$$\left.+\sum_{bc\neq a}\frac{V_{xb}V_{bc}V_{ca}}{(x)(b)(c)}+\cdots\right]. \quad (13)$$

Dirac and others have shown that the first order pole $1/(x)$ in the amplitude S_{xa} has the consequence that only states for which energy is conserved occur in the asymptotic wave function. What then can be the meaning of the additional powers of $1/(x)$ (of arbitrarily high order) present in the second square bracket? A partial and perhaps not altogether satisfactory answer is that this factor is meaningless as it stands, but can be given meaning by a process of analytical continuation. One may however consider the possibility that the theory requires modification in the sense proposed by Heitler, i.e., the more-or-less general omission of repetitive terms. Equation (13) suggests the simple modification

$$(x)S_{xa}=V_{xa}+\sum_{b\neq ax}\frac{V_{xb}V_{ba}}{(b)}$$
$$+\sum_{bc\neq ax}\frac{V_{xb}V_{bc}V_{ca}}{(b)(c)}+\cdots, \quad (14)$$

in which neither a nor x occurs as an intermediate station on the road from a to x.

THE REGROUPING PROCEDURE

The set of functions

$$E_{gh\cdots np}=E_p+\sum_{q\neq gh\cdots np}\frac{V_{pq}V_{qp}}{(q)}$$
$$+\sum_{qr\neq gh\cdots np}\frac{V_{pq}V_{qr}V_{rp}}{(q)(r)}+\cdots \quad (15)$$

represents a formal generalization of the complex energies (displaced energy levels and associated damping constants) occurring in the energy denominators of the Dirac resonance scattering theory. To establish the connection with energy denominators, observe that (for $p\neq gh\cdots n$)

$$[E-\mathcal{E}_{gh\cdots np}]^{-1}=\frac{1}{(p)}\sum_{v=0}^{\infty}\left[\frac{\mathcal{E}_{gh\cdots np}-E_p}{(p)}\right]^v$$
$$=\frac{1}{(p)}\left[1+\sum_{q\neq gh\cdots n}\frac{V_{pq}V_{qp}}{(p)(q)}\right.$$
$$\left.+\sum_{qr\neq gh\cdots n}\frac{V_{pq}V_{qr}V_{rp}}{(p)(q)(r)}+\cdots\right]. \quad (16)$$

To verify the equality, the right-hand member of the first line may be expanded as a sum of products in which the variable indices run over all values excluding $gh\cdots np$. The second line can be expressed similarly, again restricting the variable indices to values different from $gh\cdots np$. The following example serves to illustrate the procedure as regards the expansion of the sums in

the second line of Eq. (16):

$$\sum_{qrs\neq gh\cdots n}\frac{V_{pq}V_{qr}V_{rs}V_{sp}}{(p)(q)(r)(s)}=\sum_{qrs\neq gh\cdots np}\frac{V_{pq}V_{qr}V_{rs}V_{sp}}{(p)(q)(r)(s)}+\frac{1}{(p)^2}\left[\sum_{q\neq gh\cdots np}\frac{V_{pq}V_{qp}}{(q)}\right]^2. \quad (17)$$

Now Eq. (13) reduces to

$$S_{xa}=\frac{1}{E-\mathcal{E}_{ax}}\left[V_{xa}+\sum_{b\neq xa}\frac{V_{xb}V_{ba}}{(b)}+\sum_{bc\neq xa}\frac{V_{xb}V_{bc}V_{ca}}{(b)(c)}+\cdots\right], \quad (18)$$

a form similar to Eq. (14), but differing from it in important respects. Continuing the development of the regrouping procedure, write

$$(E-\mathcal{E}_{ax})S_{xa}=V_{xa}+\sum_{b\neq xa}\frac{V_{xb}}{(b)}\times\left[V_{ba}+\sum_{c\neq xa}\frac{V_{bc}V_{ca}}{(c)}+\cdots\right], \quad (19)$$

and apply the procedure leading from Eq. (11) to Eq. (13) to the factor in square brackets. The result is

$$(E-\mathcal{E}_{ax})S_{xa}=V_{xa}+\sum_{b\neq xa}\frac{V_{xb}V_{ba}}{E-\mathcal{E}_{xab}}+\sum_{bc\neq xa}\frac{V_{xb}V_{bc}}{(E-\mathcal{E}_{xab})(c)}\times\left[V_{ca}+\sum_{d\neq xa}\frac{V_{cd}V_{da}}{(d)}+\cdots\right]. \quad (20)$$

Equation (20) is designed to suggest unlimited repetition of the regrouping procedure. The limiting formula for S_{xa}, obtained by induction, is

$$(E-\mathcal{E}_{ax})S_{xa}=V_{ax}+\sum_{b\neq xa}\frac{V_{xb}V_{ba}}{E-\mathcal{E}_{xab}}+\sum_{\substack{b\neq xa\\ c\neq abx}}\frac{V_{xb}V_{bc}V_{ca}}{(E-\mathcal{E}_{xab})(E-\mathcal{E}_{xabc})}+\cdots. \quad (21)$$

In Eq. (21) *all repetitive terms in which a given station on the road from x to a is traversed more than once have been removed from the explicit numerator products* and relegated to relatively harmless positions in the generalized energy denominators.

An immediate consequence of Eq. (15) is

$$S'_{aa}=\frac{E-E_a}{E-\mathcal{E}_a}=\frac{i\gamma}{E_a-\mathcal{E}_a+i\gamma}. \quad (22)$$

Equation (22) contains two important special cases. In the first $E_a-\mathcal{E}_a$ vanishes in the limit as the fundamental volume is allowed to become infinite. Then $S'_{aa}=1$ for all values of γ and $\psi'=\psi$. The second case occurs in connection with the Dirac frequency shift and line breadth.[5] If $E_a-\mathcal{E}_a$ does not vanish Eq. (22) implies

$$\lim_{\gamma\to 0}S'_{aa}=0, \quad (E_a\neq\mathcal{E}_a). \quad (23)$$

Casual inspection of Eq. (7) suggests that the limiting value is infinity rather than zero. This observation supplies a measure of the profound modification produced in the convergence properties of the wave amplitudes by repeated applications of the regrouping transformation.

The function $\mathcal{E}_{gh\cdots np}$ is itself a proper subject for the regrouping transformation. Regrouping from left to right as in Eq. (21) the result is

$$\mathcal{E}_{gh\cdots np}=E_p+\sum_{q\neq gh\cdots np}\frac{V_{pq}V_{qp}}{E-\mathcal{E}_{gh\cdots npq}}+\sum_{\substack{q\neq gh\cdots np\\ r\neq gh\cdots npq}}\frac{V_{pq}V_{qr}V_{rp}}{(E-\mathcal{E}_{gh\cdots npq})(E-\mathcal{E}_{gh\cdots npqr})}+\cdots. \quad (24)$$

The reverse order yields

$$\mathcal{E}_{gh\cdots np}=E_p+\sum_{q\neq gh\cdots np}\frac{V_{pq}V_{qp}}{E-\mathcal{E}_{gh\cdots npq}}+\sum_{\substack{q\neq gh\cdots np\\ r\neq gh\cdots npq}}\frac{V_{pr}V_{rq}V_{qp}}{(E-\mathcal{E}_{gh\cdots npqr})(E-\mathcal{E}_{gh\cdots npq})}+\cdots. \quad (25)$$

[5] P. A. M. Dirac, *The Principles of Quantum Mechanics* (Oxford University Press, London, 1930).

REFORMULATION

An additional set of functions

$$U_{bgh\cdots mnx;xb}=V_{xb}+\sum_{q\neq bgh\cdots mnx}\frac{V_{xq}V_{qb}}{(q)}+\sum_{qr\neq bgh\cdots mnx}\frac{V_{xq}V_{qr}V_{rb}}{(q)(r)}+\cdots, \quad (26)$$

proves useful in providing a convenient formulation of the preceding results. The subscripts xb represent the indices of a matrix element in the usual sense while $bgh\cdots mnx$ stand for states excluded from the summations involved in the definition of $U_{bgh\cdots mnx;xb}$. Equation (26) is equivalent to an implicit (integral) equation; in particular

$$U_{ax;xa}=V_{xa}+\sum_{b\neq ax}\frac{V_{xb}U_{ax;ba}}{(b)} \quad (27)$$

an equation of interest because the systematic omission of states for which $E_b\neq E_a$ reduces it to the Heitler integral equation.[6]

An immediate consequence of Eqs. (15) and (26) is

$$\mathcal{E}_{gh\cdots mnp}=E_p+U_{gh\cdots mnp;pp}. \quad (28)$$

The regrouping procedure applied to Eq. (26) yields

$$U_{bgh\cdots mnx;xb}=V_{xb}+\sum_{p\neq xbg\cdots mn}\frac{V_{xp}V_{pb}}{E-\mathcal{E}_{xbg\cdots mnp}}+\sum_{\substack{p\neq xbg\cdots mn\\ q\neq xbg\cdots mnp}}\frac{V_{xp}V_{pq}V_{qb}}{(E-\mathcal{E}_{xbg\cdots mnp})(E-\mathcal{E}_{xbg\cdots mnpq})}+\cdots$$

$$=V_{xb}+\sum_{p\neq bg\cdots mn}\frac{V_{xp}U_{xbgh\cdots mnp;pb}}{E-E_p-U_{xbg\cdots mnp;pp}}. \quad (29)$$

At the end of the infinite chain of relations one has

$$U_{ax;xa}=V_{xa}+\sum_{b\neq ax}\frac{V_{xb}U_{xab;ba}}{E-E_b-U_{xab;bb}}. \quad (30)$$

DISCUSSION

The scattering of a particle by a static potential provides a trivial, but illuminating, illustration of the regrouping transformation. With plane waves for the first order eigenfunctions the matrix elements all vary inversely as L^3. Since the density of states in momentum space is proportional to this volume it is apparent from Eq. (15) that

$$\mathcal{E}_{gh\cdots np}=E_p+0(L^{-3}), \quad \gamma\neq 0.$$

Consequently the transformed energy denominators revert back to the original form if the fundamental volume is increased indefinitely while γ is held fixed at a non-zero value. At the same time the sums over intermediate states in Eqs. (11) and (21) approximate to integrals in momentum space. Both Eqs. (11) and (21) yield the same limiting amplitude for a fixed value of γ. However, using Eq. (11), the convergence to the integral form is obviously nonuniform in γ because of the second and higher order poles (in γ) produced by the coincidence of two or more variable indices in the multiple summations. Such duplications and the attendant nonuniform convergence to the limiting integral form are absent in Eq. (21).

Similar remarks apply to the problem of elastic and inelastic scattering of a particle by a composite system. In this case

$$\psi=\sum_{\alpha p}\phi_{\alpha p}S_{\alpha p\alpha_0 p_0} \quad (31)$$

with

$$_{\alpha p}=\phi_\alpha(\text{scatterer})L^{-\frac{1}{2}}e^{ip\cdot r/\hbar}. \quad (32)$$

The method of Dirac and Sommerfeld yields

$$\psi\rightarrow-\frac{2\pi L^{\frac{3}{2}}}{h^2c^2}\sum_\alpha\phi_\alpha U_{\alpha p\alpha_0 p_0}\frac{e^{ipr/\hbar}}{r} \quad (33)$$

for the asymptotic behavior of ψ. In Eq. (33) ψ is an outgoing spherical wave and $E_{\alpha_0}+E_{p_0}=E_\alpha+E_p$. The differential cross section for scattering into the element of solid angle $d\Omega$ is

$$\sigma_{\alpha p,\,\alpha_0 p_0}d\Omega=\frac{4\pi^2h^2}{c^4}\frac{E_pE_{p_0}p}{p_0}\left|\frac{L^3}{h^3}U_{\alpha p\alpha_0 p_0}\right|^2 d\Omega, \quad (34)$$

using relativistic expressions for the total energy of the incident and scattered particles. To simplify the formulae only the matrix subscripts appear explicitly on the amplitudes U (the full notation is $U_{\alpha_0 p_0\alpha p;\alpha p\alpha_0 p_0}$).

[6] W. Heitler, *The Quantum Theory of Radiation* (Oxford University Press, London, 1944), p. 240.

In the limit of infinitely large fundamental volume Eq. (27) assumes the limiting form

$$L^3U_{\alpha p\alpha_0 p_0}=L^3V_{\alpha p\alpha_0 p_0}+\frac{1}{c^2h^3}$$

$$\times\sum_{\alpha'}\int\frac{L^3V_{\alpha p\alpha' p'}L^3U_{\alpha' p'\alpha_0 p_0}p'dEp'd\Omega'}{E_{\alpha_0}+E_{p_0}-E_{\alpha'}-E_{p'}+i\gamma}$$

$$=L^3V_{\alpha p\alpha_0 p_0}+\frac{1}{c^2h^3}$$

$$\times\sum_{\alpha'}P\left[\int\frac{L^3V_{\alpha p\alpha' p'}L^3U_{\alpha' p'\alpha_0 p_0}Ep'dEp'd\Omega'}{E_{\alpha_0}+E_{p_0}-E_{\alpha'}-E_{p'}}\right]$$

$$-\frac{i\pi}{c^2h^3}\sum_{\alpha'}\int L^3V_{\alpha p\alpha' p'}L^3U_{\alpha' p'\alpha_0 p_0 p'}d\Omega', \quad (35)$$

the symbol P denoting, as usual, the principal value of the following integral. The omission of the principal value term reduces Eq. (35) to the form of Heitler's integral equation. If only $L^3V_{\alpha p\alpha_0 p_0}$ is retained one has the first order Born approximation.

The derivation of the Thomson scattering cross section, including the classical damping denominator, provides another simple application of the regrouping formalism. However, the calculation is identical with that given by Heitler,[7] since the energy denominators all reduce to the usual difference of unperturbed energies in the limit $L\to\infty$.

From the point of view of the full utilization of the advantages inherent in the regrouping formalism the foregoing applications are trivial. Non-trivial applications first appear in problems involving the interaction of quantized fields with matter. In such problems the energy displacements $U_{gh\cdots np;pp}$ do not vanish in the limit $L\to\infty$; moreover these displacements are complex numbers with negative imaginary components (in the limit $\gamma\to 0$). Thus the factor $(E-\mathcal{E}_{ax})^{-1}$ in Eq. (21) for S_{xa} is non-singular along the real energy axis (certainly an improvement over the singularities of arbitrarily high order at $E_x=E_a$ in S_{xa} defined by Eq. (13)). However, the derivation of Eqs. (33) and (34) clearly reveals that Eq. (21) cannot yield conservation of energy in the classical sense. Classically the total energy of the system is given by the sum of the energies of the several parts (scatterer and scattered particle or particles) when they are well separated in space. In quantized field theories the existence of the interaction reveals itself in the failure of additivity for the energy of field and matter. Even if the real part of the energy shift produced by the interaction is absorbed into a correction to the mass of the scattered particle, there remains the imaginary part of $\mathcal{E}_{ax}$ to cause failure of conservation. Perhaps this result is not unsatisfactory; if, however, it is rejected the modification of the theory by the substitution of (x) for $E-\mathcal{E}_{ax}$ in Eq. (21) offers a workable alternative.

A further important point is that the multiple sums in Eqs. (21), (25) and (29) have precisely the form required for a straight forward transition to multiple integrals in the limit $L\to\infty$. The nature of the complication which is here avoided appears clearly in Eq. (17), the left-hand sum having the limiting form of a double integral plus the square of a single integral.

In the light of these remarks it seems likely that the regrouping formalism will prove useful in the study of field theories, particularly where the true physical content is obscured at present by inadequate perturbation methods.

The writer is greatly indebted to Dr. Henry Primakoff for many stimulating discussions.

[7] Reference 6, p. 249.

The Internal Intensity Ratio of H_α and of D_α

CHAO-WANG HSUEH*
California Institute of Technology, Pasadena, California
(Received April 25, 1948)

A Geissler-Wood discharge tube was designed for use as the light source of H_α or D_α line. The tube was cooled in liquid air under low pressure to reveal the fine structure of the spectral lines. Four different separations, 7.6, 7.8, 8.0, and 8.2 mm, were used in the Fabry-Perot interferometer. Ten spectroscopic plates were measured for H_α and ten others for D_α. The internal intensity ratio of H_α and of D_α was found to be 0.808 ± 0.004 and 0.803 ± 0.003, respectively, as compared to the theoretical value of 0.806. This study indicates that the experimental value of the intensity ratio between the two main component groups agrees with the theoretical value when pure hydrogen or pure deuterium gas is used in the discharge tube and the discharge is at its maximum intensity.

I. INTRODUCTION

THE theoretical relative intensities of the fine structure components of the first Balmer line of hydrogen, H_α, were calculated by Sommerfeld and Unsöld[1] on the basis of Schrödinger's wave mechanics. In applying Dirac's relativistic quantum theory of electron to determine the intensity distribution of the H_α components, Saha and Banerji[2] obtained identical results. At least to the first approximation, the fine structure of D_α, 6561A, may be assumed to be the same as that of H_α, 6563A, because deuterium is an isotope of hydrogen. Detailed description of the theoretical structure of the H_α and D_α lines, including the separations of the components, has been published.[3] Experimentally, only two main components were clearly and definitely resolved from the five components predicted in the theory. It was found by some observers[4] that the relative intensities of the two main components depended largely upon the conditions of excitation and had little relationship to the theoretical value. In some cases, the intensity of the supposed weaker component was observed to be equal to or even greater than that of the stronger component of the theory.

This paper describes a further study on the intensity ratio between the two main component groups of the H_α and D_α lines.

II. THE LIGHT SOURCE FOR H_α OR D_α

In the first stage of this work, an electrodeless hydrogen discharge tube[5] excited by a high frequency oscillator was tried. It was found to have several disadvantages. One of these was observed in trying to photograph the H_α line through a Fabry-Perot interferometer. The hydrogen discharge tube was not able to provide an H_α line of sufficient intensity to give a satisfactory interferometer spectrogram. Furthermore, the discharge in the tube produced a circular image on the spectrograph slit, which caused the latter to be unevenly illuminated. A third disadvantage arose from the large bore of the tube. Its diameter of one inch was too large for efficient cooling of the hydrogen gas inside, and the H_α line thus obtained was not as sharp as desired. Therefore, another hydrogen discharge tube was designed.

A. The Discharge Tube and Its Cooling Method

There appears in Fig. 1 the new hydrogen discharge tube inside a Dewar flask. It resembled a Geissler tube in that its central part consisted of a 6-cm long capillary. To insure a rapid cooling of the tube in liquid air, a thin-walled capillary

* Now at the Research Laboratory, U. S. Naval Ordnance Plant, Indianapolis, Indiana.

[1] A. Sommerfeld and A. Unsöld, Zeits. f. Physik **36**, 259 (1926); **38**, 237 (1926).

[2] M. Saha and A. C. Banerji, Zeits. f. Physik **68**, 704 (1931).

[3] W. V. Houston and Y. M. Hsieh, Phys. Rev. **45**, 271 (1934); R. C. Williams, Phys. Rev. **54**, 559 (1938); J. W. Drinkwater, O. Richardson, and W. E. Williams, Proc. Roy. Soc. **A174**, 165 (1940).

[4] W. V. Houston, Astrophys. J. **64**, 88 (1926); R. C. Williams, Phys. Rev. **54**, 563 (1938); J. W. Drinkwater, O. Richardson, and W. E. Williams, Proc. Roy. Soc. **A174**, 175 (1940).

[5] C. W. Hsueh, Rev. Sci. Inst. **14**, 251 (1943).

having a bore of 3 mm and outer diameter of 5 mm was chosen. By concentrating the discharge in a narrow space, the capillary had the advantage of increasing the intensity of H_α. The new tube also had some of the features of a Wood's discharge tube in being longer than the Geissler tube and having a smaller diameter. A transformer was used to run it. The voltage drop across the tube was about 1200 volts, and the power consumed by the tube was approximately 20 watts. The tube was protected from overheating by means of two 9000-ohm resistors connected in series.

Inasmuch as the light emitted from the capillary discharge was used for taking spectrograms, the construction of the capillary needed special consideration. In general, when a discharge is run by a transformer or a generator, the hottest part of the tube is around the electrodes. Hence, to diminish the heating effect of the discharge on the central capillary of the tube, it is better to have the electrodes far away from the capillary. This was one of the features from the Wood's tube, which was adopted in our modification. To decrease the Stark effect at the capillary, the two ends of the tube were bent towards the same side of the capillary. The electric lines of force which joined the two electrodes would concentrate on one side of the tube without passing through the capillary, and, thereby, the electric field around the capillary was reduced.

In order to subdue the Doppler-effect broadening of the H_α and D_α lines and to make their fine structure observable, the discharge tube was cooled in rapidly evaporating liquid air which, because of its low temperature, cut down the temperature motion of the atoms. A schematic diagram of the cooling arrangement is shown in Fig. 1. Liquid air was contained in a Dewar flask of 4.5-liter capacity. The opening of the flask was closed with a brass cap and sealed airtight with layers of rubber tape and paintings of G. E. Glyptal No. 1202. A layer of wood, 2 cm thick, was placed under the cap to improve the heat insulation of the system. On top of the cap are connections to vacuum pumps and to the manometer, leads to the transformer, inlet for hydrogen or deuterium gas, and holes for pouring in liquid air. Experience proved that rapidly evaporating liquid air not only provided much lower temperature than liquid air at atmospheric pressure but also lasted longer. This apparent paradox can be explained in the following way. The speed of evaporation of the liquid air in a Dewar flask depends upon the rate at which the surrounding heat is conducted into the liquid air. When liquid air is under low pressure and thus protected by a better insulation, the heat absorbed is less than that under atmospheric pressure.

The light of the capillary discharge situated at the bottom of the liquid-air flask was transmitted to the outside through a high vacuum window which was an evacuated and sealed glass pipe, 27 cm long and 5 cm in diameter. This highly evacuated window had the desirable quality of being a good transmitter of light and an excellent heat insulator at the same time. The lateral side of the glass pipe was covered with a layer of black tape to cut off stray light. The capillary of the discharge tube was placed under the vacuum glass pipe, perpendicular to the long axis of the latter. Thus, the line of observation was normal to the direction of the discharge current. Since observation was made in a direction perpendicular to the motion of the light-emitting atoms, the Doppler-effect broadening of the spectral line was further reduced.

Several precautions in the use of the tube may be mentioned. No liquid, like acids, alcohol, or water, should be used to clean the Geissler-Wood discharge tube, because liquid contaminates the tube and decreases the efficiency of producing the H_α line. After the tube had been used for a long time a decrease in intensity of the H_α line was also observed. This was due to accumulation

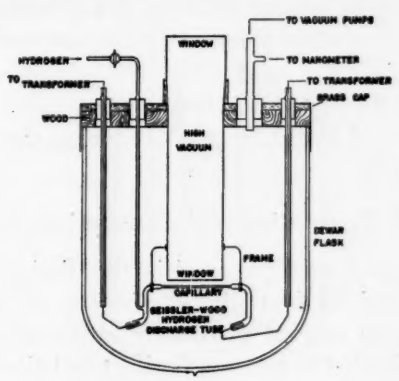

FIG. 1. The Geissler-Wood hydrogen discharge tube cooled in liquid air under reduced pressure.

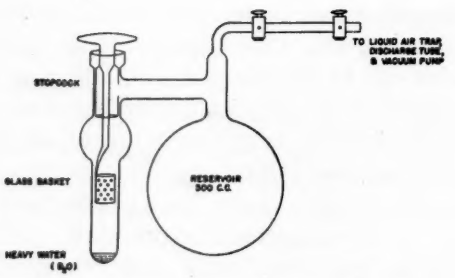

FIG. 2. Generator for the deuterium gas.

of impurities condensed inside the tube. Sometimes the efficiency can be recovered by evacuating the tube at room temperature. If this method fails, then it is better to make a new tube since a good glass blower can make a new Geissler-Wood tube in a few hours. Because mercury vapor interferes seriously with the emission of a strong H_α line, care should be exercised to prevent mercury vapor from entering into the tube by means of an efficient liquid-air trap. The current used in exciting the tube was chosen in accordance with the time of exposure and the amount of hypersensitizing of the spectroscopic plate. For example, when the plate was baked for 26 hours at 50°C and the exposure time was 30 minutes, the discharge current for a newly made tube was around 14 milliamperes.

Many workers on the D_α line used only the vapor of heavy water (D_2O) in their discharge tube. Nevertheless, according to the author's experience, pure deuterium gas gave much stronger D_α line than the heavy water vapor, especially when cooled in liquid air. This was also true with the hydrogen line. Moreover, the intensity ratio of the two main component-groups would have almost the theoretical value when gas, rather than water vapor, was admitted to the tube. The work of Spedding, Shane, and Grace[6] supported this fact. Therefore, pure deuterium and hydrogen gases were used throughout this work.

B. Preparation of the Deuterium Gas

The hydrogen gas used in the discharge tube was obtained from the electrolysis of water to which ten percent of concentrated sulfuric acid was added. The gas was purified by being passed through a liquid-air trap. In view of the scarcity of heavy water during the war, it did not seem feasible to prepare deuterium gas by means of electrolysis of heavy water, because too much of it was needed to fill the available electrolysis apparatus. Hence, another method of preparing the deuterium gas had to be developed.

Figure 2 shows the apparatus for generating deuterium gas from the reaction of deuterium oxide with sodium. The sodium metal was supplied by the Mefford Chemical Company of Los Angeles, and was kept in an airtight tin can free from oil. A few pieces of sodium were placed in the glass basket, 5 cm above the surface of heavy water. When the vapor of the deuterium oxide came into contact with the sodium metal, a chemical reaction took place liberating deuterium gas and depositing sodium deuteroxide (NaOD) on the surface. The sodium deuteroxide, similar to sodium hydroxide, has the property of absorbing water vapor. So the reaction continued until all the sodium which could be reached by the heavy water vapor changed into deuteroxide. The chief advantage of this method over the electrolysis procedure mentioned above was the economical use of heavy water. Only one gram of

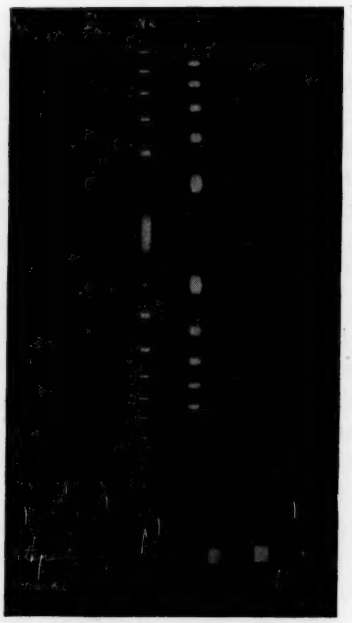

FIG. 3. Photograph showing the interferometer spectrogram of the D_α, Cd, and Ne lines and the intensity marks. White color on the photograph corresponds to black color on the plate.

[6] F. H. Spedding, C. D. Shane, and N. S. Grace, Phys. Rev. **47**, 39 (1935).

heavy water was required each time, thereby generating deuterium gas sufficient for ten days' work or longer.

The general procedure used for preparing deuterium gas is as follows: First, the apparatus was cleaned by evacuation until it was free from water or organic vapor. One gram or less of heavy water was poured into the deuterium generator, and two grams of clean sodium in small pieces were put in the glass basket. After replacement of the stopcock, the reaction chamber was partially immersed in liquid air which froze the heavy water and stopped the reaction. The apparatus was then evacuated again to remove any air enclosed. Removal of the liquid-air bath gave rise to generation of the deuterium gas. After sufficient gas was obtained, the apparatus was cooled again in liquid air. In so doing, the heavy water could be preserved for future use.

III. PROCEDURE FOR TAKING SPECTROGRAMS

The spectrograph used for taking spectrograms had a camera lens of 200 cm focal length. The dispersing system consisted of a plane reflection grating of 48,000 lines per inch, which was crossed by a resolving system consisting of a Fabry-Perot interferometer. In the interferometer were two circular optical flats which were 11.5 cm in diameter and heavily silvered. For studying the internal intensity ratio of the H_α and D_α lines, four different interferometer gaps, 7.6, 7.8, 8.0, and 8.2 mm, respectively, were used.

All exposures were made on the Eastman spectroscopic plates, type 103-H_α and size 5 in. $\times$ 7 in. To increase the speed of the plates, each plate was hypersensitized by means of heat treatment[7] a few hours before use. In the heat treatment, the plate was wrapped in layers of black paper and tin foil and packed in a cardboard box, which was placed in an electric oven kept at a temperature of 50°C for a period of about 26 hours. The exposure time for H_α or D_α was 30 minutes, during which time the temperature of the interferometer remained constant to within 1/20 of a degree centigrade. Immediately after that, the plate was exposed for another 30 minutes to the intensity-mark maker described in Section IV. Then it was developed in a high contrast Kodak developer, D-19, for 3.5 minutes with constant agitation. A short development time was chosen in order to reduce the fog or the background of the spectrogram to a minimum. Figure 3 shows a sample of the spectrogram. When not in use the red-sensitive spectroscopic plates were stored in a refrigerator in order to keep them from fogging.

[7] I. S. Bowen and L. T. Clark, J. Opt. Soc. Am. **30**, 508 (1940).

IV. CALIBRATION OF SPECTROSCOPIC PLATES

The relation between the blackness of a photographic plate and the intensity of the incident light which caused that blackness is usually expressed by the characteristic curve of the plate, also called the H and D curve. This curve is determined by means of calibration with intensities of known ratio. One of the methods for producing the various intensities is the stepweakener. The stepweakener used in this work consisted of twelve holes on a brass block, 1.75 inches wide, 2.00 inches long, and 1.50 inches high. The diameter of the holes varied from 0.537 mm to 6.312 mm. The intensity of the light which reached the plate was proportional to the area of the hole through which passed the light, or to the square of its diameter. Each hole was covered by a small lens having a focal length equal to the height of the block, and on top of the twelve small lenses was a larger lens which covered all the twelve holes. Above the block was an illuminated square at a distance from the large lens equal to its focal length. Under the block was the spectroscopic plate to be calibrated. An image of the illuminated square was formed under each hole on the emulsion of the plate. After sufficient exposure and development, twelve or less photographs of the square appeared on the plate, each

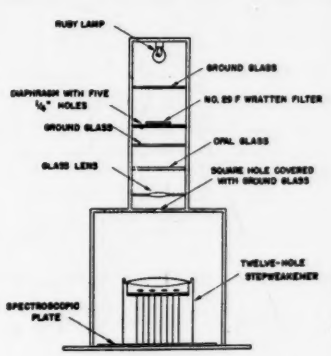

FIG. 4. Arrangement for photographing intensity marks to calibrate the spectroscopic plate.

TABLE I. Internal intensity ratio for the H_α line.

Plate no.	Interferometer separation, mm.	Intensity ratio $I(23)/I(145)$
75	7.6	0.816
76	7.6	0.820
72	7.8	0.824
73	7.8	0.810
77	7.8	0.822
80	8.0	0.789
81	8.0	0.800
62	8.2	0.798
63	8.2	0.814
64	8.2	0.789
	Mean	0.808±0.004

TABLE II. Internal intensity ratio for the D_α line.

Plate no.	Interferometer separation, mm.	Intensity ratio $I(23)/I(145)$
12	7.6	0.794
13	7.6	0.800
33	7.8	0.804
34	7.8	0.815
21	8.0	0.809
22	8.0	0.817
27	8.0	0.807
44	8.2	0.809
47	8.2	0.791
48	8.2	0.787
	Mean	0.803±0.003

displaying different degrees of blackness corresponding to the light intensity received. A sample of the intensity marks is shown at the bottom of Fig. 3.

The characteristic curve of a spectroscopic plate depends upon the time of exposure, development of the plate, and the wave-length of the incident light. In order to find the intensity of the H_α and D_α components accurately, the time of exposure for H_α or D_α and for the intensity marks was the same. The development factor also was expected to be identical because they were on the same plate. The light used to illuminate the square came from a G. E. 25-watt Mazda ruby lamp through a Wratten No. 29 F red filter. The spectrum of this red light source showed that the light from such an arrangement consisted of a narrow band with a central maximum at the H_α line, 6563A. Hence it was suitable for use in calibrating the plate in the spectral region around the H_α line. The red light was further covered with opal and ground glass to cut down the light intensity from the ruby lamp. This was required to match the intensity of the band emitted by the Mazda lamp with that of the H_α line. The detailed arrangement for photographing the intensity marks is illustrated in Fig. 4.

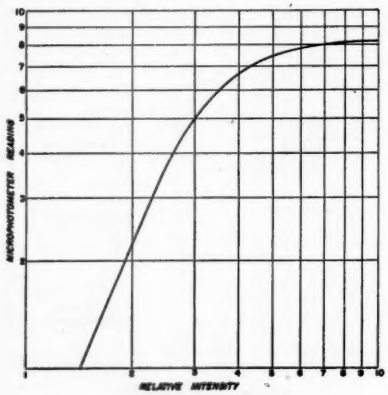

FIG. 5. Typical calibration curve of the spectroscopic plate 103-H_α.

In general, the H and D curve is obtained by plotting the optical density against the common logarithm of exposure. However, the purpose of this calibration was to find the relative intensity of the H_α and D_α components. For the sake of avoiding unnecessary steps such as reduction of the microphotometer readings to optical density and multiplication of the light intensity by the exposure time to get the value of exposure, the following simple procedure was adopted in obtaining the calibration curve of the spectroscopic plates. The intensities produced by the stepweakener were proportional to the area of the holes, and only the relative values of the various intensities were known. For convenience in plotting on the graph paper, the intensity through the largest hole was taken as 10 and the relative value of the intensity through the other holes was reduced in proportion to the square of their respective diameters. In measuring the blackness of the intensity marks, a microphotometer reading was taken for each square when the average reading of the background surrounding that black mark was made zero. In this way, the blacker intensity marks had larger microphotometer readings. Figure 5 shows a typical calibration curve of the spectroscopic plate, type 103-H_α. It was plotted on the log-log graph paper with the microphotometer reading as ordinate and with the relative intensity as abscissa.

FIG. 6. Microphotometer curve of the H_α line.

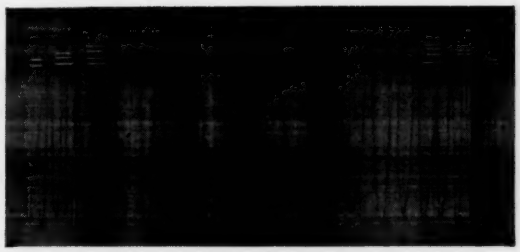

FIG. 7. Microphotometer curve of the D_α line.

V. METHOD FOR FINDING THE INTENSITY RATIO

After the microphotometer curve of an H_α line or D_α line was made, the blackness of the intensity marks on the same plate was measured immediately on the microphotometer without changing any of its adjustments. With the microphotometer readings thus obtained, the calibration curve of the said spectroscopic plate was plotted according to the method described in Section IV.

Figures 6 and 7 show, respectively, the microphotometer curve of the H_α line and the D_α line. There are, in general, eight or ten orders of the interferometer pattern on each microphotometer curve. Each order of the interferometer pattern reveals the two main components of the line, which were clearly resolved. The two components were identified by measuring their respective wave-lengths. The red of the two apparent components which has a longer wave-length is called the (145) component group and the violet which has a shorter wave-length, the (23) component group. Explanation for this denomination will be given in Section VI. The wave-lengths in air of the apparent H_α components are 6562.85A for the component (145) and 6562.72A for (23), and those of the D_α components are 6561.07A for the component (145) and 6560.93 for (23).

The white line at the bottom of Figs. 6 and 7 gives the common background of the spectroscopic plate, and the height of the microphotometer curve above the white line represents the blackness of the spectral line. For each order of a line on the microphotometer tracing, the heights of the two maxima above the line of common background were measured. The mean maximum height of all the orders on one plate gave the average degree of blackness for the component-groups (145) and (23) respectively. The intensity corresponding to each average maximum height was found from the calibration curve of that spectroscopic plate, and from these intensity values the intensity ratio was computed. The values of the intensity ratio for the H_α and D_α lines appear in Tables I and II.

As pointed out by Williams and Gibbs,[8] the intensity maximum of a complex spectral pattern does not always coincide with its center of gravity. For the component-group (23) of H_α, they computed the position difference as being equal to 0.007 cm^{-1} in comparison with their observed half-intensity width of 0.180 cm^{-1}. It appears then that the position difference is about 1/25 of the half-intensity width. For example, suppose the half-intensity width of a pattern shown on the microphotometer curve be 5 mm. The position difference between the center of gravity and the intensity peak of that pattern would be[9] approximately 0.2 mm which, being of the same order of the experimental error in taking the microphotometer readings, may be neglected. Furthermore, in the neighborhood of the intensity maximum the variation of intensity is nearly zero. Therefore, as far as the measurement of the H_α or D_α intensity from the microphotometer curve is concerned, the intensity of the center of gravity may be considered to be identical with the intensity at the peak of the curve. In view of this fact, the procedure used in this study for finding the intensity ratio is justified.

VI. RESULTS AND CONCLUSION

All the spectrograms of H_α and of D_α employed in determining the intensity ratio were made

[8] R. C. Williams and R. C. Gibbs, Phys. Rev. **45**, 476 (1934).

[9] See the Appendix.

when the discharge in the Geissler-Wood tube was at its maximum intensity. That condition was ascertained by the purple red color of the capillary discharge and by the strong intensity of the red H_α or D_α line as viewed with a direct-vision spectroscope. Moreover, the resistance of the discharge tube was at the lowest value, because the discharge current was at its maximum as measured with a milliammeter when the voltage across the tube was set at a desired value and the gas pressure in the tube was varied. Ordinary hydrogen discharge is bluish in color, but when the discharge is strong the color becomes purple red. The pressure of the hydrogen gas in the discharge tube was observed to be about 0.4 mm Hg during the period of maximum discharge.

On the basis of either Sommerfeld's fine structure formula or Dirac's quantum theory of electron, it has been theoretically predicted that the H_α or D_α line should consist of five components. In agreement with Williams's assignment,[10] they are named the components 1, 2, 3, 4, and 5 in the decreasing order of their intensity. However, on account of overlapping of the components, caused chiefly by the Doppler-effect broadening, only two groups of components can be clearly resolved. The group with the stronger intensity is composed of the components 1, 4, and 5 and has longer wave-length, while the weaker group is composed of the components 2 and 3 and has shorter wave-length. According to the theory, the value of the intensity ratio is given by[11] $I(23)/I(145)=0.806$, where $I(145)$ and $I(23)$ denote the intensity of the center of gravity of the component groups (145) and (23), respectively.

For finding the experimental value of the intensity ratio, the method given in Section V was applied. The results are tabulated in Tables I and II, in which the deviation measure was computed by using an expression described in Holman's book.[12] The deviation measure is equal to the average deviation from the mean divided by the square root of the number of measurements.

The results of measurements on the intensity ratio between the two apparent main components of the H_α and D_α line indicate the following conclusion: The value of the internal intensity ratio obtained experimentally agrees with the theoretical value, when the discharge tube is filled with pure hydrogen or pure deuterium gas and the discharge is at its maximum intensity.

The writer wishes to thank Professors W. V. Houston, I. S. Bowen, and D. M. Yost for their valuable advice.

APPENDIX

In the work done by Williams and Gibbs,[8] the abscissa of their intensity curve denoted the wave number and the unit was cm^{-1}. As we were working on the microphotometer curve directly and the abscissa represented the radius of the interferometer fringes, the unit was mm. The relation between the wave number n and the radius R of the corresponding interference fringe can be expressed by the equation

$$n=(q/2df)(f^2+R^2)^{\frac{1}{2}}, \tag{1}$$

where q is the order of interference, d the gap of the Fabry-Perot interferometer, and f the focal length of the camera of the spectrograph. Differentiate n with respect to R, and we get

$$dn/dR=(q/2df)R(f^2+R^2)^{-\frac{1}{2}}. \tag{2}$$

Let Δn and ΔR be the half-intensity width of the intensity curve and of the microphotometer curve, respectively; let dn and dR be the position difference between the center of gravity and the intensity peak of the two respective curves. According to Eq. (2), we have approximately

$$\begin{aligned}\Delta n/\Delta R &\approx (q/2df)R(f^2+R^2)^{-\frac{1}{2}} \\ &\approx dn/dR,\end{aligned} \tag{3}$$

where R represents the radius of interference fringe at the intensity peak. The approximation is due to the fact that Δn and ΔR are finite quantities and are not infinitesimal in comparison with R. From Eq. (3), we obtain

$$dR/\Delta R \approx dn/\Delta n. \tag{4}$$

[10] R. C. Williams, Phys. Rev. **54**, 559 (1938).
[11] W. V. Houston and Y. M. Hsieh, Phys. Rev. **45**, 271 (1934).
[12] S. W. Holman, *Discussion of the Precision of Measurements* (John Wiley and Sons, Inc., New York, 1904), second edition, p. 18.

PHYSICAL REVIEW VOLUME 74, NUMBER 6 SEPTEMBER 15, 1948

Some Measurements of Gamma-Ray Energies

FRANZ N. D. KURIE AND M. TER-POGOSSIAN
Department of Physics, Washington University, Saint Louis, Missouri
(Received June 2, 1948)

To examine the possibility that some radio-isotopes which have been considered to decay by K-capture do in part decay with the emission of very slow positrons careful measurements of the γ-rays emitted by two of them have been made. Preliminary measurements were made of the F and I lines of ThB as a check on the spectrometer used. Also the annihilation radiation line of Cu^{64} was measured to establish its shape and position. In the course of this, good evidence was found for radiation resulting from annihilation while the positron is in flight. The weak high energy gamma-ray previously reported was found and its energy determined to be 1.34 ± 0.01 Mev. The γ-radiation of both Be^{7} and Cr^{51} consists of a single line at 485 ± 5 kev and 320 ± 5 kev, respectively. No evidence of annihilation radiation was found in either case.

1. INTRODUCTION

THIS work began because of the necessity of examining experimentally the γ-radiation of those radioisotopes which decay by K-capture. If one plots the number of these isotopes as a function of the energy of γ-rays as recorded in the literature, one finds a clustering of energies in the neighborhood of the positron annihilation energies, 0.5 and 1 Mev. This suggests that in many cases, instead of actually disintegrating by K-capture, there might be the emission of slow positrons which could escape detection. These positrons would have a good chance, if they were slow enough, to be annihilated in the K-shell of the atom whose nucleus they had just left. This would leave a vacancy in the K-shell and, in the course of its being filled, characteristic K-radiation would be emitted. Thus the detection of K-radiation does not suffice to establish K-capture as the process whereby a particular radioisotope decays. Evidence for the emission of slow positrons might be obtained if annihilation radiation were observed in "K-capture" isotopes. Indeed, because of the proximity of a nucleus to the K-shell one should expect to find examples of single quantum annihilation perhaps somewhat more frequently than when fast positrons are annihilated. These considerations suggested that accurate determinations of γ-ray energies from isotopes which decay by K-capture might reveal such annihilation radiation.

The measurements described here include only two K-capture isotopes. Two other measurements were made for calibration purposes. The measurement of one of the internal conversion lines of Th B served to check the calibration of the magnetic field of the spectrometer, and those on Cu^{64} provided a reference line in the neighborhood of 0.5 Mev for comparison with other annihilation radiation lines, if such were found.

2. EXPERIMENTAL DETAILS

The magnet used for this work consists of two Armco iron forgings with a total weight of about two tons. The pole faces are circular, about 16″ in diameter; the gap is 4″. In this work the magnetizing current, which passed through coils of copper strip, was supplied by a bank of automobile storage batteries. No regulation other than manual was employed. Despite its somewhat massive construction and the comparatively low magnetic fields used, there was enough hysteresis in the magnet so that the same current did not give the same magnetic field. Consequently current measurements were used only to establish the increments between successive fields; the fields were measured with a 6000-turn flip coil and ballistic galvanometer. The calibration of the flip coil was made against two standard flip coils of large diameter (3″) which had been very carefully made. The area-turns of these two coils were compared in a fixed magnetic field (the remanent field of the above magnet was used) and found to be the same to one part in 1000. By mounting the flip-coil, which was used in these measurements, concentrically and consecutively in each of the standard coils it was possible to obtain an

equivalent area-turn for it. The ballistic galvanometer was calibrated against a home-made mutual inductance which, in turn, was standardized against a Leeds and Northrup mutual inductance, using the value given by the Bureau of Standards who had recently calibrated it.

Two vacuum chambers were used in this work. The first of these was a modification of a chamber which had been used for some earlier work in this Department. The modification consisted in installing lead shielding between source and counter, arranging an easily accessible source mounting, and installing slits and a Geiger-Müller counter. A radius of curvature of 13 cm was chosen for the first chamber. This was checked in the actual instrument to about two parts in 1000. Because of the diameter of the pole faces the beam of electrons is always in a very nearly uniform field. Steel lids reduced the total gap to $2\frac{1}{4}''$ of which $1\frac{3}{4}''$ was the "vacuum" gap. There were only two slits: one at the half-way point 25.4 mm wide and the other immediately before the counter window 1 mm wide. The first defining slit was aluminum-clad lead. The counter was entirely in the main vacuum, but could be filled from outside. It consisted of a block of copper with a $\frac{1}{4}$-in. hole drilled in it. To its ends were attached metal-to-glass seals and between these was stretched the central wire of about 0.003-in. tungsten. In the side of the copper block and perpendicular to the axis a hole about 3×5 mm was cut and over this a thin window was clamped. In this work all windows were 0.001-in. aluminum made vacuum-tight by being clamped against a 0.007-in. indium gasket. Such a thick window cannot pass electrons whose energy is much below 100 kev.

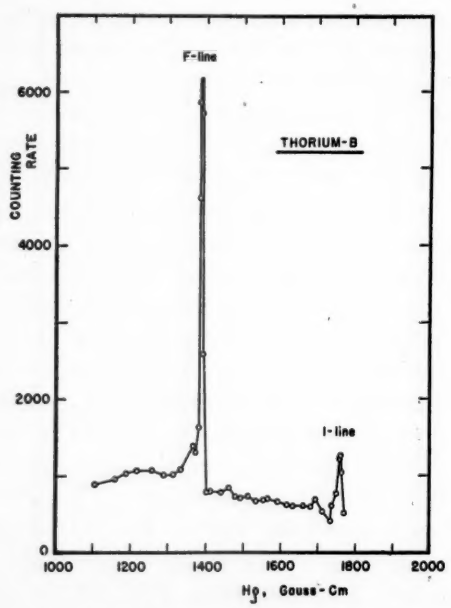

FIG. 1. The *F*- and *I*-lines of ThB. The region between these two lines and on either side was not searched carefully. There are numerous small lines in these regions. The width of the *F*-line corresponds to a resolution of 0.6 percent. The energy values deduced from the extrapolation of the high side of the line to the background are in good agreement with previous determinations.

The second chamber differs from the first in being more carefully designed and constructed. The source is inserted through an air-lock and all of the slits can readily be removed so that their aperture can be changed, if desired. The counter in the second chamber is of the end-window type and has a much larger window, $1\frac{1}{4}''\times\frac{5}{16}''$. The arrangement of the slits, the length of the magnetic air gap, and the flip coil are all identical in the two chambers. The radius of curvature of the electrons was increased to 14 cm and this figure is known with the same accuracy as in the previous case. A minor feature of the second chamber is that everything including the cover lids is positioned by metal-to-metal seats, through the use of radial *O*-ring seals. In general the vacuum used in this work was around 10^{-5} mm of mercury.

For the measurement of γ-ray energies the following procedures were used. With those substances which have particle radiation it is necessary that they be absorbed. The γ-rays are then measured by determining the energies of the secondary electrons which they eject from suitable radiators. In this paper we shall mostly be concerned with the photoelectrons ejected from a thin lamina of uranium metal. The radioactive material is placed in a small copper "boat" whose bottom is $\frac{1}{4}''\times1''$. The long dimension is mounted parallel to the magnetic field. The interior is hollowed out to form a cavity $\frac{1}{8}''\times\frac{7}{8}''$. The depth of this hollowing is such as to give a thickness of $\frac{1}{16}''$ to absorb the nuclear β-rays. This is quite adequate for most radioactive materials. To the bottom of this boat is glued a piece of uranium foil about 50-mg/sq. cm thick. When there is no particle radiation the radioactive substance is sealed in a thin glass tube

and mounted in a skeleton Lucite frame so that the glass tube is in contact with a similar piece of uranium foil.

Compton electrons are ejected from the material of the boat, from the source material and from the uranium foil. They are always present as a background. In addition photoelectrons from the uranium form sharp spires on this Compton distribution. From the known facts about the absorption and straggling of homogeneous electrons as they pass through matter, it is clear that the energy corresponding to one of the photoelectron lines is obtained by extrapolating the high energy side of such a line to the background. Usually the lines are so steep on their high energy side that this extrapolation presents no problem which might otherwise arise if there were uncertainty as to the location of this background. In all cases which have been examined both the K and the L photoelectrons are observed, and the γ-ray energies deduced from both have been found to be identical within experimental error. The γ-ray energies quoted will be those corresponding to the K-line. In all of the curves shown here irregularities on the low energy side of an intense peak are noticed. Because of their systematic regularity in all data taken with the first chamber (Cu^{64}, Be^{7}) they are thought to be caused by scattering. For the binding energy of the K-shell of uranium the value 116.4 kev was used; for the L-shell, 22 kev.

No special care was taken in preparing the counters except to have them very clean. The central wire was either heated to incandescence under a good vacuum or else was cleaned electrolytically. Various conventional quenching vapors were used without there being much noticable difference among them. Lately this laboratory has been experiencing good results with ethylene as a quenching gas. Good evacuation with a diffusion pump appears to be desirable.

The counter was connected to a scaling circuit (Instrument Development Laboratories Model 161) with a scale of 256. This had been modified so that scales of 8, 16, 32, 64, 128 or 256 could be used. No quenching circuit was used. An electric timer and a message register completed the recording equipment. In general counts were taken for a fixed length of time, so that the statistical accuracy is better at high counting rates than at low.

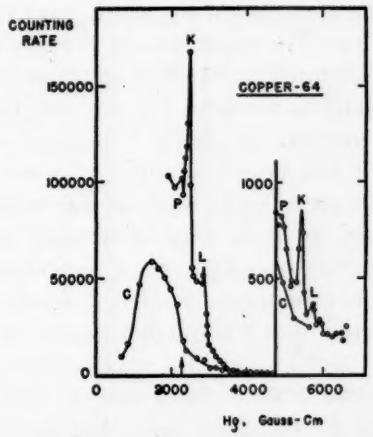

FIG. 2. The momentum distribution of photoelectrons (curve P) from a 50 mg/cm² uranium radiator due to the radiations from Cu^{64}. The lower curve, marked C, is the Compton distribution from the same γ-rays. The insert is a 100-fold magnification of the high energy end of both distributions. In the insert are seen the K- and L-photoelectron peaks from the nuclear γ-ray at 1.34 Mev. The arrow marks the position of the expected end of the Compton distribution if there were no annihilation radiation from moving positrons.

3. THORIUM—B

The original purpose of measurements on ThB was to check the accuracy of the magnetic field calibration, which was described earlier. The source was thorium active deposit on a 0.00025″ thick aluminum foil 1 mm wide. Since the gamma-rays of ThB are strongly internally converted, no radiator was needed to get the sharp peaks shown in Fig. 1. The taller of the two peaks is, in Ellis' notation, the F-line while the smaller is the I-line. These have been measured probably most accurately by Ellis[1] and Siegbahn[2] who give, respectively, 1385.8 and 1383.8 for the $H\rho$ of the F-line and 1749.6 and 1751.0 for that of the I-line.

The present work makes no claims to accuracy of the same order as that of the highly precise measurements to which reference has been made. Our values of 1395 $H\rho$ for the F-line and about 1770 $H\rho$ for the I-line merely indicates the differences between our flip-coil calibration and this more precise calibration based on these two lines. This difference of about 0.7 percent for

[1] C. D. Ellis, Proc. Roy. Soc. **A138**, 318 (1932).
[2] K. Siegbahn, Arkiv f. Mst. Astr. och Fysik, **30A**, No. 20 (1944).

the K-line is corrected for in the data to be discussed later. The resolution of the spectrograph can be estimated by the half width of the F-line and is found to be about 0.6 percent. The calculated resolution is about 1 percent and this difference has been a matter of some concern to us. No use is to be made of the resolution in this paper, so it is only interesting in understanding the operation of a spectrometer. A reasonable explanation is that the extreme outside electron path is through a somewhat weaker magnetic field which, for monochromatic electrons, would tend to throw more of them toward the head of the line, thus making it appear narrower. This same effect has been noticed in another spectrometer in this laboratory.

4. COPPER—64

A source of Cu^{64} was made by bombarding a copper plate with 11-Mev deuterons in the Washington University cyclotron. Some shavings were taken from this plate and, after they had aged for 4–5 hours to let the short-lived contaminating activities die off, they were placed in the copper boat with a uranium radiator on its bottom. The resulting distribution is shown in Fig. 2. Both the K- and L-peaks corresponding to the half-million electron volt annihilation radiation are observed on the curve marked P. The corrected $H\rho$ value as here observed is 2480 corresponding to an energy of 0.510 Mev. This establishes the position and appearance of an annihilation line in our particular spectrometer.

In the insert is shown a 100-fold magnification of the high energy end of the secondary electron spectrum, showing the K-line at 5550 $H\rho$ corresponding to 1.34 ± 0.01 Mev. This line has been observed by several authors.[3,4] Our value is seen to be in good agreement with the figure 1.35 Mev obtained by Deutsch. No attempt has been made here to estimate the intensity of this line relative to that of the annihilation line. Also shown in Fig. 2 is the distribution curve of the Compton electrons knocked out of the copper boat. This is the lower curve marked C in both the main part of the figure and the insert. It is lower and very broad because about half of the Compton electrons are contributed by the uranium radiator and because the thickness of the copper spreads the Compton distribution by straggling. The arrow arising from the axis of abscissae indicates the position of the upper limit of the Compton electrons if the annihilation radiation had a sharp energy of 0.511 Mev. That the distribution extends beyond this point is indication, as Deutsch has also shown,[3] of the existence of radiation caused by the positrons being annihilated in flight. As suggested by the curve on the insert to Fig. 2 this Compton distribution seems to extend at least up to $H\rho$ 5250, corresponding to an energy of 1.35 Mev, which is the maximum energy expected theoretically. The data are not sufficiently good statistically to argue that the extension beyond this point is real.

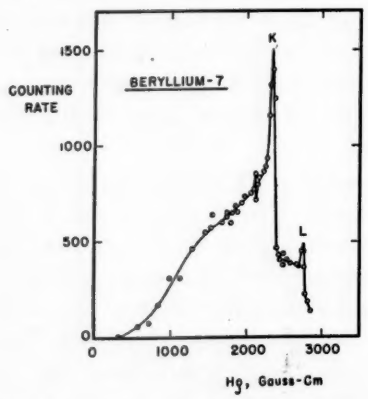

FIG. 3. The momentum distribution of photoelectrons from the same uranium radiator due to the γ-radiation from Be^7. There appears to be only one strong γ-ray from this element. The energy of it found here is 485 kev.

5. BERYLLIUM—7

Beryllium-7, which decays with a half-life of 53 days, can easily be made by bombarding lithium with deuterons according to the process: $Li^6(d,n)Be^7$. Such a source was prepared by bombarding pure lithium metal for 10,000 microampere hours with 11 Mev deuterons in the cyclotron. The beryllium was chemically separated, following a procedure suggested by Dr. Gerhard Friedlander. The resulting activity was sealed in a thin-walled glass tube and placed in immediate contact with a thin uranium radiator of the same size as had been used in our other measurements. The energy distribution of the photoelectrons ejected from the uranium is shown in Fig. 3. The corrected $H\rho$ of the K-peak

[3] M. Deutsch, Phys. Rev. **72**, 729 (1947).
[4] Bradt, Gugelot, Huber, Medicus, Preiswerk, Scherrer, Steffen, Helv. Phys. Acta **19**, 219 (1946).

is 2380 corresponding to a gamma-ray energy of 0.485 ± 0.005 Mev.

Previous work on this γ-ray has followed two lines of attack, as summarized by Zlotowski and Williams[5] and by Siegbahn.[6] One of these has been, of course, the direct measurement of the γ-ray energy. The other has been to study the excited states of Li^7 formed in the reactions: $Li^6(d,p)Li^7$, $Be^9(d,\alpha)Li^7$, $B^{10}(n,\alpha)Li^7$. Results obtained to date have not shown very good agreement with each other. In general the excitation energy of Li^7 has been somewhat higher than the measured γ-ray energy. Thus the following values (quoted without limits of error) have been found for the energy of the excited state of Li^7: (see reference 5 for bibliography) 455, 495, 494, 470, 480 kev. These are to be contrasted with the following γ-ray energies: 425, 459 kev. Zlotowski and Williams, using Bothe's coincidence method, found a value of 485 kev for this γ-ray, while Siegbahn, using a β-spectrometer, finds a value of 453 kev. Both of these authors had, as compared to ourselves, quite weak sources and, as suggested by Siegbahn, it would be possible to deduce appreciably different values from the data of Zlotowski and Williams. To get the value he gives, Siegbahn seems to have chosen the top of the K-line peak. Since there is some debate as to what is the proper point on a photoelectron line to use in deducing the γ-ray energy and since this point may differ for different types of spectrometers, it is possible that Siegbahn's data could be interpreted to give a higher energy. As previously stated, on the basis of measurements of the straggling of homogeneous electrons, we subscribe to the method of extrapolating the high energy side of a photoelectron peak to get its energy, at least in the case of a 180° spectrometer.

The value which has been found here seems to be in good agreement with the measurements on the excitation energy of Li^7. The deviation of this value from that of the 0.511 Mev of annihilation radiation is well outside of experimental error so we must conclude that there is no evidence here for the process discussed at the beginning of this paper.

[5] I. Zlotowski and J. H. Williams, Phys. Rev. **62**, 29 (1942).

[6] K. Siegbahn, Arkiv f. Mat., Astr. o. Fysik **34B**, No. 6 (1946).

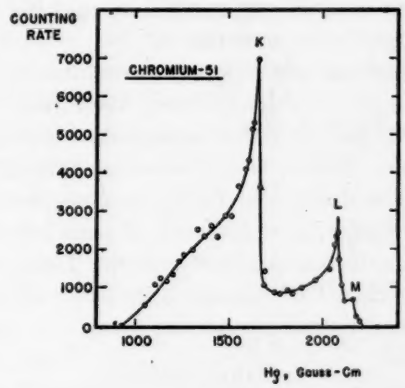

FIG. 4. The momentum distribution of photoelectrons from the same uranium radiator due to the γ-radiation from Cr^{51}. There appears to be only one strong γ-ray from this element. The energy of it found here is 320 kev.

6. CHROMIUM—51

A radioactive substance whose half-life is about 26.5 days and which has been identified as Cr^{51} was discovered and studied by Walke, Thomson and Holt.[7] These authors ascertained that it decays by K-capture and, by absorption, measured γ-ray energies of 0.5 and 1.0 Mev. They also report that the 1.0-Mev γ-ray is internally converted to the extent of 0.1 percent. Later Miller and Curtiss[8] listed the Cr^{51} γ-ray as 0.32 Mev. This appeared to be a likely substance to use to examine the notion of slow positron annihilation.

A sample of Cr^{51} was obtained from Oak Ridge and carefully purified chemically following a procedure suggested by W. H. Burgus. The purified sample was divided into several parts and the largest of these was mounted in a thin-walled lucite tube close to a uranium radiator as in the case of Be^7. Figure 4 shows the momentum distribution of the photoelectrons from this radiator. It will be noticed that there appears to be only one γ-ray as is evidenced by the K- and L-peaks. The corrected $H\rho$ for the upper limit of the K-line is 1670, corresponding to a gamma-ray of 320 ± 5 kev. This is in very good agreement with the value found by Miller and Curtiss. The region where one would expect to find photoelectrons from a 1.0-Mev gamma-ray

[7] H. Walke, F. C. Thomson and J. Holt, Phys. Rev. **57**, 171 (1940).

[8] L. C. Miller and L. F. Curtiss, Phys. Rev. **70**, 983 (1946).

was very carefully searched but nothing above background was detected.

Another sample of the same material was mounted on a thin foil and used as a β-ray source to look for the conversion electrons reported by Walke, in an attempt to find some positron emission. In both cases no detectable particle radiation was found of sufficient energy to penetrate our counter window. These results indicate that Cr^{51} decays simply by K-capture with the emission of one soft γ-ray.

7. CONCLUSIONS

In the two K-capture elements tested there is no evidence of annihilation radiation resulting from the emission of very slow positrons. In our experiments no positron of energy lower than about 100 kev could enter our counter. It is believed that it would be profitable to pursue this problem further, however, since in many cases the evidence for $\bar{K}$-capture would not exclude the possibility of slow positron emission.

We take great pleasure in thanking Mr. J. E. Robinson for the very able assistance he rendered in the many long "runs" which were involved in this work and its preliminaries. Our grateful thanks are also due to Dr. Lin-Sheng Tsai, to Dr. Gerhard Friedlander, and to Mr. W. H. Burgus for their assistance and counsel on matters chemical.

This work has been supported in part by a grant from the Research Corporation to one of us (FNDK) and by the Office of Naval Research under Contract N6ori-117.

PHYSICAL REVIEW VOLUME 74, NUMBER 6 SEPTEMBER 15, 1948

The Beta- and Gamma-Rays of Rb^{86}

DANIEL J. ZAFFARANO, BERNARD D. KERN, AND ALLAN C. G. MITCHELL
Indiana University, Bloomington, Indiana

(Received June 1, 1948)

The beta- and gamma-rays of Rb^{86} (19.5 d) have been measured in a magnetic lens spectrometer. Measurement of the energies of photoelectrons produced in a lead radiator shows one line corresponding to a gamma-ray of energy 1.081 Mev. The beta-ray spectrum is resolvable into two groups with end point energies of 1.822 and 0.716 Mev.

I. INTRODUCTION

TWO rubidium isotopes of 18 minutes and 19.5-day half-lives were reported by Snell.[1] Later Helmholz, Pecher, and Stout[2] showed that the activity of 19.5 day half-life must be attributed to Rb^{86}. They measured the beta-ray end point by absorption in aluminum and obtained a value of 1.56 ± 0.05 Mev. Haggstrom[3] measured the beta-ray spectrum of this isotope in a solenoid type magnetic analyzer. She made a Fermi plot of her data and found a beta-ray end point of 1.60 ± 0.03 Mev. The Fermi plot was not a straight line at the low energy end, but she attributed this to the fact that Rb^{86} belongs to the second forbidden class.

Preliminary work in this laboratory showed that a low intensity gamma-ray accompanies this activity. A rough estimate of the energy of the gamma-ray was obtained by measuring the coincidence absorption of Compton electrons produced in an aluminum radiator. The value obtained for the energy of this gamma-ray was approximately 1 Mev. In order to determine the disintegration scheme, the authors decided to investigate the spectrum in a magnetic lens spectrometer. The spectrometer has been described elsewhere.

II. PURIFICATION OF SOURCE MATERIAL

Strong sources of Rb^{86} were obtained from Oak Ridge. The main impurity in the source

[1] A. H. Snell, Phys. Rev. **52**, 1007 (1937).
[2] A. C. Helmholz, C. Pecher, and P. R. Stout, Phys. Rev. **59**, 902 (1941).
[3] E. Haggstrom, Phys. Rev. **62**, 144 (1942).

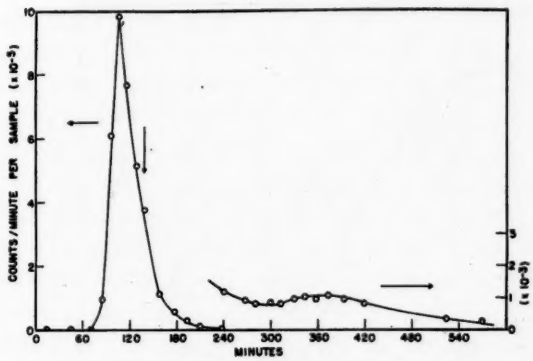

FIG. 1. The separation of Rb^{86} from Cs^{134} in an ion exchange column.

appeared to be Cs. The activity of Cs^{134} was found to be present and the gamma-rays of Cs^{134} were identified when the gamma-ray spectrum from the unpurified sample was measured. The separation of small quantities of Cs from Rb has, until recently, been quite a tedious process. However, with the advent of the ion exchange resins, and tracer techniques, the separation of these two elements has become quite simple.[4]

The ion exchange column used in these experiments was 1.5 meters long and 1 cm in diameter. It was filled with the resin called "Amberlite 200." The column was prepared by filling it with

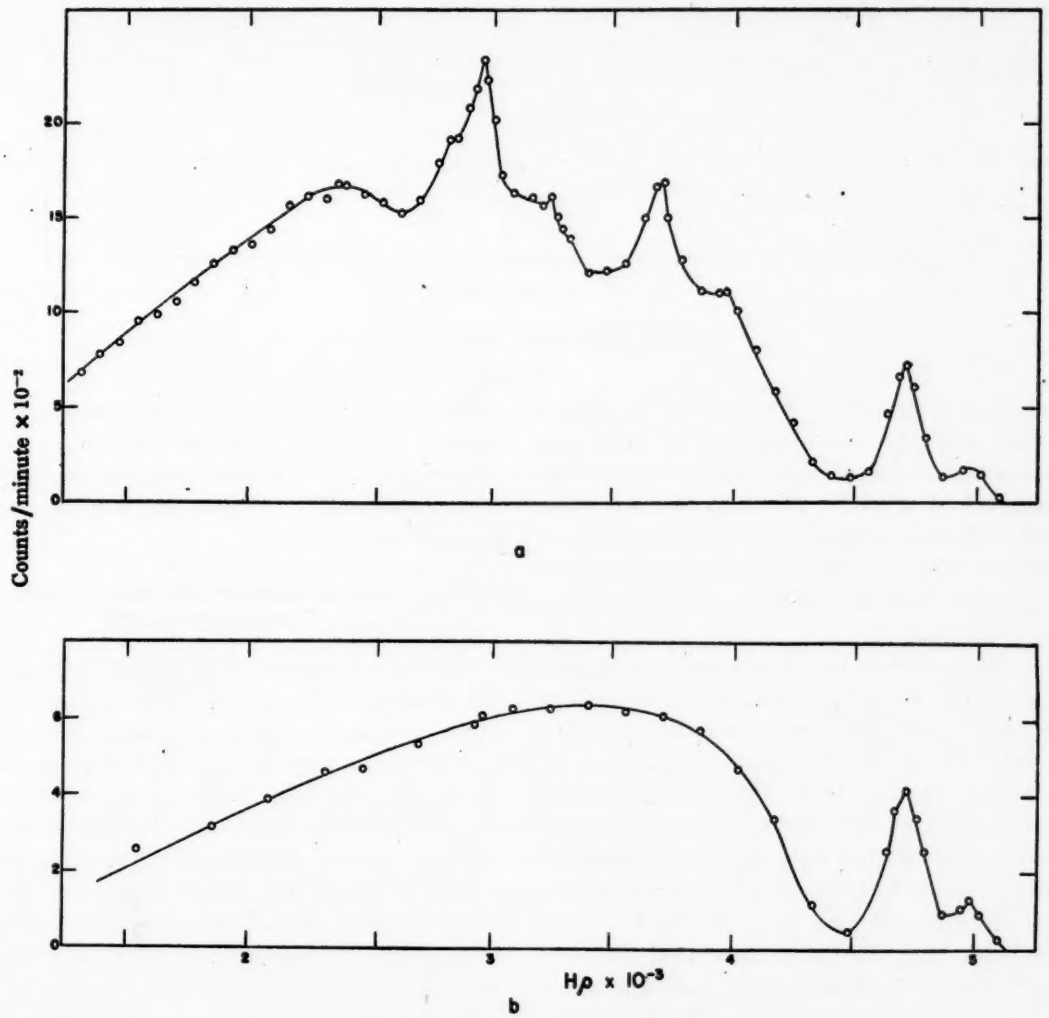

FIG. 2. Photoelectrons ejected from lead by gamma-rays. 2a. Unpurified source, showing gamma-rays of Cs^{134} and Rb^{86}. 2b. Purified source; gamma-ray of Rb^{86}.

[4] The authors are indebted to Dr. G. E. Boyd of Clinton Laboratories for calling their attention to this method. Many papers describing this method are to be found in the *Journal of the American Chemical Society* for November, 1947.

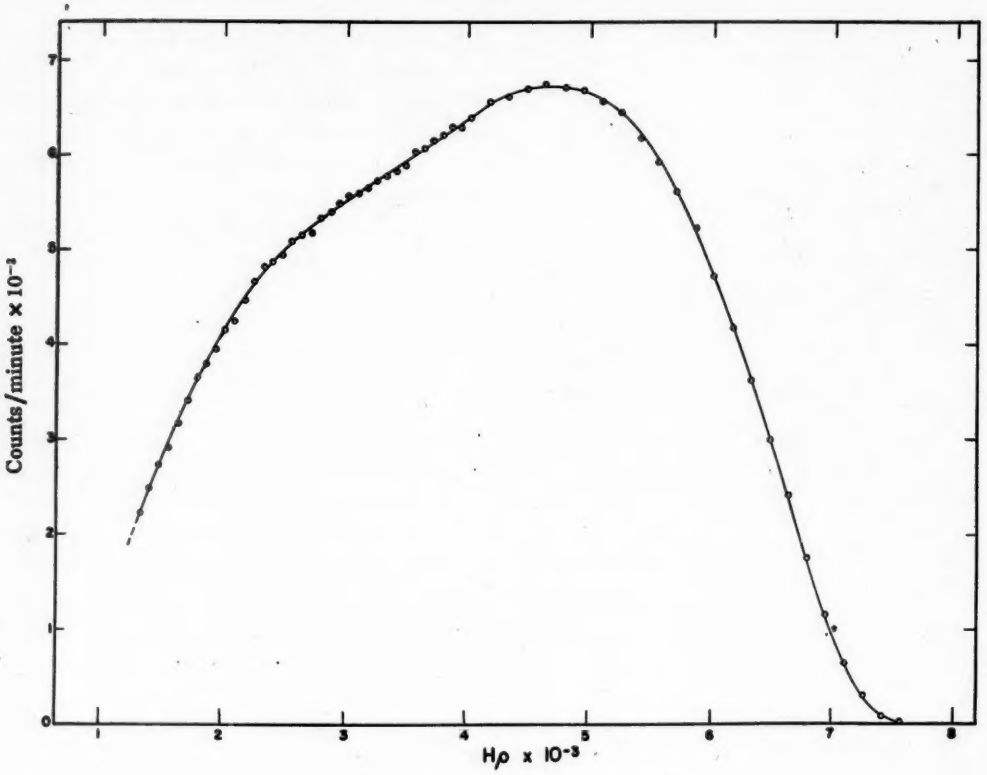

FIG. 3. The beta-ray spectrum of Rb^{86}.

the resin and a solution of 0.1 N HCl. The source material, Rb_2CO_3, was dissolved in HCl and enough additional acid was added to make the solution 0.1 N in HCl. The solution was then poured into the column and the column was washed, or eluted, with 0.1 N HCl at a constant rate. The flow rate used in these experiments was about 2 cm^3/min.

In order to follow the separation, a standard volume of the solution issuing from the bottom of the column was taken every few minutes. The activity of this standard sample was then measured with a counter. When the activity became too strong for counting, the sample was suitably diluted and an aliquot part therefrom taken for counting. A plot of the activity of successive samples against the time is shown in Fig. 1. It will be seen that the peak associated with rubidium is quite well separated from the small peak associated with cesium. The rubidium sample separated for study was taken off shortly after the rubidium peak had been passed, as indicated by the vertical arrow in Fig. 1. In some experiments the purified rubidium was again run through a freshly prepared ion column. After purification the solution containing rubidium was evaporated to dryness and was used in the preparation of sources.

III. MEASUREMENT OF THE GAMMA RADIATION

Gamma-ray sources were prepared by packing the solid salt into a cylindrical copper capsule whose walls and base were just thick enough to stop all beta-rays. A lead radiator, of surface density 26 mg/cm^2, covered the base of the cylinder to serve as a source of photoelectrons. The capsule was then placed in the magnetic lens spectrometer and the number of secondary electrons (photoelectrons and Compton electrons) were counted as a function of the current through the coil.

The results of the measurement on the purified source are shown in Fig. 2b, in which the counting rate is plotted as a function of the momentum of the electrons (in gauss-cm). There are

two peaks, one at 4685 $H\rho$ and one at 4950 $H\rho$. These are the K and L photo lines excited in lead from a gamma-ray of 1.081 ± 0.006 Mev. If the binding energies of the K (0.088 Mev) and L (0.016 Mev) shells of lead are added to the energies of the respective photo-lines, one obtains $E_\gamma = 0.993 + 0.088 = 1.081$ Mev and $E_\gamma = 1.068 + 0.016 = 1.084$ Mev. In addition the distribution of the accompanying Compton electrons may be seen.

In Fig. 2a the results of a similar measurement taken earlier using the unpurified sample are shown. In addition to the lines shown in Fig. 2b, K and L lines from a gamma-ray at 0.795 Mev, and K lines from gamma-rays at 0.604 and 0.568 Mev are to be seen. These lines have been observed previously by Elliott and Bell[5] and are to be attributed to Cs^{134}.

Since the original source contained impurities, it was necessary to show that the 1.081 Mev line is to be attributed to Rb^{86}. This was done by measuring the K-photo peak and selected points on the Compton distribution for the purified source over a long period of time. These measurements were monitored by a small uranium source which could be placed in front of the counter window in the instrument. All points followed a 19.5-day period to within ± 5 percent.

IV. MEASUREMENT OF THE BETA-RAY SPECTRUM

The beta-ray spectrum was measured with sources of surface densities 0.45 mg/cm² to 9 mg/cm², on backings of Zapon film, paper, or aluminum foil weighing less than 1 mg/cm². A typical example is shown in Fig. 3. It will be noticed that the shape appears to indicate a complex spectrum. The Fermi plot for this spectrum is shown in Fig. 4.

An inspection of the Fermi plot reveals that the points near the end point drop slightly below

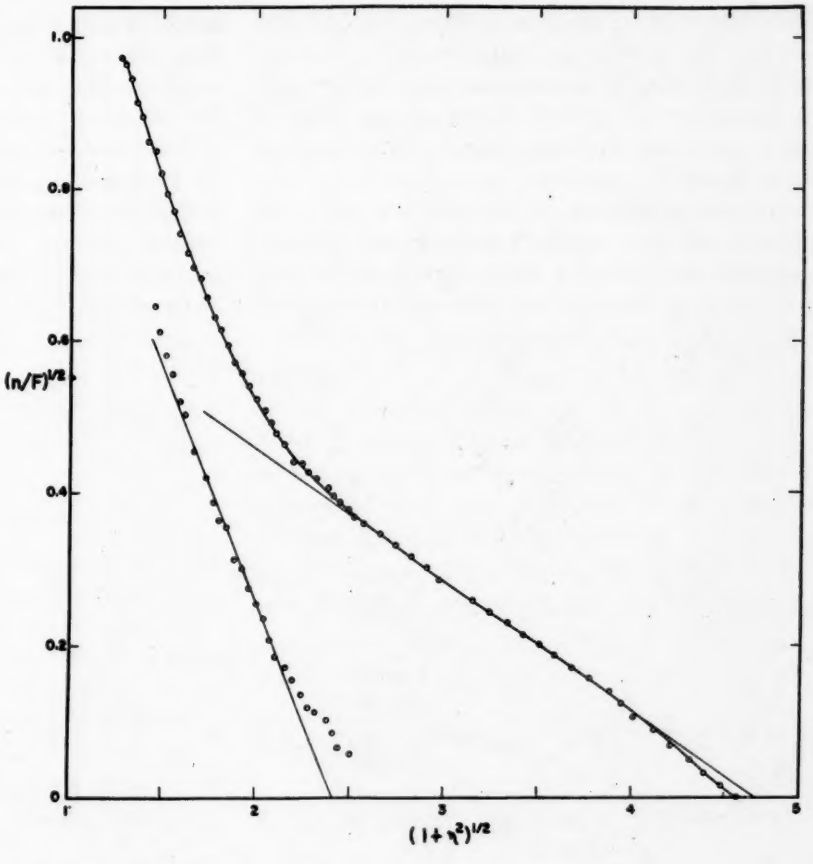

FIG. 4. Fermi plot of the beta-ray spectrum of Rb^{86}.

[5] L. G. Elliott and R. E. Bell, Phys. Rev. 72, 979 (1947).

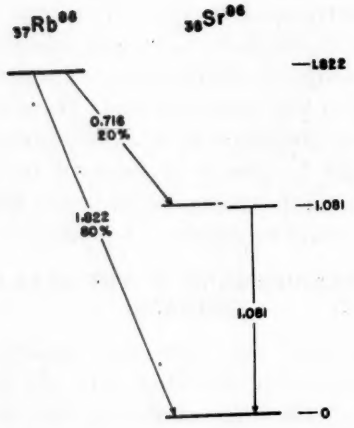

FIG. 5. Disintegration scheme of Rb^{86}.

the best straight line that can be put through the remainder of the points in the high energy group. This effect was found in every spectrum which was analyzed. The explanation is probably to be found in the fact that the spectrum of Rb^{86} belongs to the second forbidden class. The end point obtained for the extrapolated straight line is 1.855 Mev, while the actual end point is 1.822 Mev. A definite deviation from this straight line at the lower energy end allows one to separate out a second beta-group with an end point of 0.716 Mev.

Six determinations of the high energy end point have been made. These give an average value of 1.822 ± 0.014 Mev. The lower energy group has an average end point of 0.716 ± 0.02 Mev. The difference between these two end points is 1.106 Mev, which is to be compared with the gamma-ray energy of 1.081 Mev previously mentioned. The small discrepancy is probably due to the difficulty of determining accurately the end point of the inner beta-group.

The low energy beta-group comprises 20 percent of the total beta-emission. This fraction has been observed to remain approximately constant in data taken over a period of two half-lives.

V. DISCUSSION

An energy level scheme can now be drawn up for the disintegration of Rb^{86} into Sr^{86}. This is shown in Fig. 5. It will be seen that in 80 percent of the disintegrations there is a direct transition to the ground state with the emission of a beta-ray of 1.822 Mev, and in the remainder, a transition to an excited state of Sr^{86} with the subsequent emission of a gamma-ray of energy 1.081 Mev. A confirmation of this scheme has been found by Mr. E. T. Jurney who has made coincidence measurements on this material. He finds that there are no gamma-gamma-coincidences and that there are beta-gamma-coincidences only for beta-energies less than 0.6 Mev.

The authors wish to express their indebtedness to Professor L. R. Merritt of the Chemistry Department for his help in work on ion exchange columns. This work has been supported by the Office of Naval Research under Contract N6ori-48, T.O. 1.

The Spectral Emissivity of Iron and Cobalt

H. B. WAHLIN AND HARRY W. KNOP, JR.
Department of Physics, University of Wisconsin, Madison, Wisconsin

(Received June 2, 1948)

The spectral emissivity of iron and cobalt has been determined as a function of the temperature. Sharp, definite changes in the emissivity have been observed in iron at the A_3 and A_4 point and at the Curie temperature for cobalt. A gradual change takes place in cobalt in the region where, presumably, the cobalt structure changes from hexagonal to cubic. A decrease in the neighborhood of 1370°K has been observed for iron.

IN an earlier report[1] it has been shown that when the temperature of iron is increased through the A_3 point there is a decrease in the emissivity. In the results submitted below the earlier findings have been extended and improved and a new series of values for both iron and cobalt have been found.

The technique used in determining the emissivity has been described in reference 1. Briefly, it consists in forming a hollow cylinder of the material by wrapping a flat, uniform strip of the material 12–15 cm long around a 3-mm rod and spot-welding the overlapping portion. A hole about $\frac{1}{2}$ mm in diameter is drilled in the side of the tube at the midpoint. This hole serves as a source of blackbody radiation. The tube is mounted in a glass bulb fitted with a flat glass window and is connected to a vacuum system so that it can be degassed and heat-treated.

The procedure in determining the spectral emissivity is then to match a disappearing-filament optical pyrometer on the hole and on the outside of the cylinder, and from these two temperatures to compute the emissivity, using the relation

$$ln\epsilon=(c_2/\lambda)[(1/T_1-(1/T_2)],$$

where T_1 is the true or hole temperature and T_2 is the apparent temperature determined by the radiation from the outside of the cylinder.

The iron used in these determinations was prepared electrolytically by depositing on a stainless steel strip from a ferrous chloride bath. This deposit was removed from the stainless steel and used as anode in a second bath from which the final deposit, again on stainless steel, was obtained. It was found that a sulfate bath was unsuitable for the deposition because of the inclusion of sulfur in the deposit. In fact, enough sulfur was included so that in subsequent annealing in hydrogen a distinct odor of hydrogen sulfide was detectable.

The final strip from the chloride bath was annealed in hydrogen and rolled with frequent annealings to a final thickness of 0.07 mm.

It was necessary to make the emissivity determinations on iron in an atmosphere of hydrogen in order to reduce the sublimation of the metal. The hydrogen pressure used was about 15 cm.

Figure 1 shows the results obtained for iron. The values shown here are lower than those reported in the reference above. This may be due to the presence of hydrogen in solution in the metal although this is doubtful for the following reasons:

After the data had been obtained the hydrogen pressure was reduced and no change in emissivity was noted before the pressure reached a value of about 0.01 mm. When the gas was removed completely the emissivity at a temperature of 1220°K rose gradually from 0.325 to 0.36 over a period of days. However, if the cylinder was flashed for a few seconds to a temperature of 1500°K after the 0.36 value was reached,

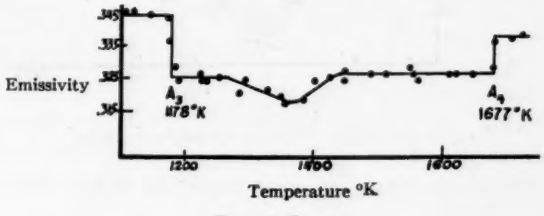

FIG. 1. Iron.

[1] H. B. Wahlin and Rufus Wright, J. App. Phys. **13**, 40 (1942).

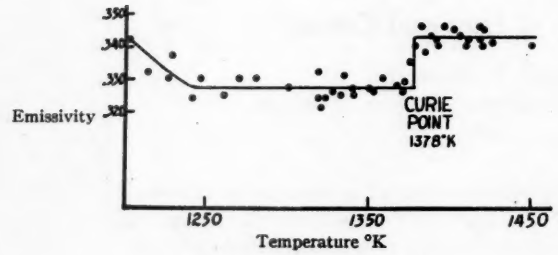

FIG. 2. Cobalt.

the emissivity at 1220°K was reduced to a lower value. Unfortunately, the life of a cylinder was short with this strenuous treatment, so that the effect could not be repeated more than two times. Even though it is qualitative, it is indicated that the low value obtained here is not due to the solution of hydrogen in the iron. It is hoped that this effect can be studied for another metal more suited to the experiment than is iron.

The temperature of the A_3 point as determined here is 1178.3°K, in good agreement with the accepted value of 1179°K. The temperature found for the A_4 point is 1677°K. The dip in plot at around 1360° cannot be correlated with any known phenomenon in iron.

Figure 2 shows the results on cobalt prepared electrolytically from a chloride bath. These data were obtained in a vacuum. The gradual decrease in the emissivity with increasing temperature at the lower temperature end of the curve is possibly due to a change from the cubic to the hexagonal form, a change for which some evidence exists.[2] The gradual slope suggests that the change is sluggish just as it is for the change from the hexagonal structure at room temperature to the cubic form above 713°K. However, the evidence for the existence of the higher temperature hexagonal form is not definite. In fact, Marick[3] made a careful crystallographic x-ray analysis of cobalt as a function of temperature and found no evidence for the existence of the hexagonal structure.

More recently, W. P. Sykes[4] in a discussion of a paper by Ellis and Greiner tells of results which indicate that a prolonged heating of cobalt powder at a temperature of 1200°C increases the amount of hexagonal cobalt at room temperature relative to the cubic.

That the increase in the emissivity with decreasing temperature is not due to the formation of an oxide is indicated by the following test. A determination of the emissivity was made at a temperature above the point where the rise begins and the temperature was lowered to a point on the rising part of the curve and a second value found. This value was higher than the high temperature one. The cylinder was left at this lower temperature for 24 hours and no further rise was noted. The temperature was now lowered still further and a still higher value was found. Then, the temperature was raised again to the second value and a determination was made as soon as the temperature equilibrium was established. This value agreed with the other two values obtained at this temperature.

Hydrogen was next introduced and, while it seemed to lower the temperature at which the rise begins by about 35°, it did not cause a disappearance of the rise.

The sharper rise in the emissivity at about 1378°K corresponds to the Curie temperature. In this curve this change is indicated as a rather sharp break. It is doubtful whether the change is as sudden as indicated.

Figure 3 shows the results from a Co-Ni alloy (65 percent Co) kindly prepared by E. M. Wise of the International Nickel Laboratories. The dip in the curve corresponds to the Curie temperatures. These data were obtained shortly after the cylinder was mounted and before extensive heating. With continued heating the emissivity rose and the dip became less pronounced. This probably was due to the diffusion to the surface of impurities which masked the effect. The sample admittedly was not pure.

A possible application of variation of the emis-

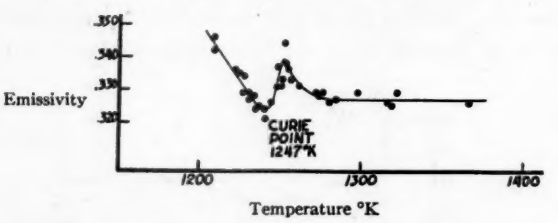

FIG. 3. 65 percent cobalt, 35 percent nickel.

[2] *Metals Handbook* (American Society for Metals, 1939), p. 1628.
[3] Louis Marick, Phys. Rev. **49**, 831 (1936).
[4] W. P. Sykes, "Ellis and Greiner," Trans. Am. Soc. for Metals **21**, 415 (1941).

sivity with structural change is shown in Fig. 4. Here the difference in the pyrometer current when it is matched on the hole in the cylinder and that when matched on the outside is plotted against the pyrometer current when matched on the hole. This plot is for points in the neighborhood of the A_4 point for iron. As is seen from this plot, a rather sharp break occurs. The two points on either side of the break are $1\frac{1}{2}°$ apart. This suggests that such breaks can be used as convenient secondary-temperature standards for checking the calibration of optical pyrometers. A series of such standards can probably be prepared at desired temperatures. Unfortunately, two pyrometers were used around the A_3 point, so a similar plot could not be made for this region.

As far as the authors know, no adequate explanation exists to account for the changes observed. However, a justification for this work can be made as follows:

(a) The change in emissivity with change in structure or with change in intermetallic compound introduces a variable which should be of help in the search for a theoretical explanation of the radiation from metals when heated.

(b) A plot of emissivity as a function of temperature will, in the case of many alloys, show the temperature at which structural changes take place.

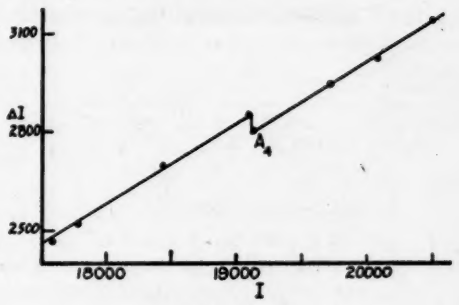

FIG. 4. Iron.

(c) The method gives a means of determining the Curie temperature pyrometrically and at zero magnetic fields.

(d) It also raises the possibility of establishing standard temperatures in addition to the well established melting-point standards.

The method is being extended to alloys, the results on which will be published at a later date.

Since this manuscript was prepared, the authors have been advised that emissivity determinations on iron obtained by A. G. Worthing and his co-workers show a drop at the A_3 point similar to that reported here.

In conclusion the authors wish to extend their sincere thanks to Mr. E. M. Wise of the International Nickel Company for furnishing the Co-Ni alloy.

This work was supported in part by a grant from the Wisconsin Alumni Research Foundation

---

PHYSICAL REVIEW VOLUME 74, NUMBER 6 SEPTEMBER 15, 1948

Configurations of the Low Terms of Ti II

HENRY NORRIS RUSSELL
Princeton University Observatory, Princeton, New Jersey

(Received June 1, 1948)

Series relations among the high even terms of Ti I afford conclusive evidence that the lower of the two ^4F terms in Ti II arises from the configuration d^2s, and the other from d^3.

THE Ti II spectrum is unique in having as its lowest levels a pair of terms of the same multiplicity and name, less than 1000 cm^{-1} apart. One of these ^4F terms undoubtedly arises from the configuration $3d^24s$, and the other from $3d^3$, but they are so close together that it is hard to be sure which is which. The writer[1] concluded, from the intensities of the combinations, that the lower term, a^4F, arose from d^2s. Dr. A. Many,[2] from theoretical calculation of the levels of the

[1] H. N. Russell, Astrophys. J. 66, 283 (1927).
[2] A. Many, Phys. Rev. 70, 511 (1946).

TABLE I. Rydberg denominations for limit d^n.

Added Electron		4s	5s	6s	4d
Ca I	l				
	h	1.604	2.657		
Sc I	l	1.598			
	h	1.541	2.634		
Ti I	l	1.569			
(a)	h	1.489	2.545	3.577	2.997
V I	l	1.545	2.582		
	h	1.449	2.522		2.981
Cr I	l	1.529	2.567	3.578	
	h	1.418	2.493		2.989
Ti I	l	1.596			
(b)	h	1.514	2.678	3.979	3.221

low even terms, attributed it to d^3. Independent evidence, resolving the uncertainty, is provided by the series limits of the higher even terms of Ti I.

In all the spectra of the iron group, these high terms—which arise from configurations in which the excited electron is 5s, 6s, 4d, or 5d—combine almost exclusively with the lower odd terms of the same family, produced by the addition of a 4p electron to the same state of the ionized atom (or the same term in its spectrum). There are two sets of such terms in Ti I, one combining with terms to which both the writer's study of line intensities[3] and Dr. Rohrlich's later calculations of energy levels[4] assign the configurations $3d^24s4p$, and the other with terms to which both assign $3d^34p$.

The first set includes one series of three members and five more of two, which agree in showing that their limit $d^2s\ {}^4F_{4\frac{1}{2}}$ is close to the value 55531 calculated in 1927. The other ${}^4F_{4\frac{1}{2}}$ is 823 cm^{-1} distant, and must be either at 54708 or 56354. Only one known series runs to this limit. It has three members and a Ritz formula gives the limit 56500. Further evidence is obtained by comparing the Rydberg denominators n^* for all the even terms with the d^3 limit with those for the d^n limit in neighboring elements. Table I gives the results for the component of greatest J in each term and the term of highest L in each pentad (which suffice for the test). Thus lower and higher multiplicity are denoted by l and h. The results for the $d^{n-1}s$ limits, which run quite smoothly for Ti, are omitted to save space. The entries (a) for Ti I are found if $d^3\ {}^4F$ is higher than $d^2s\ {}^4F$, (b) if it is lower. The former are in good agreement with the run of the values for other elements, the latter greatly discordant.

This appears to be conclusive evidence that a^4F in Ti II comes from d^2s, and b^4F from d^3. This involves no criticism of Dr. Many's calculations, nor of the theory on which they are based, beyond the well-recognized fact that the latter takes account only of the major terms in the very complex interactions, so that the outstanding residuals are considerable, having a mean square value of ± 440 cm^{-1}, though the observed levels are accurate to a unit. The high even terms are much less subject to perturbation, both in position and in line-intensity, and afford the decisive test. The computed levels are sometimes also decisive. The terms called by the writer a^1s in Ti I and a^2s in Ti II are more than 9000 cm^{-1} below Many's calculated positions. Re-examination of the data indicates that the first is probably spurious, and the second very doubtful.

[3] H. N. Russell, Astrophys. J. 66, 412 (1927).
[4] F. Rohrlich, kindly communicated by letter.

The Dielectric Constant of Several Gases at a Wave-Length of 3.2 Centimeters

C. M. CRAIN
*Electrical Engineering Research Laboratory, University of Texas, Austin, Texas**

(Received December 22, 1947)

The dielectric constants of dry air, oxygen, water vapor, ethyl alcohol, ethyl chloride, chloroform, and acetone have been measured at a frequency of 9340 megacycles using the beat frequency method. With the exception of water vapor, the measurements were made at room temperature. For water vapor measurements were made over a temperature range of 293 to 342 degrees Kelvin.

I. DESCRIPTION OF APPARATUS

THE apparatus makes use of a method of frequency stabilizing very high frequency oscillators developed by Pound.[1] The frequency of the oscillator is controlled to a factor of approximately 10^7 by the resonant frequency of a cavity.

Figure 1 shows a block diagram of the electrical system used. The beat frequency between two stabilized oscillators is fed into a communication receiver where it is compared to the output of a frequency standard.

Figure 2 is a block diagram of the Pound oscillators shown in Fig. 1. The principal difference between the stabilized oscillators used and the system described by Pound is that higher gain was used in the intermediate frequency amplifiers of the former.

The system used for varying the gas pressure in one of the cavity resonators is shown in Fig. 3. The pressure was measured by means of the manometer or modified Fortin type mercurial barometer, depending on the magnitude of the pressure, and the gas temperature was measured by means of a thermocouple system. By measuring the change in beat frequency caused by allowing gas to enter the previously evacuated cavity resonator, the dielectric constant of the gas for the given pressure and temperature was calculated from the relation:

$$\Delta f/f = e^{\frac{1}{2}} - 1,$$

where f = change in beat frequency in cycles per second, f = resonant frequency of cavity containing gas, and e = dielectric constant of gas.

II. RESULTS OF MEASUREMENTS

1. Dry Air

The dry air was obtained by allowing room air to enter the previously evacuated system through a glass drying tube 12 feet long alternately packed with steel wool and phosphoric anhydride. Measurements were made at room temperature (20° to 27°) and at a pressure of from 24 to 28 inches of mercury. It was necessary to restrict the flow of air such that about an hour was required to raise the cavity gas pressure to the above pressures. The results obtained for faster rates of entry indicated incomplete drying. When the results obtained were converted to 0° Centigrade and one atmosphere the dielectric constant was found to be 1.000572.

2. Oxygen

The oxygen used was of the commercial variety of 99.6 percent or better purity. Measurements were made at room temperature and pressure. When the results obtained were converted

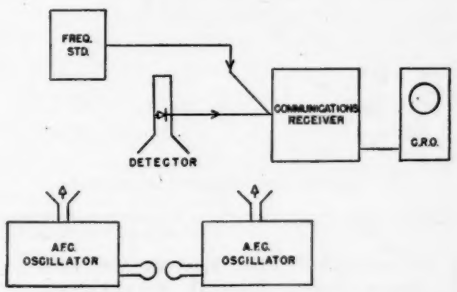

FIG. 1. Block diagram of electrical system.

* Sponsored by the Office of Naval Research, at the University of Texas, Austin, Texas.

[1] R. V. Pound, *An Improved Frequency Stabilization System for Microwave Oscillators* (Radiation Laboratory, Massachusetts Institute of Technology, 1945), Report 837.

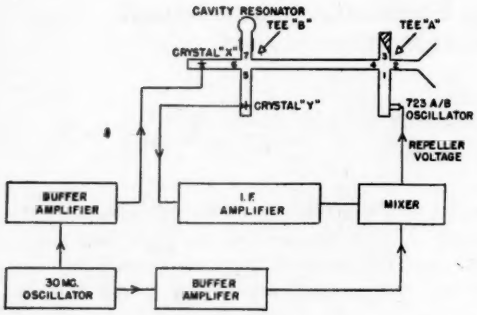

FIG. 2. Block diagram of stabilized oscillators.

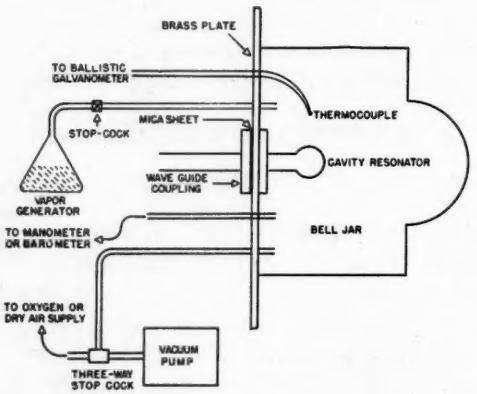

FIG. 3. Gas system.

to 0° Centigrade and one atmosphere by means of the gas law the dielectric constant was found to be 1.000530.

3. Water Vapor

The water vapor was obtained by allowing distilled water to evaporate into the gas system as shown in Fig. 3. Measurements were made over a temperature range of 293 to 342 degrees Kelvin. The pressure of the vapor varied for the different measurements; in all cases it was kept to a value below the saturation pressure by keeping the water temperature below that of the temperature controlled chamber in which the cavity resonator was placed. Since water vapor is a polar molecule the results are best described in Fig. 4. In plotting Fig. 4, all measured results were converted to a pressure of 1 inch by means of the gas law. The results obtained are almost identical to those obtained at 0.5 megacycle by Stranathan[2] and are very near to those reported by Sanger,[3] who measured at 1.0 megacycle. Also shown in Fig. 4, is a curve based on values used[4] by the Radiation Laboratory at the Massachusetts Institute of Technology. These values were based on a rounded average of the results of Stranathan and Sanger and were used for plotting nomograms for determining the refractive index of atmospheric air at micro-wave frequencies. Saxton measured the dielectric constant of water vapor at a wave length of 3.2 centimeters over a temperature range of 100–200 degrees Centigrade and re-

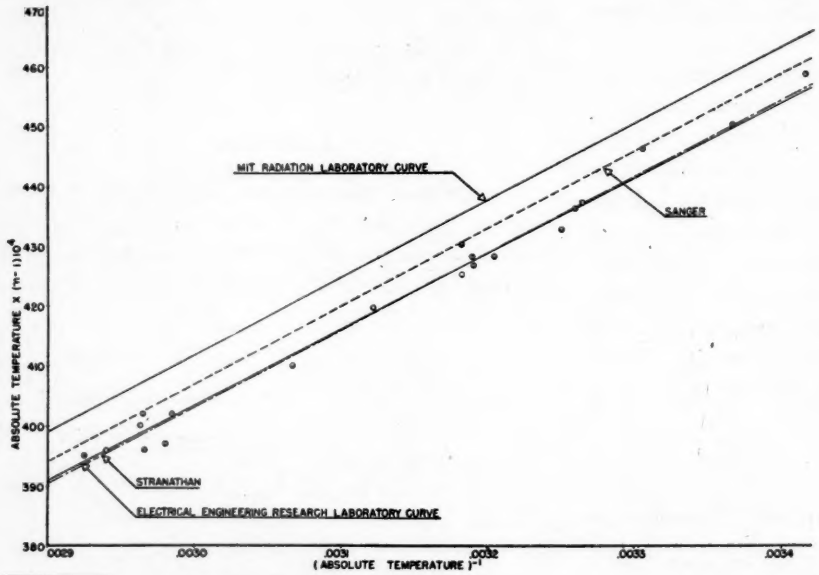

FIG. 4. Absolute temperature $\times(n-1)10^4$ *vs.* (absolute temperature)$^{-1}$ for a water vapor pressure of 1 in. of Hg (33.86 millibars).

[2] J. D. Stranathan, Phys. Rev. **48**, 538 (1935).
[3] R. Sanger, Physik. Zeits. **31**, 306 (1930).
[4] R. H. Burgoyne, *Nomograms for Computation of Modified Index of Refraction* (Radiation Laboratory, Massachusetts Institute of Technology, 1945), Report 55.

TABLE I. Dielectric constant of one atmosphere of chloroform.

Temperature Degrees C	Dielectric Constant $(\epsilon-1)10^3$
22.5	4.78
24.7	4.64
26.0	4.52
26.9	4.50
27.0	4.53
27.2	4.46
28.2	4.47
28.5	4.47

TABLE II. Dielectric constant of one atmosphere of acetone.

Temperature Degrees C	Dielectric Constant $(\epsilon-1)10^3$
24.8	23.5
25.0	23.3
25.2	23.2
26.0	23.2
28.1	22.8
29.8	22.7

ported[5] values some 10–15 percent lower than were obtained by the above and other observers at lower frequencies. The dipole moment[6] of the water vapor molecule as calculated from the results shown in Fig. 4 is 1.84×10^{-18} esu-centimeter.

4. Chloroform

The chloroform vapor was obtained by allowing purified anesthesia chloroform to evaporate into the vapor system. Measurements were made over a temperature range of 22.5 and 28.5 degrees Centigrade at pressures near 4 inches of mercury. Results obtained are shown in Table I. The pressure was converted to one atmosphere by means of the gas law.

5. Acetone

Chemically pure acetone was allowed to vaporize into the gas system in the same manner. The acetone had been previously dried by allowing it to stand over calcium sulphate crystals for several days. Measurements were made over a temperature range of from 24.8 to 29.8 degrees Centigrade at pressures of from 5 to 7 inches of mercury. The results, when converted to standard pressure, are given in Table II.

TABLE III. Dielectric constant of one atmosphere of ethyl alcohol.

Temperature Degrees C	Dielectric Constant $(\epsilon-1)10^3$
23.3	8.45
23.5	8.44
23.8	8.42
23.9	8.40
24.3	8.46
25.5	8.29
27.1	8.18
27.3	8.16
27.4	8.12
27.5	8.20
27.6	8.13

TABLE IV. Dielectric constant of one atmosphere of ethyl chloride.

Temperature Degrees C	Dielectric Constant $(\epsilon-1)10^3$
26.3	11.75
26.7	11.76
27.3	11.68
27.7	11.61
27.9	11.70
28.0	11.70

6. Ethyl Alcohol

Ninety-five percent ethyl alcohol was allowed to stand over calcium sulphate crystals for several days and was then vaporized into the gas system. Measurements were made over a temperature range of from 23.3 to 27.6 degrees Centigrade at pressures of from 1.7 to 2.2 inches of mercury. The results, when converted to standard pressure by means of the perfect gas law, are given in Table III.

The measurements at 24.3 and 27.5 degrees appear to be in error for unknown reasons.

7. Ethyl Chloride

Measurements were made on ethyl chloride of U. S. P. standards over a temperature range of 26.3 to 28.0 degrees Centigrade at pressures close to 17 inches of mercury. The results when converted to standard pressure by means of the gas law are given in Table IV.

Since the ethyl chloride was probably the purest gas measured the variation in $(\epsilon-1)10^3$ in the above table is an indication of the accuracy of the measuring process.

[5] J. A. Saxton, *The Dielectric Constant and Absorption Coefficient of Water Vapor for Wavelengths of 9 cm and 3.2 cm* (Radio Research Board Paper No. RRB/S.11, 1943).

[6] P. Debye, *Polar Molecules* (The Chemical Catalogue Company, Inc., New York, New York, 1929).

Letters to the Editor

PUBLICATION of brief reports of important discoveries in physics may be secured by addressing them to this department. The closing date for this department is five weeks prior to the date of issue. No proof will be sent to the authors. The Board of Editors does not hold itself responsible for the opinions expressed by the correspondents. Communications should not exceed 600 words in length.

Tracks in Emulsions at 100,000 Feet*

E. O. SALANT, J. HORNBOSTEL, AND E. M. DOLLMANN
Brookhaven National Laboratory, Upton, Long Island, New York
July 26, 1948

NUCLEAR emulsions (Ilford C2, unloaded, 50 microns thick), placed with surfaces horizontal, well above heavy material, were carried by balloon to 100,000 feet (temperature range at ceiling: +20°C to −60°C). Particles were identified by known methods from ranges and grain densities,[1] and from scattering[2] of tracks. Control plates showed negligible fading and established the background for observed events.

Both single tracks and stars show mesons, protons, alpha- and heavier particles. Examination so far has shown 211 stars of many (=5 or more) prongs, 4 stars produced by mesons (these σ-mesons being the only star-initiating particles observed), 1 star emitting a meson, and $1\pi-\mu$-decay.

At first, grain density and scattering measurements of a number of prongs were inconsistent; when grain densities indicated mesons or protons, scattering indicated protons or alpha-particles, respectively. But neutron-irradiated plates at various temperatures established that tracks in the colder plates and reduced grain densities (at −60°C, about ⅓ less than at +20°C), and when the aforementioned prongs were corrected for temperature effect, the inconsistencies disappeared. Details will appear later, but it seems definite that temperature regulation of plates must be considered.

In Table I is shown the distribution of prongs among stars. In row *B* is the distribution found on this flight; in row *W* is the distribution read from a histogram of Wambacher,[3] for emulsions exposed at an altitude of 7700 feet. At both altitudes, as prongs increase, stars appear, in general, less frequently; but, as seen in the last row of Table I, the very-many-particle disintegrations are present in greater proportion at the high altitude. This is, of course, consistent with the prevalence of more energetic primary particles at 100,000 feet.

TABLE I. Distribution of prongs in stars.

Number of Prongs	4	5	6	7	8	9	10	11	12	13	14	15	19
B = No. of stars, this flight	39	35	36	45	26	17	13	11	6	11	4	5	2
W = No. of stars, mountain*	35	17	5	4	4	2	0	1	1	0	1	0	0
Ratio *B/W*	1.1	2	7	11	6.5	8.5	∞	11	6	∞	4	5	∞

* See reference 3.

On a 10,000-foot mountain, the ratio of π- or σ-mesons to many-pronged stars is about 1/10, according to Lattes, Occhialini, and Powell (Table 5),[4] who indicate, too, that the observed heavy mesons originate locally, e. g., in the glass of the plates. On our balloon flights, the ratio of σ-mesons to many-pronged stars is 1/50, and only one $\pi-\mu$-decay was observed (for the 211 stars). The greater scarcity of heavy mesons relative to stars is consistent with the more energetic nature of the spectrum of primary particles, if one considers that a meson, produced in a disintegration by a more energetic primary particle, could acquire greater velocity and so become less observable in the emulsion.

Schein and Lord[5] report 6000 stars, of 4 or more prongs, are produced per cc per day on a flight to 60,000 feet. Because both course and duration are uncertain, the actual rate of production on our flight is unreliable, but an upper limit can be set quite definitely. For stars of 4 or more prongs this limit is 2000 per cc of emulsion per day. Plates at various altitudes are being examined.

Judging a star's asymmetry by absence of a track in a sector of 180°, and calculating the probability of such absence on the basis of uniform (horizontal) distribution, the ratio of observed to calculated asymmetry is found to increase with the number of prongs in the star.

We find no evidence for a "close neighbor" effect,[6] but with our relatively few stars, this means only that the effect is less than fivefold as frequent as at low altitude.

Our thanks are due the Special Devices Center of the Office of Naval Research for the balloon flight, and the Physics Department of Columbia University for cyclotron bombardments. Invaluable aid in scanning, grain density, and scattering measurements was given by Messrs. E. J. Downs, H. A. Veillette, J. E. Smith, B. Demarest, and S. Millman of this Laboratory.

* Research carried out at Brookhaven National Laboratory under the auspices of the Atomic Energy Commission.

[1] Lattes, Occhialini, and Powell, Nature **160**, 453 (1947).
[2] S. Lattimore, Nature **161**, 518 (1948).
[3] H. Wambacher, Wien. Ber. **149**, 157 (1940).
[4] Lattes, Occhialini, and Powell, Nature **160**, 436 (1947).
[5] M. Schein and J. J. Lord, Phys. Rev. **73**, 189 (1948).
[6] L. Leprince-Ringuet and J. Heidmann; D. H. Perkins, Nature **161**, 844 (1948).

The Discharge Spread in Geiger-Mueller Counters

S. H. LIEBSON
Naval Research Laboratory, Washington, D. C.
July 26, 1948

IN a recent review article by Corson and Wilson[1] results of a paper by Alder, Baldinger, Huber, and Metzger[2] are compared with results obtained by Liebson[3] on the discharge mechanism of self-quenching Geiger-Mueller counters, filled with organic vapors and inert gas. The conclusions drawn therefrom merit further clarification.

Corson and Wilson compare the absolute distances traversed by photons in the double counter experiments of

Alder *et al.*, and those of Liebson, using the distances shown in the latter's curves. However, these distances correspond to distances between the ends of the cathodes. Since the discharge in each counter is not limited to the cathode length, but extends along the anodes beyond the cathodes, these distances do not represent the absolute distance between the effective counters. Rough measurements on the spread of the discharge along the wire beyond the cathode indicated that the effective absolute distances would be decreased by about 1 cm. The difficulty of accurately defining this distance and its comparative irrelevance in determining the slopes of the probability curves was responsible for omitting the absolute distances from the data.

On the other hand, the measurements of Alder *et al.* are not suitable for comparison with results using organic vapors and inert gas. Their mixtures consisted of 1.5 cm Hg of argon plus 6.5 cm Hg of air and small admixtures of alcohol. The large amount of air contamination renders the extrapolation of their measurements to alcohol-argon counters questionable. Furthermore, no allowance was made for the fact that the addition of alcohol vapor to the argon-air counters may have reduced the number of photons produced. This would effectively produce a decrease in the number of quanta propagated across the 11-cm gap, acting as though an increase in absorption had taken place.

[1] D. R. Corson and R. R. Wilson, Rev. Sci. Inst. 19, 207 (1948).
[2] Alder, Baldinger, Huber, and Metzger, Helv. Phys. Acta 20, 73 (1947).
[3] S. H. Liebson, Phys. Rev. 72, 602 (1947).

Artificial Collateral Chains to the Thorium and Actinium Families

A. GHIORSO, W. W. MEINKE, AND G. T. SEABORG
Department of Chemistry and Radiation Laboratory, University of California, Berkeley, California
August 9, 1948

WE have produced and identified two new series of alpha-particle emitting radioactive elements; one is a "collateral" branch of the actinium ($4n+3$) radioactive family and the other is collateral to the thorium ($4n$) family. The series are of considerable interest in that they are the first whose early members lie on the neutron deficient side of beta-stability. They have been produced in high yield by irradiation of thorium with deuterons of energy about 80 Mev in the Berkeley 184-inch cyclotron. So far as the present observations are concerned, both of these series begin with isotopes of protactinium (atomic number 91), although progenitors with higher atomic numbers are to be expected and will possibly be produced and identified. These protactinium isotopes are Pa^{227} and Pa^{228} formed by $d,7n$ and $d,6n$ reactions, respectively.

After bombardments of the order of one-half to four-hour duration, the metallic thorium was dissolved and the element protactinium was isolated in essentially weightless fractions. The decay of the alpha-particles from these was measured both through the use of standard alpha-particle counting devices and also with the help of an alpha-particle pulse analyzer[1] equipped with a fast sample-changing mechanism. Through the use of the latter, a number of alpha-particle groups were observed and their energies determined.

TABLE I.

Isotope	Type of radiation	Half-life	Energy of radiation (Mev)
$_{91}Pa^{227}$	α	38 min.	6.46
$_{89}Ac^{223}$	α	~2 min.	6.64
$_{87}Fr^{219}$	α	$\sim10^{-4}$ sec.	7.30
$_{85}At^{215}$	α	$\sim10^{-4}$ sec.	8.00
$_{83}Bi^{211}$(Ac*C*)	α(99.7%)	2.16 min.	6.62
$_{81}Tl^{207}$(Ac*C''*)	β^-(0.3%)	4.76 min.	1.47
$_{82}Pb^{207}$	stable		
$_{91}Pa^{228}$	α	22 hr.	6.09
$_{89}Ac^{224}$	α	~2.5 hr.	6.17
$_{87}Fr^{220}$	α	~30 sec.	6.69
$_{85}At^{216}$	α	$\sim10^{-3}$ sec.	7.79
$_{83}Bi^{212}$	α(34%)	60.5 min.	6.05
	β^-(66%)		2.20
$_{81}Tl^{208}$(Th*C''*)	β^-	3.1 min.	1.82
$_{84}Po^{212}$(Th*C'*)	α	3×10^{-7} sec.	8.78
$_{82}Pb^{208}$	stable		

Prominent soon after bombardment are a number of alpha-particle groups, which decay with the 38-minute half-life of the protactinium parent. These are due to the following collateral branch of the $4n+3$ radioactive family:

$$_{91}Pa^{227} \xrightarrow{\alpha} {}_{89}Ac^{223} \xrightarrow{\alpha} {}_{87}Fr^{219} \xrightarrow{\alpha} {}_{85}At^{215} \xrightarrow{\alpha} {}_{83}Bi^{211}(\text{Ac}C) \xrightarrow{\alpha} {}_{81}Tl^{207}(\text{Ac}C'') \xrightarrow{\beta^-} {}_{82}Pb^{207}(\text{stable}).$$

The branch which arises from orbital electron capture by Pa^{227} is not shown. The mass type was identified by observation of the characteristic energy and half-life of the Bi^{211}(Ac*C*) alpha-particles, the half-life of the beta-particle emitting Tl^{207}(Ac*C''*), and the growth of 18.9-day Th^{227}(RdAc) as an orbital-electron-capture branching decay product of the Pa^{227} (ratio $K/\alpha=\sim0.2$). The energy obtained for these At^{215} alpha-particles is several hundred kilovolts less than that reported[2] for At^{215} as formed by the beta-particle branching decay of Po^{215}(Ac*A*).

Identification of members of the series was aided by a simple method of recoil collection. Recoil atoms were collected from a plate which contained the entire series in equilibrium and measurements using the plate upon which these were collected established the half-life and the energy of the Ac^{223} alpha-particles. In a "second-order" recoil experiment recoils were collected from the plate containing Ac^{223} (and daughters) in order to check the half-life of the alpha-particles attributed to Bi^{211}(Ac*C*) and similarly a third-order recoil experiment was effected in order to isolate the beta-particle emitter and prove that it decayed with the known half-life of Tl^{207}(Ac*C''*). The very short half-lives of the Fr^{219} and At^{215} were estimated, and their energies identified through crude coincidence experiments using the pulse analyzer apparatus to operate the driven sweep of a cathode-ray oscillograph. The measured half-lives and energies for the members of this series are summarized in Table I.

After the decay of the above-described series, a second group of alpha-particle emitters can be resolved. This second series, which decays with the 22-hour half-life of

its protactinium parent, is a collateral branch of the $4n$ radioactive family as follows:

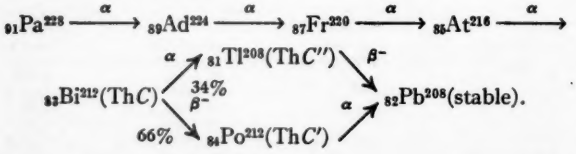

The branch which arises from orbital electron capture by Pa^{228} and Ac^{224} is not shown. The mass type was identified through observation of the characteristic radioactive properties of the Bi^{212}(ThC) and its daughters, chemical identification of Bi^{212}(ThC), the growth of Th^{228}(RdTh) as an orbital-electron-capture branching decay product of the Pa^{228} (ratio $K/\alpha=\sim 50$) and the growth of Ra^{224}(ThX) as a similar product of the Ac^{224} (ratio $K/\alpha=\sim 10$). Of interest is the check, within about 0.15 Mev, of the energy of these At^{216} alpha-particles with the energy reported[3] for At^{216} as formed by the beta-particle branching decay of Po^{216}(ThA). The half-life of the Ac^{224} could be measured and the energy of its alpha-particles identified as the result of its collection in recoil experiments. Similarly, the half-life and alpha-particle energy of the Fr^{220} could be determined by second-order recoil experiments from plates containing only Ac^{224} (and daughters). The very short half-life at At^{216} was estimated as described above and its energy could be determined by measurements on samples containing its progenitors. The half-lives and energies are summarized in Table I. The radioactive properties of ThC (and AcC) and daughters are the accepted values taken from the literature.[4]

These data extend the information on the isotopes of protactinium, actinium, francium, and astatine so that more interesting correlations[5] of mass and atomic numbers, etc., with alpha-particle decay energies and half-lives are possible.

The cooperation of Professor R. L. Thornton, Mr. J. T. Vale, and the 184-inch cyclotron group is gratefully acknowledged.

This paper is based on work performed under the auspices of the Atomic Energy Commission.

[1] See, A. Ghiorso, A. H. Jaffey, H. P. Robinson, and B. Weissbourd, "An Alpha-Pulse Analyzer Apparatus," Plutonium Project Record 14B, 17.3 (1948), to be issued.
[2] B. Karlik and T. Bernert, Naturwiss. 32, 44 (1944).
[3] B. Karlik and T. Bernert, Naturwiss. 31, 492 (1943).
[4] See G. T. Seaborg, Rev. Mod. Phys. 16, 1 (1944).

The Half-Life of C^{14}

R. C. Hawkings, R. F. Hunter, W. B. Mann, and W. H. Stevens
National Research Council, Atomic Energy Project, Chalk River, Ontario, Canada
August 4, 1948

FROM experiments which have recently been described,[1] Norris and Inghram conclude that the half-life of C^{14} is 5100 years; earlier experiments[2] by the same authors had given somewhat higher values, namely, 6100 and 5300 years, the former being, however, a preliminary value. A value of 4700 years was obtained by Reid, Dunning, Weinhouse, and Grosse.[3]

Experiments have also been carried out in the standardization laboratory of this project for the purpose of providing C^{14} standards. With this end in view the activity of C^{14} in samples of carbon dioxide has been measured in gas counters similar to those which have been described by Miller.[4,5] In order to eliminate possible errors arising from end effects, compensated counter units each consisting of a long and a short copper cathode of the same radius and having as nearly similar end geometries as possible have been used. To investigate the errors which might arise on account of β-particles entering the wall from a thin layer of gas at the wall and not giving rise to a pulse, experiments were carried out using compensated counter units of different radii and with fillings at different pressures. The counters were quenched by means of a Parkinson multivibrator quenching unit.[6]

The results obtained assuming a 100 percent counter efficiency, in conjunction with a mass-spectrometer, isotope-abundance determination, lead to a value for the half-life of C^{14} of 6400 ± 200 years.

Further experiments are to be carried out to check the efficiencies of the counters, but the investigation into the effect of radius referred to above would indicate that the counters are not less than 95 percent efficient. Such an efficiency would correspond to a half-life of 6100 ± 200 years, which is still considerably higher than that obtained by Norris and Inghram.

We wish to acknowledge with thanks the help which we have received from Mr. G. B. Parkinson and Mr. F. N. MacGillivray. We also wish to express our thanks to Professor H. Thode of McMaster University for placing at our disposal the facilities of his laboratory, and to Mr. C. Collins who operated the mass spectrometer. A more detailed account of these experiments together with a description of the preparation of the active carbon is to be submitted for publication in the near future.

[1] L. D. Norris and M. G. Inghram, Phys. Rev. 73, 350 (1948).
[2] L. D. Norris and M. G. Inghram, Phys. Rev. 70, 772 (1946).
[3] Reid, Dunning, Weinhouse, and Grosse, Phys. Rev. 70, 431 (1946).
[4] W. W. Miller, Science 105, 123 (1947).
[5] S. C. Brown and W. W. Miller, Rev. Sci. Inst. 18, 496 (1947).
[6] W. B. Mann and G. B. Parkinson: Submitted to the Review of Scientific Instruments for publication.

The Half-Life of C^{14}

L. Yaffe and Jean M. Grunlund
Chemistry Branch, Atomic Energy Project, National Research Council, Chalk River, Ontario, Canada
August 4, 1948

THE half-life of C^{14} has recently been checked by several investigators. Values found were 4700[1] and 5100[2] years. Hawkings, Hunter, Mann, and Stevens[3] have, by mass spectrographic analysis and gas counting, obtained a value of 6400 ± 200 years.

Since this last value was so much higher than the previously accepted values, it was decided to check this using a calibrated end-window Geiger counter. We used an aliquot of the same Na_2CO_3 solution used by Mann *et al.* from which they generated CO_2. The samples were mounted on very thin (50 $\mu g/cm^2$) Formvar films. Correc-

tions were made for back-scattering, absorption in the air gap, and counter window.

The value we obtained was 7200±500 years.

[1] Reid, Dunning, Weinhouse, and Grosse, Phys. Rev. **70**, 431 (1946).
[2] L. D. Norris and M. G. Inghram, Phys. Rev. **73**, 350 (1948).
[3] See preceding letter.

The Absorption of Charged Particles from the 2.2-μsec. Meson Decay

E. P. Hincks and B. Pontecorvo
National Research Council of Canada, Chalk River Laboratory, Chalk River, Ontario, Canada
July 26, 1948

THE energy spectrum of the charged particles (commonly assumed to be electrons) emitted in the 2.2-μsec. meson decay is still unknown. Conversi and Piccioni[1] in 1944 deduced from the relative numbers of decay electrons escaping from iron plates 0.6 cm and 5 cm thick that their mean range is about 2.5 cm of iron. According to the range-energy relationships of Bethe-Bloch-Heitler,[2] this corresponds to an energy of about 50 Mev, which was consistent with the Yukawa β-process picture of a meson decaying into an electron and a neutrino, each of about 50 Mev. Subsequently, Anderson and co-workers[3] observed two instances of meson decay in a cloud chamber, and were able to measure accurately the energy of the decay electron. This was found in both cases to be close to 25 Mev. To explain this low energy they postulated that the decay process might be

$$\text{charged meson} \rightarrow \text{electron} + \text{neutral meson}, \qquad (1)$$

with the kinetic energy of the electron having a unique value of about 25 Mev. Since the present experiment was initiated there have been reported a few results[4] obtained with cloud chambers that seem to indicate a considerable spread in the energies of the decay particles. A 3-particle decay process in which the electrons may be emitted with any energy up to about 50 Mev has been suggested recently.[5]

Our experiment, carried out in the Chalk River Laboratory, is an attempt to derive some information about the energy of the decay electrons by measuring their penetration through a solid absorber. The method differs from that used by Conversi and Piccioni; in particular, a low atomic number absorbing material (carbon*) for the electrons was used in order to decrease the energy losses by radiation which complicate the interpretation of the experiment.

A section of the counter arrangement, together with a block diagram illustrating the function of the electronic circuits, is shown in Fig. 1. A meson beam entering the apparatus is defined by a coincidence between counter trays A and B. The positive and negative mesons which are stopped in a graphite block 20 cm×40 cm×4.2 g/cm² thick are detected by the anticoincidence $(AB-C)$, which initiates a grating pulse 4.6 μsec. in width and delayed by ~1 μsec. This pulse is then mixed separately with the outputs from A, B, and C, so that if the decay electron passes through A, B, or C between 1 and 5.6 μsec. after an anticoincidence $(AB-C)$, a delayed coincidence is recorded which we designate by $(A)_{del}$, $(B)_{del}$, or $(C)_{del}$. In particular, a decay electron passing through both B and A gives an event $(AB)_{del}$.

In order to measure the penetration of the decay electrons, the rate $(AB)_{del}$ is measured as a function of the thickness of a graphite absorber placed between A and B.** Some events $(AB)_{del}$ are also events $(ABC)_{del}$ and are caused essentially by a meson traversing the three trays by chance within the delayed interval. The events $(ABC)_{del}$ are also recorded and enable us to disregard most of the chance $(AB)_{del}$.

It will be noticed that A and B have two functions: (i) detecting the passage of the primary meson and (ii) detecting the passage of a decay electron. Because of the counter dead time, only those decay electrons will be detected which pass through a different counter from that traversed by the meson. This decrease in the effective sensitivity of tray B would be serious if the meson absorber (i.e., the "source" of decay electrons) were placed very close to B; a favorable position of the source (4.1 cm below B) was determined graphically.

The results are summarized in Table I.

The interpretation of an electron absorption curve is made difficult by the inherent presence of scattering and radiation, and, in our experiment in particular, by the low intensity and "poor geometry." Nevertheless, the following conclusions can be drawn.

Let us assume first that the energy of the decay electrons is always 25 Mev. The *maximum* range of a 25-Mev electron (defined as $\int_0^{25\ \text{Mev}} dE/-(dE/dx)_{ion}$, where $-(dE/dx)_{ion}$ is the rate of energy loss in Mev×cm²/g due only to non-radiative collisions), is estimated[2,6] to be 15 g/cm² in carbon. Now we have calculated (cf. reference

Table I.

Absorber thickness	Total thickness* (g/cm²)	Hours of observation	$(B)_{del}$ (counts)	$(C)_{del}$ (counts)	$(AB)_{del}$ (counts)	$(ABC)_{del}$ (counts)	$(B)_{del}+(C)_{del}$ (cts./hr.)	$(AB)_{del}-(ABC)_{del}$ (cts./hr.)
No absorber	4.2	212	840	1856	176	6	12.7±0.3	0.80±0.06
5.1 g/cm² C	9.3	67	246	588	38	2	12.4±0.4	0.54±0.09
13.7 g/cm² C	17.9	142	695	1301	30	6	14.1±0.3	0.17±0.04
16.2 g/cm² C	20.4	250	1009	2073	31	6	12.3±0.3	0.10±0.02
16.2 g/cm² C+2.7 g/cm² Fe	23.1	158	683	1373	12	3	13.0±0.3	0.06±0.02
96.5 g/cm² Pb+5.8 g/cm² Fe (control run)	106.5	158	637	1494	2	2	13.5±0.3	0 in 158 hr.**

* To the absorber thickness has been added the thickness of counter walls (2.1 g/cm² Cu) and half the thickness of the graphite source (2.1 g/cm² C).
** The computed casual rate is about 0.003/hr.

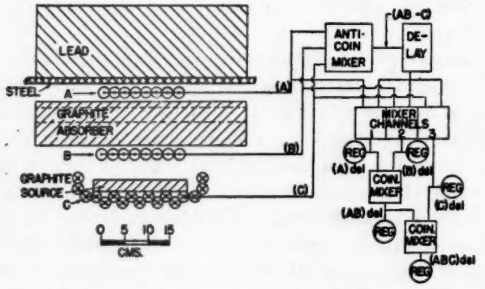

FIG. 1. Experimental arrangement. The geometry in the plane perpendicular to the paper can be inferred from the length of the counters, which is 35 cm.

2) that less than 0.03 count per hour can be due to radiation from 25-Mev electrons in our arrangement. Consequently, it may be seen from Table I that at least a substantial fraction of the electrons must have a range greater than 15 g/cm² of carbon. Therefore, we conclude that there are decay electrons having energies greater than 25 Mev and therefore that the 2-particle decay process (Eq. (1)), with a *unique* energy of about 25 Mev for the decay electron, is incompatible with our results.

We observe, however, that a *maximum* energy of about 50 Mev for the decay electrons would be consistent with the data of Table I.

* For one run a small thickness of iron was added on top of the graphite.

** The absorber for the decay particles, when placed between *A* and *B*, produces a negligible change in the number of mesons stopped in the graphite below *B*, so that the strength of the "source" of decay electrons is sensibly constant as indicated by the rate $(B)_{del}+(C)_{del}$.

[1] M. Conversi and O. Piccioni, Phys. Rev. **70**, 874 (1946).
[2] H. Bethe and W. Heitler, Proc. Roy. Soc. **A146**, 83 (1944).
[3] C. D. Anderson, R. V. Adams, P. E. Lloyd, and R. R. Rau, Phys. Rev. **72**, 724 (1947); R. V. Adams, C. D. Anderson, P. E. Lloyd, R. R. Rau, and R. C. Saxena, Rev. Mod. Phys. **20**, 334 (1948).
[4] W. Y. Chang, reported at the Am. Phys. Soc. Washington Meeting, April 1948; J. G. Retallack, Phys. Rev. **73**, 921 (1948); E. C. Fowler, R. L. Cool, and J. C. Street, Phys. Rev. **74**, 101 (1948); J. L. Zar, J. Hershkowitz, and E. Berezin, Phys. Rev. **74**, 111 (1948).
[5] O. Klein, Nature 161, 897 (1948); J. A. Wheeler, reported at the Am. Phys. Soc. Washington Meeting, April, 1948.
[6] E. Fermi, Phys. Rev. **57**, 485 (1940); G. C. Wick, Ricerca Scient. **12**, 858 (1941); O. Halpern and H. Hall, Phys. Rev. **73**, 477 (1948).

The Self-Diffusion Coefficient of Nitrogen*

E. B. WINN
Rouss Physical Laboratory, University of Virginia, Charlottesville, Virginia
July 29, 1948

AN approximation to the self-diffusion coefficient of nitrogen at room temperature has been determined, using a method originated by Ney and Armistead and previously applied to uranium hexafluoride[1] and methane.[2] This consisted of allowing nitrogen having 7.4-atom percent enrichment of N^{15}, supplied by the Eastman Kodak Company, to diffuse into normal nitrogen at the same temperature and pressure. Because of the chemical similarity and the small mass difference between the molecules $N^{14}N^{14}$ and $N^{14}N^{15}$, the coefficient of diffusion of the one into the other should be very nearly the same as the coefficient of self-diffusion of either.

The apparatus used consisted of two cylindrical copper bulbs, having volumes of 924 cm³ and 249 cm³, mounted on a common axis and connected through a copper tube and brass ground-joint stopcock, the tube and stopcock assembly having a uniform bore of 0.635 cm and an over-all length of 16.23 cm. In performing the diffusions heavy nitrogen was placed in one bulb and the normal gas in the other at the same temperature and pressure. After opening the connecting stopcock a continuous analysis of the concentration of $N^{14}N^{15}$ in the small bulb was performed with a 60° Nier-type mass spectrometer, the rate at which this concentration changed providing a means of evaluating the coefficient of diffusion. In order to obtain a relaxation time of about an hour and a half all diffusions were performed at room temperature and at pressures of from five to six cm of mercury.

In the kinetic theory of transport phenomena there is derived the relation $\rho D=\epsilon\eta$, where ρ is the density, D the coefficient of self-diffusion, η the coefficient of viscosity, and ϵ a constant related to the intermolecular forces. Taking ρ for nitrogen to be 1.2506×10^{-3} g/cm³ at 0°C and 760 mm of mercury pressure, and assuming the ideal gas law to hold, the mean of five diffusions referred to 20°C is: $(\rho D)_{20°C}=258\pm10$ micropoises. The precision measure assigned is the most probable cumulative error arising from errors in the measurement of the geometrical constants, pressure, and temperature, as well as instrument error.

Taking η at 20°C to be 174.7 micropoises,[3] it is found that $\epsilon=1.48$. If the nitrogen molecules be represented as point centers of repulsive force, Chapman and Cowling[4] compute that $\epsilon=1.44$, using the experimentally verified relation $\eta\propto T^{0.756}$. This theoretically determined figure agrees with the observed value within the limits of experimental error. This agreement between experiment and theory is of especial interest, since the values reported for ϵ for uranium hexafluoride,[1] methane,[2] and argon[5] show a departure from the simple theory and yet agree with each other within the limits of error. This unexpected result led at first to the suspicion that ϵ might have the same value for all gases, but the figure reported here does not support such a belief.

Experimentally determined values of ϵ for various gases are listed in Table I, which, with the addition of the result for nitrogen, is reproduced from a paper by Hutchinson[5] and illustrates the as yet unexplained behavior of this quantity.

Amdur[6] has already pointed out that the molecular model assumed by Chapman and Cowling may be incomplete, it being more appropriate to represent the interactions as a sum of both repulsive and attractive forces.

TABLE I. Reported values of ϵ.

Gas	Temperature, °C	ϵ
H_2	20	$1.37_0\pm0.003$
	−188	1.32 ±0.06
	−252.8	1.28 ±0.02
Ne	20	$1.27_8\pm0.006$
A	22	1.31 ±0.01
Kr	20	1.30 ±0.06
Xe	20	1.24 ±0.06
CH_4	20	1.33
UF_6	30	1.31
N_2	20	1.48

Furthermore, the temperature variation of the coefficient of viscosity by itself does not supply reliable information as to the nature of the attractive force, so that no final conclusions regarding the force field of the nitrogen molecule should be drawn from this work alone.

The writer would like to express his thanks to Dr. E. P. Ney for suggesting the problem and for valuable discussions in the initial stages of the project.

* This work was supported by Contract Nord 7873 with the U. S Navy Bureau of Ordnance.

[1] E. P. Ney and F. C. Armistead, Phys. Rev. **71**, 14 (1947).
[2] E. B. Winn and E. P. Ney, Phys. Rev. **72**, 77 (1947).
[3] M. Trautz and R. Zink, Ann. d. Physik **7**, 427 (1930).
[4] S. Chapman and T. G. Cowling, *The Mathematical Theory of Non-Uniform Gases* (Cambridge University Press, Teddington, 1939), p. 172.
[5] F. Hutchinson, Phys. Rev. **72**, 1256 (1947).
[6] I. Amdur, Phys. Rev. **72**, 642 (1947).

Erratum: The Radial Dependence of the Tensor Force in the Deuteron

[Phys. Rev. **74**, 145 (1948)]

WILLIAM G. GUINDON
Massachusetts Institute of Technology, Cambridge, Massachusetts

IN the above article, on page 149, Eq. (33) should read

$$\langle J_1(r)\rangle_{Av} \geq \gamma \langle J_2(r)\rangle_{Av}.$$

Cloud-Chamber Observations of the Decay of Tritium

W. J. BYATT, F. T. ROGERS, JR., AND ARTHUR WALTNER
The University of North Carolina, Chapel Hill, North Carolina
August 5, 1948

THE introduction of a small amount of tritiated water[1] into a cloud chamber operating at atmospheric pressure, thus providing a weakly radioactive vapor in the chamber, has enabled us to observe a significant number of beta-particle tracks from the decay of $_1H^3$. The chamber had a diameter of 9 cm; and photography was non-stereoscopic, using an optical system with a 4-mm depth of focus. The photographs were measured at a magnification of 10.83 diameters, and only those tracks were recorded which were entirely in focus. 1565 tracks were acceptable, and the differential distribution of the lengths of their projections is shown in Fig. 1. Although all photographs were searched very carefully for very short tracks, we cannot be sure that the distribution as shown is accurate for projections smaller than 0.5 mm.

In view of the preliminary nature of this investigation, and of the uncertainties in available data relative to straggling and to the energy-range relation, it seems possible to reach only limited conclusions from Fig. 1. Apart from the fact that the data do not indicate any highly unusual form for the energy distribution, it is possible to report only that the maximum track length was observed to be 4.12 mm (referred to dry air at 15°C and 760-mm pressure). An application of Alper's[2] energy-range relation, as extrapolated to higher energies concordantly with Wilson's,[3] indicates an energy of 11 ± 1 kev as the corresponding maximum energy for the tritium beta-particles. The uncertainty in the 4.12-mm measured range leads to a corresponding undertainty in the maximum-energy determination, but it is considerably less than the ±1 kev attributed to the uncertainties in the energy-range relation.

FIG. 1.

[1] The authors are indebted to the Carnegie Institution (DTM), and particularly to Drs. M. A. Tuve and P. H. Abelson and Mr. W. D. Whitehead of that Institution, for the gift of tritiated water.
[2] T. Alper, Zeits. f. Physik **76**, 172 (1932).
[3] C. T. R. Wilson, Proc. Roy. Soc. **A104**, 1 (1923).

Cloud-Chamber Observation on Low Energy Portion Ra*E* Beta-Spectrum

ARTHUR WALTNER AND F. T. ROGERS, JR.
The University of North Carolina, Chapel Hill, North Carolina
August 5, 1948

SINCE measurements of the low energy behavior of continuous beta-spectra of Ra*E* have been somewhat contradictory, it seems that cloud-chamber measurements might provide significant new information. We have made cloud-chamber measurements of this spectrum using Ra*E* deposited on a collodion film having a thickness of about 0.15 micron, and have observed 716 tracks. The diameter of the cloud chamber was 9 cm and the effective depth of focus was about 4 mm; only those tracks were used which were entirely in focus. Tracks were photographed non-stereoscopically and measured according to the method of Petrova,[1] in which the projection of the track in the photographic plane is determined; all data were reduced to 15°C and 760 mm Hg. Corrections were applied to compensate for the change in effective solid angle with projected length of track. A second series of 262 tracks was obtained by using a source deposited electrolytically on a platinum wire, to exhibit the effects of a massive source support.

The data are shown as differential distributions in Fig. 1, indicating the intensity of each spectrum as a function of the "projected range." It is clear from this figure that the energy distribution of the Ra*E* beta-particles seems to vanish at zero (or some small energy); this result has not been reported by earlier workers,[2] presumably because of instrumental difficulties at very low energies.

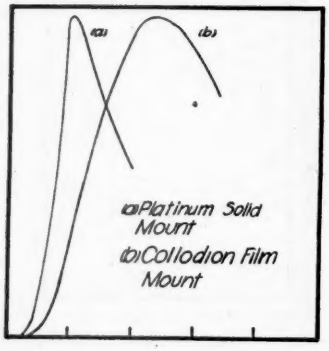

FIG. 1.

Preliminary measurements have also been made using Ra*E* in the form of a radioactive vapor formed by the interchange of Ra*E*, an isotope of Bi, with Pb in $Pb(CH_3)_4$, as described by Richardson and Leigh-Smith.[3] These measurements, though incomplete, indicate the same general behavior for the spectrum.

[1] J. Petrova, Zeits. f. Physik **55**, 628 (1929).
[2] A. Flammersfeld, Zeits. f. Physik **112**, 727 (1939).
[3] H. O. W. Richardson and Alice Leigh-Smith, Proc. Roy. Soc. **162**, 391 (1937).

On the Positive Particles Occurring from P^{32} in the Cloud Chamber

J. S. BARLOW AND F. T. ROGERS, JR.
The University of North Carolina, Chapel Hill, North Carolina
August 5, 1948

THE ratio of occurrence of "positive" tracks from beta-emitters as determined from cloud-chamber measurements has been consistently higher than the ratio found by other methods of investigation by at least an order of magnitude. In order to determine if the ratio is dependent on the type of source mount used for the active material in the chamber, we have taken a number of stereoscopic pictures of the tracks arising from a source of P^{32} supported between two films of collodion, approximately 0.15 micron thick, in a cloud chamber filled with air and operated at approximately atmospheric pressure. A source having a very high specific activity was obtained by using the separated isotope P^{32} available from the United States Atomic Energy Commission at Oak Ridge. A total of 1493 pictures was taken using a chamber 7 inches in diameter and $2\frac{1}{4}$ inches deep, using a magnetic field strength of 400 gauss. Analysis of the pictures showed 7240 electron tracks and 11 positive tracks, a ratio of 0.15×10^{-2}. In order to obtain the best statistics possible all positives and negatives arising from the source were considered, regardless of their age. The ratio obtained is somewhat smaller than the values given by Sizoo, Barendregt, and Griffioen,[1] who used a glass capillary source mount in the center of the chamber, and Smith and Groetzinger[2] who mounted the P^{32} source at the end of a short aluminum channel which led into the chamber; but the ratio is in agreement with the values given by Pi and Chao,[3] who use glass capillary source mounts. Calculations made from the relation for multiple scattering given by Bethe[4] showed that only approximately 20 percent of the positives could be accounted for by multiple scattering of electrons, which is in agreement with the result of Heine,[5] who found no decrease in the ratio when a H_2+He mixture was used as the gas in the chamber. Since our ratio is not significantly different from those given by Pi and Chao, it appears that the behavior of the positives is not dependent on the nature of the source support used for the active material in the chamber.

In order to investigate the discrepancy between cloud-chamber results and the results of other methods of investigations, two experiments appear possible. An increase in the ratio of positives to negatives found by operating a magnetic beta-ray spectrograph with a small amount of the vapor used in the cloud chamber compared to the value with an evacuated spectrograph would indicate that the positives could be ascribed to scattering of electrons. Secondly, measurements made with a cloud chamber of at least twice the dimensions of the present chamber and filled with a H_2+He mixture would be relatively free from any uncertainty in the origin of the positive tracks. The very intense light available from flashtubes would enable pictures to be taken using such a deep chamber without loss of definition because of a small depth of focus which would occur if less intense light sources were used. Such an experimental arrangement could be used to test effectively the hypothesis given by McCusker[6] that the positives arise either from multiple scattering of electrons or from electrons which travel a full circle and return to the source.

[1] Barendregt, Griffioen, and Sizoo, Physica **7**, 860 (1940).
[2] L. Smith and G. Groetzinger, Phys. Rev. **70**, 96 (1946).
[3] T. H. Pi and C. Y. Chao, Phys. Rev. **72**, 639 (1947).
[4] H. A. Bethe, Phys. Rev. **70**, 821 (1946).
[5] H. G. Heine, Helv. Phys. Acta **17**, 273 (1944).
[6] C. B. A. McCusker, Nature **161**, 564 (1948).

A Comparison of the Beta-Spectra of C^{14} and S^{35}*

L. E. GLENDENIN
Department of Chemistry and Laboratory for Nuclear Science and Engineering, Massachusetts Institute of Technology, Cambridge, Massachusetts

AND

A. K. SOLOMON
Biophysical Laboratory, Harvard Medical School, Boston, Massachusetts
August 2, 1948

IN a recent paper[1] by one of us, absorption curves and Feather analyses[2,3] were presented for the β-radiations of C^{14} and S^{35}. In view of the fact that there was a marked difference in the shape of the Feather plots of the two β-emitters, which in turn would indicate a difference in the shape of their energy spectra,[3] it seemed advisable to repeat the absorption work under carefully controlled and identical conditions in order to determine whether or not a real difference exists.

For the absorption measurements essentially weightless sources (<0.1 mg) of high specific activity were evaporated in stamped copper cups over an area of about 0.5 cm^2.

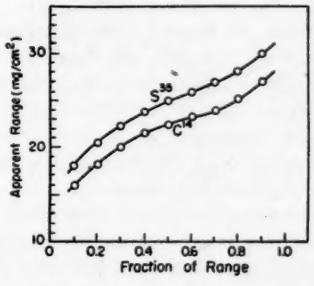

FIG. 1. Feather plots for C^{14} and S^{35}.

The prepared sources were placed in an aluminum shelf arrangement[4] at a distance of 1 cm from the thin mica window (2.8 mg/cm²) of a Victoreen (model V G 15) counter. The initial intensities of the sources were 11,000 c/m for C^{14} and 9300 c/m for S^{35}. Absorption curves were obtained in the customary manner by observing the activity through aluminum foils of varying thickness placed between the source and the counter. Feather analyses of the absorption curves were made using the absorption curve of the β-radiations of UX_2 (rather than Ra E) as a standard. The Feather plots are presented in Fig. 1.

The extrapolated ranges obtained are 28.5 ± 0.5 mg/cm² for C^{14} and 31.7 ± 0.5 mg/cm² for S^{35}, in good agreement with the previous determinations.[1] It will be noticed, however, that over the whole range of absorption there is a constant ratio between the two Feather plots, i.e., the shapes of the absorptions curves for C^{14} and S^{35} are identical. The difference in the absorption curves previously reported[1] was probably due to the use of sources of appreciable thickness which exerts a marked effect on the lower energy electrons in the initial portions of the curves. To the extent that the shape of an absorption curve is indicative of the shape of the energy spectrum,[3,5] the curves of Fig. 1 may be taken to indicate that the shapes of the energy spectra of C^{14} and S^{35} are essentially identical, at least for energies greater than about 50 kev. (Electrons of energy less than this value are stopped by the external absorption of 4 mg/cm² due to window and air.) This is a rather interesting result in view of the great difference in the half-lives of C^{14} (5100 years) and S^{35} (87 days).

In a recent investigation of the β-spectra of C^{14} and S^{35} using a magnetic lens spectrometer, Berggren and Osborne[6] have found that the energy distributions of both spectra are of the same allowed shape for energies above 40 kev. From a similar investigation with a magnetic spectrometer, Langer, Cook, and Price[7] report, however, that the β-spectra of C^{14} and S^{35} differ slightly in shape.

* This work was supported in part by the Office of Naval Research.
[1] Solomon, Gould, and Anfinsen, Phys. Rev. **72**, 1097 (1947).
[3] N. Feather, Proc. Camb. Phil. Soc. **34**, 599 (1938).
[5] L. E. Glendenin, Nucleonics **2**, 12 (1948).
[4] C. D. Coryell, "Detection and measurement of radioactivity," in *Isotopes in Biology and Medicine* (University of Wisconsin Press, Madison, Wisconsin, 1948), p. 121.
[5] D. J. Hughes and C. Eggler, Bull. Am. Phys. Soc. **23**, No. 3, 45 (1948).
[6] J. L. Berggren and R. K. Osborne, Bull. Am. Phys. Soc. **23**, No. 3, 46 (1948).
[7] L. M. Langer, C. S. Cook, and H. C. Price, Bull Am. Phys. Soc. **23**, No. 4, 15 (1948).

Hall and Kerr Effects at Microwave Frequencies*

S. P. COOKE
Cruft Laboratory, Harvard University, Cambridge, Massachusetts
August 9, 1948

WE have recently observed the Hall or Kerr effect at microwave frequencies for bismuth, iron, nickel, Permalloy (45 percent Ni), Moly-Permalloy (4 percent Mo, 79 percent Ni), Kovar, and various other metals.

The apparatus consists of a cylindrical cavity resonator driven in the TE_{11} mode so that the primary current for the Hall effect measurement flows across the plane end plates of the resonator, one or both of these end plates being made of the material whose Hall coefficient is to be determined. An external magnetic field is applied normal to the end plates. The transverse voltage arising from the Hall effect sets up an oscillation of the cavity in the same mode type except that the E-vector is at right angles to the driving E-vector. The transverse oscillation is detected by means of an output coupling hole located in a rotatable section of the cavity. This is equivalent to measuring the Kerr effect, i.e., rotation of the plane of polarization on reflection from a surface in the presence of a normal magnetic field.

Since the first observation of the effect last fall, three different versions of the equipment have been built, of which the two most recent are shown in Figs. 1 and 2.

Certain qualitative facts have been observed:

1. The measured rotations are not in good agreement with those calculated on the assumption that the Hall effect, as measured under direct current conditions, is the only contributing mechanism. Rotations in certain cases,

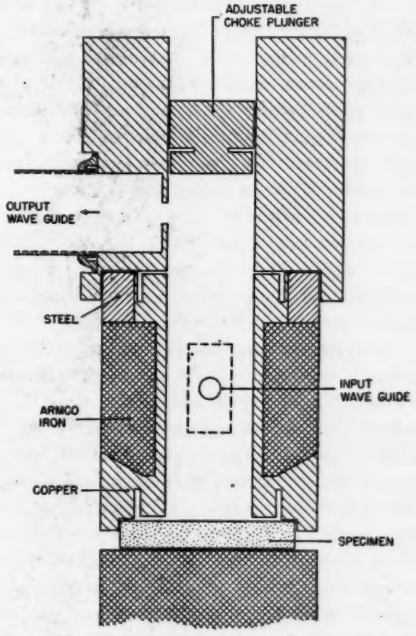

FIG. 1. Wave-guide assembly for the measurement of rotation of plane of polarization.

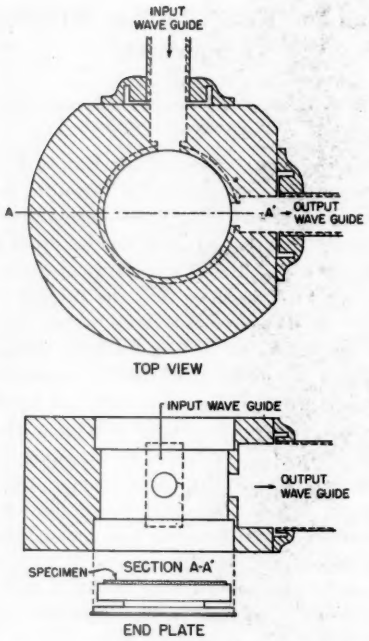

FIG. 2. Wave-guide assembly with fixed coupling holes. End plate shown retracted.

bismuth for instance, are opposite in sign to the predicted rotation on the basis of the above assumption. This suggests the possibility of more than one mechanism for the observed effect.

2. All rotations produced by magnetic fields are accompanied by time-phase shifts relative to the primary current. In other words, the reflected wave is elliptically polarized.

3. Since any asymmetry of the resonant cavity gives rise to coupling between the two above-mentioned modes of oscillation, great care must be taken with machining operations and preparation of specimens. Random scratches resulting from polishing the specimen surfaces cause no effect but any regularity resulting from polishing produces a residual rotation. No time-phase changes result from rotations produced by mechanical asymmetry.

4. Transverse (perpendicular to the cavity axis) magnetization of ferromagnetic specimens, in general, produces a rotation in the absence of any external magnetic field. Effects of this type are easily detected by mechanically rotating the specimen relative to the cavity.

The preliminary measurement of rotation was made in the apparatus shown in Fig. 1, in which the homogeneity of the magnetic field was not better than 10 percent. The angle of rotation increases with magnetic field strength but in such a field it is easily possible that fine structure with respect to field strength be unresolved.

The cavity shown in Fig. 2 sacrifices the feature of relative rotation of coupling holes in order to reduce the over-all axial length of the cavity, and hence permits its use in a magnet of more uniform field strength.

Since some part of the observed effects may be due to electron spin transitions, and since such transitions are in the nature of precessional rotations, it was reasonable to suppose that a ferromagnetic salt crystal would produce similar rotations. In order to test the sensitivity of the apparatus, a 50-mg specimen of dilute iron alum (0.0085: iron to aluminum) was symmetrically mounted in a cavity of the type shown in Fig. 2. Operating at 9310 Mc/sec. (the resonance frequency of the cavity) with magnetic fields in the vicinity of 3360 gauss, the main resonance and two satellite lines were observed.

We are indebted to Dr. E. M. Purcell[1] for permission to use his excellent magnet, and to Mr. C. D. Slichter[1] for the specimen of dilute iron alum referred to above.

* The research reported in this document was made possible through support extended Cruft Laboratory, Harvard University, jointly by the Navy Department (Office of Naval Research) and the Signal Corps, U. S. Army, under ONR Contract N5ori-76, Task Order I.

[1] Lyman Laboratory of Physics, Harvard University.

Atmospheric Absorption of Water Vapor between 1.42μ and 2.50μ

ORREN C. MOHLER
McMath-Hulbert Observatory of the University of Michigan, Lake Angelus, Pontiac, Michigan
W. S. BENEDICT
National Bureau of Standards, Washington, D. C.

August 2, 1948

IN our high resolution recordings of the infra-red solar spectrum[1] there appear a very large number of lines resulting from atmospheric water vapor. We have undertaken the rotational analysis of this material, and wish to report briefly on the principal results.

Between 1.34μ and 1.42μ there is complete absorption, due principally to the well-known perpendicular band ($v_1v_2v_3=101$). At the long wave-length edge of this region there appears the perpendicular band (021).[2] It is well developed and well resolved on our spectra; it has been possible to locate most of the rotational levels up to $J=9$. It is overlapped to some extent by high J transitions in the P branch of (101) and its weaker satellite, the parallel band (200).[3] It is also overlapped at longer wave-lengths by a weaker, previously unreported parallel band (120), of which we have identified most of the rotational levels up to $J=6$. Practically all of the strongest lines between 1.42μ and 1.54μ have been accounted for by these four bands.

There is again complete absorption between about 1.82μ and 1.97μ caused by the strong perpendicular band (011), which is accompanied by the much weaker parallel band (110).[3] The short wave-length wing of this region is well resolved, and we have been able to assign the strongest lines, from 1.71μ to 1.82μ, to transitions of the type $\Delta J=+1$, $\Delta\tau=+3$, for J up to 8, and $\Delta J=+1$, $\Delta\tau=-1$, for J up to 11, in the (011) band. In the long wave-length wing, from 1.97μ to 2.05μ, the H_2O absorption is complicated by strong bands of CO_2, but some of the corresponding transitions with $\Delta J=-1$ have been found, as well as lines of (110).

Between 2.00μ and 2.22μ a number of relatively weak lines have been identified as belonging to the parallel band (030), the previously unreported second overtone of

TABLE I.

v_1	v_2	v_3	ν_0 cm^{-1}	A cm^{-1}	B cm^{-1}	C cm^{-1}
0	2	1	6871.37	33.50	14.84	8.87
1	2	0	6775.00	34.43	14.67	8.78
0	3	0	4666.70	42.05	14.98	8.88
1	0	1	7249.8	25.89	14.12	8.98
2	0	0	7201.4	26.38	14.20	8.94
0	1	1	5331.2	29.52	14.61	8.98
1	1	0	5235.0	30.13	14.45	8.93

the bending fundamental. Most of the levels up to $J=6$ have been found, but the analysis is complicated by the overlapping in the R branch with the stronger CO_2 absorption. Further measurements with relatively large amounts of H_2O in the absorbing path are planned in order to develop this band more fully. The third overtone (040), which should fall in the relatively clear region 1.54–1.64μ, will also be sought under these conditions.

Between 2.22μ and 2.50μ, the latter being the approximate limit of complete absorption as a result of the strong ν_3 fundamental, resolved lines have been assigned principally to the $\Delta J=+1$, $\Delta\tau=+3$ transitions of that fundamental up to $J=10$. A few lines of the $\Delta J=+1$, $\Delta\tau=+7$ type have been located, and a number of the strong lines near 2.5μ doubtless result from the $\Delta J=+1$, $\Delta\tau=-1$ transitions, with J from 10 to 15, but definite assignments for these lines must await corresponding measurements in the long wave-length wing of the band.

The position of the zero rotational level and the approximate effective reciprocal moments of inertia for the three newly resolved bands are shown in Table I.

The relative intensities of the various bands may be estimated approximately, by comparing, for fully resolved lines of equal absorption in the several bands, the calculated intensities.[4] If the probability of vibrational transition in (001) is assigned the value 5000, the probabilities for the other bands are: (101)=80; (200)=20; (021)=8; (120)=1; (011)=150; (110)=3; (030)=1.

Further details of the analysis will be published by one of us, together with results obtained in the photographic region.[5]

[1] R. R. McMath, O. C. Mohler, and L. Goldberg, Phys. Rev. **73**, 1203 (1948).
[2] T. G. Cowling, Nature **152**, 694 (1943).
[3] R. C. Nelson and W. S. Benedict, following communication.
[4] P. C. Cross, R. M. Hainer, and G. W. King, J. Chem. Phys. **12**, 210 (1944).
[5] W. S. Benedict, Bull. Am. Phys. Soc. **23**, 54 (1948).

Absorption of Water Vapor Between 1.34μ and 1.97μ

R. C. NELSON
Northwestern University, Evanston, Illinois
AND
W. S. BENEDICT
National Bureau of Standards, Washington, D. C.
August 2, 1948

THE absorption of water vapor between 1.34μ and 1.97μ has been recorded using the PbS photoconductive cell with the spectrograph and amplifier described by Nelson and Wilson.[1] The absorption path within the spetcrograph was 11 meters long, and the extent of absorption was controlled by varying the humidity in the instrument. There are two principal regions of absorption, 1.34 to 1.48μ and 1.78 to 1.97μ. In the former, the effective slit width was 0.18 cm^{-1}; this permitted 70 scale divisions deflection on the Speedomax recorder with a noise level (illuminated) of one division. In the longer wave-length region the lower sensitivity of the detector required slits of 0.40 cm^{-1}.

The spectrum obtained bears a general resemblance to that previously reported,[2] but the resolution is markedly improved and there is a systematic deviation in the wave-lengths—our values, after correction to vacuum, being from 1.5 to 2.0 cm^{-1} lower in the 1.4μ-region, and 0.8 to 1.2 cm^{-1} lower in the 1.9μ-region. The present values, obtained by comparison with lines of Ne in higher orders, are believed accurate to $\pm$0.1 cm^{-1}. Agreement to within this limit is found with measurements made with atmospheric path lengths with both photo-cell[3] and photographic[4] recording.

A rotational analysis of the lines has been made, using the known rotational levels of the ground state[5] to locate groups of lines with a common upperstate level. The calculated energy and intensity tables for the rigid asymmetric rotor[6] served as valuable guides in making the assignments. The principal absorption between 1.36μ and 1.42μ is due to the well-known perpendicular band ($v_1v_2v_3$ =101), but, as was found to be the case with corresponding bands in the photographic region,[7] there are many lines that must be attributed to a weaker band of parallel symmetry type (200). The relative intensity of the two bands is about 4:1, except for a few lines going to close-lying rotational levels of equal J and the same total symmetry, when perturbations of the Coriolis type occur, giving rise to displacements of the calculated term values and enhancement of the intensity of the weaker band. The rotational levels of (101) have been completely located up to $J=6$, together with many of the stronger, low τ, levels of higher J, and of (200) up to $J=5$. These account for practically all the lines in the central region. At longer wave-lengths a number of weaker lines may be assigned to the perpendicular band (021), and a few to the parallel band (120), in agreement with the rotational analysis previously made from the solar absorption.[2] At the shortest wave-lengths there remain a few unassigned lines which undoubtedly belong to the second parallel band (002). A tentative analysis of the present data together with the photographic atmospheric absorption[3] locates most of the levels of this band up to $J=3$, giving $\nu_0=7445.0$ cm^{-1}, but further studies of the region from 1.30–137μ with long absorbing paths are required to confirm this identification.

In the 1.9μ-region the absorption is due almost entirely to the (011) band. With the aid of the weaker lines in the

atmospheric absorption, all levels up to $J_r=8_8$, and many of higher J, have been located. The accompanying parallel band (110) has also been found; its intensity relative to (011) is about 1:50, so that only the strongest transitions, or those strengthened by Coriolis perturbation, are resolved.

The zero rotational levels and approximate effective reciprocal moments of inertia of these bands are as shown in Table I. The moments for (101) and (011) are in fair agreement with those given by Nielsen,[1] but our term values, except for the lowest levels, are in many cases quite different.

Further details of the experimental and theoretical aspects of this work will be published separately.

The experimental portion of this work was sponsored by the Bureau of Ships, U. S. Navy.

[1] R. C. Nelson and W. R. Wilson, Proc. Nat. Electronics Conf. **3**, 579 (1947).
[2] H. H. Nielsen, Phys. Rev. **62**, 422 (1942).
[3] See preceding letter.
[4] H. D. Babcock and C. E. Moore, *The Solar Spectrum from λ6600 to λ13495* (Carnegie Institute of Washington, 1947), p. 579.
[5] D. M. Dennison, Rev. Mod. Phys. **12**, 189 (1940).
[6] G. W. King, R. M. Hainer, and P. C. Cross, J. Chem. Phys. **11**, 27 (1943); *ibid.* **12**, 210 (1944).
[7] W. S. Benedict, Bull. Am. Phys. Soc. **23**, No. 3, 54 (1948).

Tracks of Low Ionizing Particles in Photographic Emulsions

J. SPENCE, J. CASTLE, AND J. H. WEBB
Kodak Research Laboratories, Eastman Kodak Company, Rochester, New York
August 9, 1948

THE improvement in photographic emulsions for the registration of charged particles of low ionizing power has been very great in recent months, as may be seen from the accompanying pictures of tracks of electrons and mesons. One year ago it was doubtful that electrons could be registered as recognizable trails of grains at all by the photographic emulsion, although at that time a few tracks of several grains' length had been observed[1] that were attributed to electrons of a few kev energy. In a paper by Berriman[2] early this year, unmistakable tracks of electrons were obtained using the NTP-2*a* plate made by Kodak Limited, in Harrow, England. More recently, electron tracks of considerably greater range were observed using the NTP-2*a* plate of Kodak Limited[3] and the NTB plate of the Eastman Kodak Company in America.[4] The longest of these tracks were of the order 20–30-microns emulsion range corresponding to electron energies of around 40–60-kev energy.

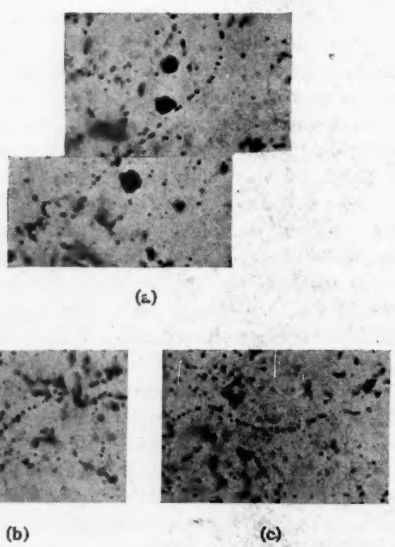

(a)

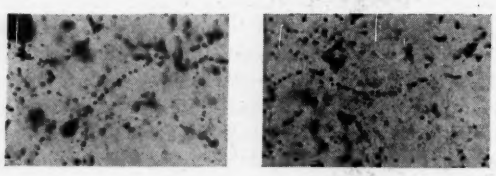

(b) (c)

FIG. 1. Electron tracks obtained on Eastman NTB emulsion to beta-rays from RaD+RaE in electron mass spectrograph.

The tracks shown in Fig. 1 are records of electron paths recently obtained on Eastman NTB emulsions exposed to beta-rays from a source of RaD+RaE in an electron mass spectrograph. The tracks shown represent some of the longer tracks selected from the high energy end of the spectrum. The longest track shown here, Fig. 1a, had a range in the emulsion of approximately 56 microns, which corresponds to an electron energy of about 100 kev.

FIG. 2. Meson track in Eastman NTB emulsion obtained by exposure in University of California cyclotron.

The particle track shown in Fig. 2 is of a meson on an Eastman NTB emulsion exposed to laboratory-produced mesons obtained in the University of California cyclotron.

The track shown was 400 microns in length in the emulsion, corresponding to an energy of 3.6 Mev, if we assume the mass of the meson to be 313 electron masses, as seems probable.[5]

In order to give some idea of the sensitivity of the present Eastman NTB plate in terms of specific ionizing power required to produce a track, Fig. 1a is to be noted. As stated above, this track of 56-micron range in the emulsion corresponds to an energy value at the beginning of the track of around 100 kev. The space rate of energy loss due to ionization by an electron of 100-kev energy in air is approximately 0.005 Mev/cm.[6] The minimum of the energy loss curve for charged particles in air is 0.0022 Mev/cm. Thus, it may be seen that the photographic emulsion has been pushed to a point in sensitivity where it will register a particle of twice the energy loss rate of the minimum for any charged particle whatsoever. On the basis of the above figure of 0.005-Mev/cm energy loss for 100-kev electrons, mesons of 40-Mev energy should be recorded by the highest sensitivity emulsions now available.

The authors wish to express their indebtedness to the Radiation Laboratory of the University of California for their kind cooperation in exposing the NTB plate to mesons. Also the authors wish to thank the Physics Department of the University of Rochester for the loan of the electron mass spectrograph on which the electron exposures were made.

[1] P. Demers, Can. J. Research **A25**, 223 (1947).
[2] R. W. Berriman, Nature **161**, 432 (1948).
[3] R. H. Herz, Photographic J. (in press).
[4] J. H. Webb, Phys. Rev. **74**, 511 (1948).
[5] E. Gardner and C. M. G. Lattes, Science **107**, 270 (1948).
[6] J. H. Smith, Phys. Rev. **71**, 32 (1947).

On the Ammonia Molecule

MASATAKA MIZUSHIMA
Physics Department, Tokyo University, Tokyo, Japan
July 16, 1948

THE well-known inversion doubling of the ammonia molecule has a peculiar effect on its properties. From this point of view, the intensity change in molecular beam and the half-width of inversion absorption line are calculated for this molecule.[1]

Each vibrational ground state of this molecule is composed of two nearly degenerate states whose wave functions are, respectively, positive and negative for a reflection of all particles at the origin (inversion doubling).[2] If we designate these wave functions by ψ_+ and ψ_- we can set

$$\Psi_{+,J,K,M}=\psi_+\Theta_{J,K,M}\Phi, \quad \text{or} \quad \Psi_{-,J,K,M}=\psi_-\Theta_{J,K,M}\Phi \tag{1}$$

for the total wave function of each state, where Θ is the rotational wave function of a symmetric rotator and Φ is the rest of the parts of the wave function.

Thus assuming the factorizability of Ψ, we can easily prove by Van Vleck's theory[3] that the quantity μ in Debye's formula of polarization,

$$P=\frac{N\mu^2}{3kT}+\alpha,$$

TABLE I. Intensity change at the center in the molecular beam experiment for ammonia.

Experimental number	$J(0)/J_0$ obs.	$J(0)/J_0$ calc.
1	0.87	0.88
4	0.63	0.55
7	0.41	0.38

is equal to the following matrix element of dipole vector μ:

$$\mu^2=\left(\int\psi_+/\psi_-d\tau\right)^2$$

using the fact that energy difference $\epsilon_{J,K}$ between $\Psi_{+,J,K}$ and $\Psi_{-,J,K}$ states is nearly independent of J and K and small compared with kT. Thus we can obtain numerical value of this matrix element:

$$d\equiv\left|\int\psi_+/\psi_-d\tau\right|=1.48\cdot10^{-18}\ \text{e.s.u./c.g.s.} \tag{2}$$

The experimental measurement on the deflection of the molecular beam of ammonia in an inhomogeneous electric field was performed by Schoeffers.[4] He attempted to calculate the dipole moment of this molecule from his results, but did not succeed. In his experiment, energy perturbation was smaller than ϵ; hence, remembering that $\int\psi_+\mu\psi_+d\tau$ and $\int\psi_-\mu\psi_-d\tau$ vanish identically because of the symmetry properties of these wave functions, second-order perturbation should be considered. Thus, starting from (1), we obtain for the perturbation energy of each state in the form

$$E^{(2)}{}_{+,J,K,M}=-\frac{d^2}{\epsilon}\left(\frac{KM}{J(J+1)}\right)^2$$

or

$$E^{(2)}{}_{-,J,K,M}=+\frac{d^2}{\epsilon}\left(\frac{KM}{J(J+1)}\right)^2.$$

By these formulae and (2) we can calculate in the usual manner intensity change under the electric field.[5] In Table I we compare the results with Schoeffers' experimentel data; agreement is satisfactory.

Recently Good[6] observed fine structure in the inversion spectrum of ammonia, and he reported the line form for the $J=3$, $K=3$ absorption line.

It can be shown that the half-width of an absorption line can be expressed by the following formula,

$$A=\frac{4}{(\pi)^{\frac{1}{2}}}\left(\frac{m}{4kT}\right)^{\frac{1}{2}}\sum_{J,K,M}\int_0^\infty\int\left(\exp-\frac{m}{4kT}V^2\right)\times V^3\rho(1-\cos\alpha)dVd\rho P(J,K,M)n,$$

$$\alpha=\int_{-\infty}^{\infty}\frac{p_i(t)-p_f(t)}{\hbar}dt,$$

where m is the mass of molecule, V the relative velocity of collision, ρ the distance from the absorbing molecule to

TABLE II. Intermolecular potential between ammonia molecules A and B.

State of B \ State of A	$+,J,K$	$-,J,K$
$+,J,K$	$\epsilon-(\epsilon^2+\epsilon_m^2)^{\frac{1}{2}}$	$\pm\epsilon_m$
$-,J,K$	$\mp\epsilon_m$	$-\epsilon+(\epsilon^2+\epsilon_m^2)^{\frac{1}{2}}$

TABLE III. The half-width of $J=3$, $K=3$ line in the inversion spectrum of ammonia.

Pressure 10^{-2} mm Hg	A obs. Mc/sec.	A calc. Mc/sec.
5	1.27	1.15
2.5	0.57	0.58
1.5	0.34	0.34

the asymptote of relative motion of the colliding one, $P(J, K, M)$ the probability that a molecule is in J, K, M state, n the number of molecules in unit volume, and $p_i(t)$, $p_f(t)$ the perturbation energies of initial and final states of the absorption process as a function of time t; α is the function of J, K, M, V, and ρ where J, K, and M represent the rotational state of colliding molecules.

Using (1) we can calculate intermolecular potential in the usual manner, resulting in Table II. In this table $\pm$ means that the sign must be taken corresponding to that of $\epsilon_{J,K}-\epsilon_{J',K'}$, and e_m is the mth eigenvalue of a matrix whose element is[7]

$$(M_j, M_j'|\,V|\,M_i, M_i')=\frac{d^2}{R^3}\frac{KK'}{J(J+1)J'(J'+1)}$$
$$\times\{-2M_iM_i'\delta(M_i, M_j)\delta(M_i', M_j')$$
$$\pm\tfrac{1}{2}[(J-M_i+1)(J+M_i)(J'-M_i')(J'+M_i'+1)]^{\frac{1}{2}}$$
$$\times\delta(M_i, M_j+1)\delta(M_i', M_j'-1)$$
$$\pm\tfrac{1}{2}[(J+M_i+1)(J-M_i)(J'+M_i')(J'-M_i'+1)]^{\frac{1}{2}}$$
$$\times\delta(M_i, M_j-1)\delta(M_i', M_j'+1)\},$$

R being intermolecular distance. Since an absorption line in the inversion spectrum corresponds to $\psi_{+,J,K}\rightarrow\psi_{-,J,K}$ transition, we can calculate α for it by means of the above table. Making some approximation and again resorting to (2), we can obtain values as in Table III, showing good agreement with the experiment. The half-width of other lines can be easily calculated.

In all these calculations Boltzmann distribution was assumed over rotational states from $J=0$ to $J=10$. On statistical weight of each state one may refer to Herzberg's book.[2]

[1] These results were published in The Research in Chemical Physics (in Japanese) 9, 1 (1947); 11, 11 (1948). Details of them will be published in the near future in J. Phys. Soc. Japan.
[2] G. Herzberg, *Infra-Red and Raman Spectra of Polyatomic Molecules* (D. Van Nostrand Company, Inc., New York, 1945), pp. 26, 221.
[3] J. H. Van Vleck, *The Theory of Electric and Magnetic Susceptibilities* (Oxford University Press, New York, 1932), p. 186.
[4] H. Schoeffers, Physik. Zeits. 41, 89, 98 (1940).
[5] O. Stern, Zeits. f. Physik 41, 563 (1900).
[6] W. Good, Phys. Rev. 70, 213 (1946).
[7] H. Margenau and D. T. Warren, Phys. Rev. 51, 748 (1935).

Erratum: Theory of High Frequency Discharges. IV

[Phys. Rev. 73, 326 (1948)]

H. MARGENAU
Sloane Physics Laboratory, Yale University, New Haven, Connecticut

IN this paper the original authorship of the similarity principle was given erroneously. I offer my apologies to Dr. R. Holm, who introduced and discussed it in Physik. Zeits. 15, 289 (1914).

Primary and Secondary Meson Event in Photographic Emulsions

ADAIR MORRISON AND ERIC PICKUP
Physics Division, National Research Council, Ottawa, Canada
July 29, 1948

THROUGH the courtesy of the British Overseas Airways Corporation in carrying plates for us on consecutive transatlantic flights, we have had Ilford nuclear research emulsions exposed to cosmic radiation over a period of time. Examination of these emulsions has yielded many interesting cosmic-ray events, some involving mesons.

In a total of 3.26 cc of emulsion of various types of loading so far examined and yielding just over 1000 cosmic-ray stars, we have noted one double meson event of the type first described by Lattes, Muirhead, Occhialini, and Powell[1] ($\pi-\mu$-process) in which the secondary meson lies wholly in the emulsion. This event was found in a C_2 emulsion, boron-loaded, 60 microns thick after processing. The primary meson enters through the surface and passes downward through the emulsion, ending 18 microns above the glass. The secondary meson also travels upward through the emulsion and is scattered downwards about 50 microns from the end of its range.

The ranges of the primary and secondary meson as measured in horizontal projection are 176 and 627 microns, respectively. A profile showing the vertical path of the mesons through the emulsion is given in Fig. 1. The vertical coordinates have been corrected for the shrinkage of the emulsion in processing by multiplying by a factor of 2.5. After correction for vertical travel, the primary and secondary ranges become 213 and 655 microns, respectively. The accuracy of the range measurement is believed to be ± 0.5 percent. The corrected range of the secondary is somewhat longer than the average range, 614 ± 8 microns given by Lattes, Occhialini, and Powell.[2] A mosaic of photomicrographs of the tracks is shown in Fig. 2.

Identification of the tracks as due to mesons was made by their scattering, which is greater than that of protons of comparable range, and by the grain counts as compared with that of protons. The total number of grains in the primary or π-meson track is 141, and the grain counts for the last 50, 100, and 150 microns are 46, 77, and 106. For the secondary or μ-meson the corresponding figures are 263 grains and 43, 80, and 112 grains (average grain size in the emulsion = 0.4 micron). The distances are corrected for slant in the emulsion as deduced from the profile given above, and are thus the distances along the path of the mesons when the event took place.

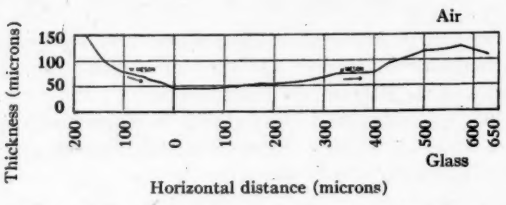

FIG. 1. Vertical profile along the tracks of the primary and secondary mesons.

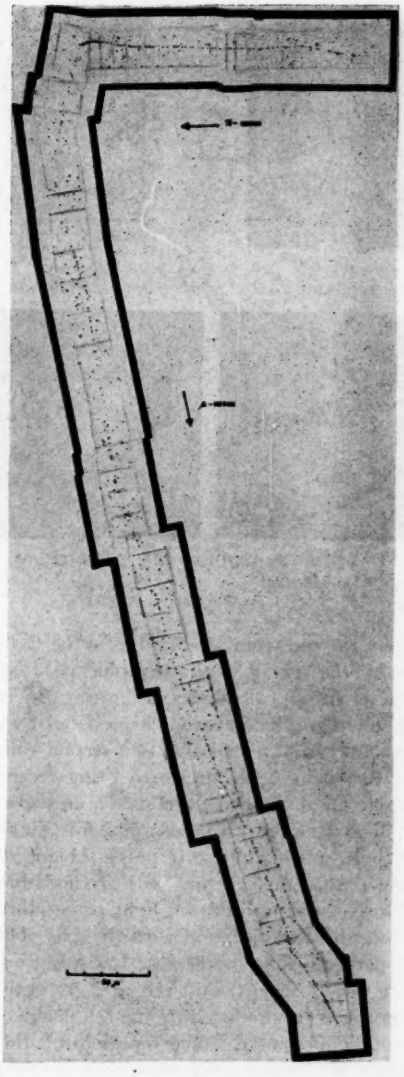

FIG. 2. Mosaic of photomicrographs of tracks of primary and secondary mesons. Leitz 114X, apochromatic objective. Observation by Joan Young.

The differences in the grain counts of the π- and μ-mesons are not great enough to give any positive indication of mass difference. In view of the shortness of the primary track and the statistical uncertainty involved because of the small number of grains, all we can say is that the possibility of a difference in mass cannot be excluded.

The plates were exposed over a six-week period, during which time they were flown 202, 187, 137, and 15 hours above 10,000, 15,000, 18,000, and 20,000 ft. respectively. They were developed for 15 minutes at 68°F in Kodak D-19 diluted with two parts of water to one of developer, with continuous agitation by mechanical means during development and fixing.

The photomicrographs were made by projecting the microscope image through a prism and mirror system onto a flat surface, each track being recorded on a strip of film in a film holder with two slides which could be moved to expose short intervals of the track, brought successively into focus on the top surface of one of the slides. The mosaic was constructed from a series of such strips.

We wish to acknowledge most gratefully the cooperation given by the British Overseas Airways Corporation in carrying the plates and in making available the time-altitude data, the painstaking work of the three observers who did most of the preliminary searching, Misses Joan Young, Shirley Young, and Berverley Mear, and the assistance of Mr. F. Morton in developing the projection scheme.

[1] Lattes, Muirhead, Occhialini, and Powell, Nature 159, 694 (1947).
[2] Lattes, Occhialini, and Powell, Nature 160, 453 (1947).

A Tentative Explanation of the Observed Mass of Mesons and Other Particles

E. G. CULLWICK
Defense Research Board, Department of National Defense, Ottawa, Ontario, Canada
July 19, 1948

THE continued experimental discovery of elementary particles whose rest masses appear to have a wide range of values intermediate between those of the electron and the proton evidently calls for some simplifying principle.

The following suggestion, although entirely unorthodox and a reversion to pre-relativistic physics, may possibly be of some interest in this connection.

The following phenomena may be accepted as experimental facts:

(a) the mass of an elementary particle varies with velocity, and the relation $m=m_0[1-(v^2/c^2)]^{-\frac{1}{2}}$ has been verified as describing this variation, at least up to about $v=0.8c$.
(b) energy is directly convertible into mass according to the relation $W=mc^2$.

In relativistic physics, the velocity v in the mass-variation law is measured relative to the observer or, in actual practical experiments, relative to the laboratory. Suppose now that a Newtonian description of all physical phenomena is found to be possible (for example, Ritz's[1] work in electrodynamics and Dewar's tentative hypothesis of non-relativistic radiation[2]). Then velocities relative to the observer are not involved, and v in the mass-variation law (now regarded as empirical) must be measured relative to some specific inertial system.

Let us define this inertial system as the parent body from which an elementary particle is originally ejected. Then if the velocity of the parent body relative to the laboratory is small compared with that of light, there will be no appreciable difference in the mass of the ejected particle as deduced by the two theories. But if the velocity of the parent body is comparable with that of light at the moment a particle is ejected, there will be a difference.

Suppose, for example, that a nucleon (neutron or proton) of high energy, say of the order 10^{10} ev, collides with an atomic nucleus and that as a result it emits one or more electrons (+ or −) in random directions with very high

energies, say of the order 10^9 ev. An emitted particle will move with velocity almost equal to that of light *relative* to the incident nucleon. A particle emitted sideways or forewards (if it escapes) will be detected as a high energy electron, but one emitted *backwards* will have a velocity in the laboratory equal to the *difference* between the velocity of the nucleon and the velocity of the electron relative to it. Thus its laboratory velocity will be sensibly less than c, the velocity of light. Its mass, however, according to the hypothesis suggested here, will be of the order 2000 m_0 in *all* reference systems, including that of the laboratory. Depending on its velocity, it will be interpreted by the usual experimental methods as possessing a rest mass somewhere in the range m_0 to 2000 m_0.

The excess of mass may be regarded as the storage of part of the energy which has been expended in giving the particle its high velocity relative to its original inertial system, the bombarding nucleon.

If also we suppose the surplus mass to be rather loosely tied to the electron, it seems reasonable to expect that it will be rapidly, or suddenly, converted back into other forms of energy, as it moves comparatively slowly in its new inertial system. One might also suppose that the instability of the particle would be a function of the increment of mass above that value appropriate to its velocity in the new inertial system.

In this hypothesis variable mass appears not as a relativistic effect, but as a result of true conversion of energy into mass according to the relation $W=mc^2$.

[1] W. Hovgaard, "Ritz's electromagnetic theory," J. Math. Phys. 11, 218–254 (1932).
[2] M. J. S. Dewar, "An interpretation of light and its bearing on cosmology," Phil. Mag. 38, 488–494 (1947).

Study of Turbulence by Light Diffraction*

J. C. Hubbard, J. A. Fitzpatrick, W. J. Thaler, Laura Cheng, and R. J. Beeber
The Catholic University of America, Washington, D. C.
August 3, 1948

In the course of experiments on the distortion of progressive ultrasonic waves[1] we have been accustomed to estimate the complexity of the wave form by viewing the spectrum produced by the photographic negative of the acoustic wave system used as an optical grating in a spectrometer of small aperture, or by viewing or photographing the Debye-Sears pattern produced by portions of the sound field itself.

It has been found that turbulence in a fluid, however produced, may conveniently be examined by the same methods. A field of turbulence, instead of a system of sound waves, may be studied by visual or photographic

Fig. 1.

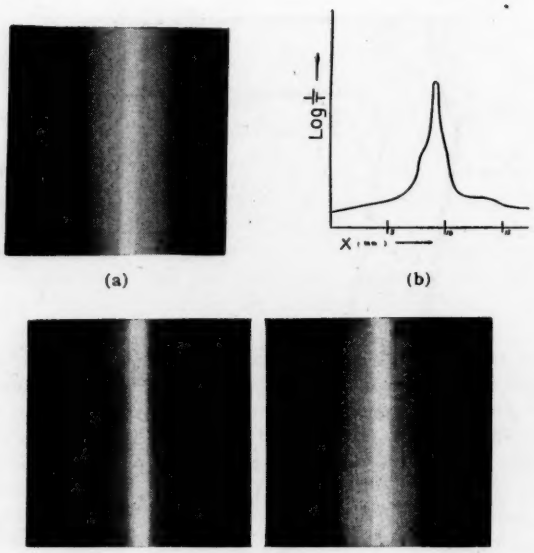

Fig. 2.

inspection of the spectrum produced as in the Debye-Sears effect, or by the use of a photographic negative of the turbulence as an optical diffraction grating. In the latter method a photographic negative is prepared by allowing collimated light from a spark of 10^{-7}-second duration to enter the turbulent field, afterward being received on a photographic plate. A print from such a negative is given in Fig. 1, showing a jet of CO_2 escaping into air through a nozzle of 2-mm opening, the static pressure being 90 lb./in.^{2}. When used as an optical grating, with the negative masked so that most of the transmitted light passes through the region affected by the jet, and with the axis of the jet in this case perpendicular to the slit, the spectra shown in Fig. 2 are produced; (a) and (b) are, respectively, the diffraction spectrum produced by the full image of the jet, and the photomicrometer trace representing the density of the image of the spectrum (logarithm of the reciprocal of transmission *vs.* distance along axis perpendicular to the slit); (c) shows the diffraction effect when the half of the jet image near the orifice is used. This half contains less of the turbulent structure and more of the line structure, some of which is found to be closely associated with segment dimensions. In the spectrum (d), formed by the half of the jet image farther from the orifice, the continuous part indicates more turbulence and a finer structure (broadening of spectrum limits).

Direct visual observation of the diffraction spectrum of light passed through the jet, as in the Debye-Sears experiment, shows to better advantage the line system in which the intensity and number of lines is a function of pressure. These lines doubtless result in part from the system of sound waves which can be seen to originate in jet structures of sufficient intensity, as photographed by transmitted light from the very short spark.[2] Both methods of observation show the progressive change of turbulence to finer structure, an effect analogous to that previously found for

ultrasonic waves of high intensity which develop higher frequencies and enhanced absorbtion as they progress.

* Supported by contract with the Office of Naval Research.
[1] Hubbard, Fitzpatrick, Kankovsky, and Thaler, Phys. Rev. 74, 107–108 (1948).
[2] Hubbard, Larkin, and Zartman, Radiation Laboratory, Johns Hopkins University, Report C. F.-764 (1947).

A Suggested Mechanism for the Generation of Thunderstorm Electricity

E. J. Workman and S. E. Reynolds
New Mexico School of Mines, Albuquerque, New Mexico
July 30, 1948

IN October 1946 the authors undertook laboratory investigations of the electrical properties of water and ice with the hope of discovering a physical process for the development of thunderstorm electricity which would be consistent with what is now known about thunderstorms.[1]

Initial tests reported to the sponsors in January 1947 showed effects wherein large differences of potential were developed between the liquid and solid phases of water when rapid freezing was in progress. These investigations were interrupted and work was not resumed until early 1948.

In continuing, attention was first directed toward determining whether our earlier observations were related to the phenomena reported by Dinger and Gunn wherein observations suggestive of the same phenomena were interpreted as contact potential differences of from 6 to 10 volts.[2]

The authors, using apparatus similar to that of Dinger and Gunn, were able to obtain relatively larger electrical effects, but having such differences in sign, magnitude, and character as to indicate a different interpretation than that of contact potential. In further tests samples of relatively pure water (resistivity about 10^6 ohms-cm) were frozen in a small nickel-plated copper dish floated on a mercury pool at about $-16°$C. The cup was grounded and the surface of the water was connected to an electrometer through a platinum wire. As soon as a thin film of ice separated the water from the cup, the electrometer indicated a negative potential which usually increased to about 40 volts. Occasionally values of -90 volts were obtained. Frequently, a reversal in potential was observed as the freezing approached completion. These potentials varied in magnitude, but 20 or 30 volts was expected. The measured resistivity of the remaining water was less during the reversed polarity phase than that of the sample before freezing started.

When water samples of one-tenth the resistivity (contaminated with sodium chloride) were used, a positive, instead of negative, potential developed as the ice covered the metal cup reaching a maximum value of something like 25 volts. For water of intermediate conductivity (4×10^5 to 8×10^5 ohm-cm) little or no electrical activity was observed.

Amounts of charge transferred during the freezing process were determined by measuring voltage across an electrometer shunt (5×10^6 ohms). As much as 30,000 e.s.u. per cc of water was common in the low resistivity cases.

Other tests including the impingement of water drops on cold ice in a cold chamber indicated that this process appears to satisfy the requirements for the initial electrification in thunderstorms. Water drops in the low resistivity range caused the ice to become negatively charged as the drops sheared and partially froze on the ice surface; the residue of the drops leaving the ice after impact was positively charged. After the ice was warmed by continued dropping to the extent that the drops no longer partially froze, successive drops drained negative charge from the ice by the process of charge sharing. This, or a similar process of cycling, appears necessary in a thunderstorm for consistency with field observation, showing that the negative charge center does not descend much below the zero isotherm. Our limited information on the resistance of water from melted hail gives values consistent with the negative ice and positive water situation.

A more complete report giving definite information bearing on the nature of the effects here reported is in progress, and further applications to possible thunderstorm formation will be discussed.

[1] This work has been supported by the Signal Corps of the United States Army.
[2] J. E. Dinger and Ross Gunn, Terr. Mag. 51, 477 (1946).

Preparation and Radiation of U^{237}

Lars Melander and Hilding Slätis
Nobel Institute for Physics, Stockholm, Sweden
June 21, 1948

LITERATURE contains very little information about the uranium isotope U^{237}. Only the half-life, 6.5–7 days,[1,2] and the upper limit of the β-spectrum, 0.26 Mev,[2] are reported. Starke[3] pointed out the possibility of using the Szilard-Chalmers reaction for the concentration of U^{237}, obtained in the process $U^{238}(n,2n)U^{237}$. We have modified the method[4] used in earlier experiments[5] on U^{239} and Np^{239}, carried out in this institute, for the case of U^{237}.

Solid uranyl salicylaldehyde-orthophenylenediimine[6] was shielded by boron and cadmium and irradiated with fast neutrons from lithium, bombarded with deuterons in the

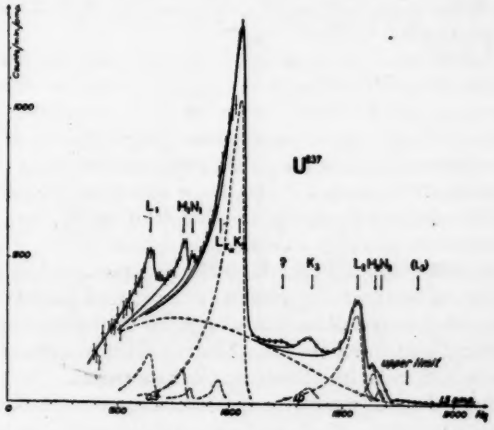

FIG. 1. The β-spectrum of U^{237}.

TABLE I. β-ray lines of U^{237}.

Notation	$H\rho$	E_β kev	W kev	E_γ kev	Origin
L_1	635	34.3	22.3	56.6	γ_1
M_1	781	51.0	5.7	56.7	γ_1
N_1	820	56.0	1.5	57.5	γ_1
LK_α	944	73.1	22.3	95.4	K_α
K_2	1029	85.9	118.2	204.1	γ_2
?	1224	118.2	118.2	236.4	?
K_3	1354	141.7	118.2	259.9	γ_3
L_2	1556	181.0	22.3	203.3	γ_2
M_2	1634	196.9	5.7	202.6	γ_2
N_2	1660	202.0	1.5	203.5	γ_2
(L_3)	1823	236.6	22.3	258.9	(γ_3)

cyclotron. In the case of U^{237} the concentration of the activity was almost exactly the same as with U^{239} and Np^{239} and will be discussed but shortly here. The purification, however, had to be changed, since in the present case it was desired to remove Np^{239} which might have been formed by possible slow neutrons, and all UX_1 had to be removed after the irradiation.

After the irradiation and after a time lag sufficient for possible U^{239} to vanish, the sample was dissolved in pyridine and the solution treated as in the former experiments: the activity was adsorbed on charcoal and the charcoal shaken with ammonium carbonate solution in the presence of some barium. The result was an ammonium carbonate solution containing those activities which are soluble under these conditions.

Precipitation as fluorides in acid solution was supposed to be the best method to get rid of such active impurities as UX_1 (thorium), four-valent neptunium, and three-valent rare earth metals (cerium, for example). During such a precipitation, uranium should be kept in the valence state six, the fluoride of which is soluble. In order to ensure the six-valent state to uranium, the solution was acidified with hydrochloric acid and some solid ceric sulfate added (it evolves chlorine and forms cerous ion). After that, sulfur dioxide was introduced into the solution. It is known to reduce neptunium but not uranium from the valence six to four, and hence the solution now contained its uranium, neptunium, and cerium as the ions UO_2^{2+}, Np^{4+}, and Ce^{3+}, respectively. Hydrofluoric acid was added and precipitated cerous fluoride, which carried such activities as neptunium, UX_1, etc.

Among the methods tried for the precipitation of uranium from the filtrate the following was the simplest and best one. By means of zinc powder the uranium was reduced to U^{4+} and a small amount of cerous ion added. The cerous fluoride then carried the uranium as tetrafluoride. (The amount of uranium is always very small and hardly visible.) The precipitate, washed and ignited, was used for the physical measurements.

In order to establish the yield and the concentration factor, a part of the originally irradiated sample was converted into sodium uranyl acetate in the presence of sulfur dioxide (and thus freed from foreign activities) and the specific activity of that uranium measured.

According to β-activity measurements on the concentration product and the sodium uranyl acetate, the latter of which represents the specific activity attainable without any concentration, the yield was 15–25 percent and the concentration factor at least 500. These values are in accordance with those found for slow neutrons.[4] The purification methods, however, were different and hardly permit close comparison.

Figure 1 shows the β-spectrum of U^{237}. The statistical error in each point is represented. The resolving power is limited by the granulate structure of the sample rather than by the properties of the magnetic lens spectrograph,[7] as shown by the anomalously small slope at the low energy side of the lines. This circumstance and the occurrence of many internal conversion lines mask the continuous β-spectrum almost completely.

From the assumption of a single Fermi distribution, an upper limit at $H\rho=1784$ ($E_\beta\approx0.23$ Mev), and visibility of the continuous spectrum at $H\rho=1120$, the latter was calculated and is represented by a dotted line. There is, however, some indication for a complex β-distribution (see below).

At least eight internal conversion lines and one converted x-ray line have been found. The thin curves belong to the construction of the individual conversion lines, which are plotted separately with dotted lines.

In Table I the data for the lines are given. The first column contains the symbols for the lines, as also marked in Fig. 1. The other columns give the momentum $H\rho$, the energy of the β-particles E_β, the ionization work W, the energy of the corresponding γ- quanta E_γ, and the origin of the lines, respectively.

The ionization work W for Np was obtained by extrapolation of the known ionization works[8] of the corresponding electrons in bismuth, thorium, and uranium.

The evidence for the line LK_α in the β-spectrum is not very strong, but it seems natural that this line should appear, because the K-conversion of γ_2 is high (see below), and K_α-radiation is to be emitted when the K-shell is completed. The energy of this K_α-radiation, then, is $118.2-22.3=95.9$ kev in agreement with the computed value in Table I.

The two hardest γ-components, γ_2 (204 kev) and γ_3 (260 kev), did not appear as two separated components in absorption measurements. Their mean value, however, corresponds to the hardest γ-component, 230 kev, found in such measurements. The energy of the weak component γ_1 (57 kev) is in good agreement with the absorption value 59 kev.

Weak γ-radiation, 32 kev and x-radiation, was also found in the absorption measurements, but because of the low energy, which is still reduced by the ionization work, possible conversion lines from these radiations cannot be recorded.

The weighted means for the energies of γ_1 and γ_2 are 56.7 and 203.9 kev, respectively. The sum of these is 260.6 kev, within the limit of experimental error agreeing with the energy of γ_3, 259.9 kev. Thus the latter probably is a crossover transition, and the three γ-radiations, γ_1, γ_2, and γ_3, belong to two excited levels in the Np^{237} nucleus. The intensities of the different conversion lines give evidence for the existence of more than one way of β-decay.

The half-life was found to be 6.63 ± 0.05 days.

A more complete description of these experiments will be published soon.[9]

[1] Y. Nishina, T. Yasaki, H. Ezoe, K. Kimura, and M. Ikawa, Phys. Rev. **57**, 1182 (1940).
[2] E. McMillan, Phys. Rev. **58**, 178 (1940).
[3] K. Starke, Naturwiss. **30**, 577 (1942).
[4] L. Melander, Acta Chem. Scand. **1**, 169 (1947).
[5] H. Slätis, Arkiv. Mat. Astr. Fys. **35A**, No. 3 (1947); Nature **160**, 579 (1947).
[6] R. B. Duffield and M. Calvin, J. Am. Chem. Soc. **68**, 1129 (1946).
[7] K. Siegbahn, Phil. Mag. **37**, 162 (1946).
[8] M. Siegbahn, *Spektroskopie der Röntgenstrahlen* (Berlin, 1931), p. 467.
[9] L. Melander and H. Slätis, Arkiv. Mat. Astr. Fys., in print.

On the Faraday Effect at Microwave Frequencies†

M. Carr Wilson and G. F. Hull, Jr.
Wilder Laboratory, Dartmouth College, Hanover, New Hampshire
July 29, 1948

A MICROWAVE analog of the Faraday effect has been found experimentally at a wave-length of 3.338 centimeters. The sensitivity of the apparatus was adequate to measure Verdet constants as small as 0.5×10^{-3}, with a probable error of 25 percent under worst conditions.

The effect was found by use of a TE_{11} wave in circular pipe. The dielectric was placed within this pipe, and the pipe inserted on the longitudinal axis of a solenoid having a maximum field strength of 1350 gauss. Position of the electric vector within the pipe was determined by side probes extending into the pipe at each end of the solenoid. Angular displacement of the electric vector caused by the applied magnetic field was measured by rotating one of the side probes about the axis and reading the angle on a scale accurate to one minute of arc.

Two of the materials measured have Verdet constants of the customary order of magnitude. The materials are paramagnetic salts, $MnCl_2\cdot4H_2O$ and $MnSO_4\cdot H_2O$. These salts are known to exhibit microwave absorption at 3 and 10 centimeters in the presence of a magnetic field.[1] The chief results for these two salts are given in Table I.

The basic equation for the Faraday effect is $\theta=RLH$, where θ is the angular rotation of the polarization plane in minutes, L is the path length, H is the magnetic field strength, and R is the Verdet constant (a function of wave-length).

Table I.

L (cm)	H (gauss)	λ (cm)	θ (min.)*	Dev.	R ($\times10^3$)
Substance: manganous sulfate; $MnSO_4\cdot H_2O$					
9.2	1350	3.34	9.5		0.766
9.2	1350	3.45	12.5		1.01
9.2	1350	3.338	12.5		1.01
Substance: manganous chloride; $MnCl_2\cdot4H_2O$					
9.2	1350	3.338	22.7	±35%	1.83 (*a*)
9.65	1350	3.338	28.7	±19%	2.21 (*b*)
23.4	1350	3.338	61.5		**1.94 (*c*)
30.5	1350	3.338	73.3	±13%	1.78 (*d*)
30.5	920	3.338	55.2	±17%	1.96 (*e*)
30.5	460	3.338	25.9	±23%	1.84 (*f*)
30.5	1350	3.442	25.7	±23%	***0.62 (*g*)
30.5	1350	3.553	46.9	±12%	***1.14 (*h*)

* Rotation to left when wave was in direction of magnetic field.
** Percentage deviation ±14 percent; additional possible error 15 percent; total possible error 29 percent. Material in this specimen was loosely packed. Mean Verdet constant for values $(a-f)=1.90\times10^{-3}$.
*** One large deviation omitted from percentage calculation.

Table II.

Ethyl alcohol	Polystyrene (clear)
Nitrobenzene	Ammonia (gas)
Carbon disulfide	Sodium chloride
Methyl alcohol	Glycerine
Ammonium nitrate	Ferrous sulfate (crystal)
Ammonium hydroxide	Ferric chloride (powder)
Water (distilled)	Carbon tetrachloride
Ether (anhydrous)	Manganous carbonate
Chloroform	Ferric nitrate
Ethylene chloride	Ferric sulfate
Methylene chloride	Cobalt chloride
Benzene	Cobalt sulfate
Ferrous ammonium sulfate	

For the material most thoroughly investigated, manganous chloride, three principal observations may be made from the table:

(1) The Faraday rotation was proportional to the path length L; see table values (*a*) and (*d*).

(2) The Faraday rotation was proportional to the field strength H; values (*d*) and (*f*).

(3) There was some variation in the Verdet constant with wave-length; values (*d*), (*g*), (*h*). This suggested an absorption band within the wave-length region measured; however, available data was not adequate to substantiate this.

The salts were in crystalline form, in general no greater than 2 millimeters in the largest dimension. The crystals were tamped slightly when inserted into the pipe.

A large number of materials gave no measurable effect; these are listed in Table II. For some of these, measurement was doubtful, since very small path lengths L were used because of high attenuation. The substances were in various forms; ammonia gas was at atmospheric pressure.

† Abstract of M.A. thesis, submitted by the first author at Dartmouth College, June 1948.

[1] R. L. Cummerow and D. Halliday, Phys. Rev. **70**, 433 (1946); *ibid.* **72**, 173 (1947).

The Change of Photo-Conductivity of Cadmium Sulfide between Room Temperature and the Temperature of Liquid Air

J. C. M. Brentano and D. H. Davis
Northwestern University, Evanston, Illinois
July 27, 1948

THE photo-conductive properties of cadmium sulfide crystals have been described by R. Frerichs.[1] He showed that crystals prepared by a reaction between cadmium and H_2S become conductive when exposed to light and lose their conductivity after illumination with a certain decay time. He showed that at liquid air temperature the decay period is increased and that delay is also observed between the onset of illumination and the time when conductivity begins. In our experiments we examined the photo-conductivity of such cadmium sulfide crystals at intermediate temperatures between room temperature and that of liquid air. Two facts were observed: (1) When using unfiltered radiation from a metal filament as illumi-

nant the photo-conductivity increases with lowering of the temperature to a maximum at −125°C with a rise which is approximately linear in the middle temperature range and falls off steeply between −130°C and −160°C. (2) The delay time between the beginning of illumination and that of photo-conductivity, which is large (of the order of 10″ and depending on the intensity of illumination) below −150°C, falls off very rapidly for higher temperatures.

The reason for drawing attention to these findings, in particular the first one, is that this parallels the change of the magnitude of the photographic Herschel effect with temperature, which will be described in a paper by L. C. Spencer; this could be interpreted as a possible relationship between the two phenomena. A similar temperature dependency exists for *F* centers which suggests a common mechanism.

The range of temperatures was obtained by placing the cadmium sulfide crystal in a double-walled jacket immersed in liquid air; by evacuating the air space of the jacket the rate of heat exchange could be controlled, a method developed at the Bureau of Standards.

We are indebted to the Navy Bureau of Ships, and to Dr. Frerichs for having made available to us the crystal used in these experiments.

[1] R. Frerichs, Phys. Rev. **70**, 594 (1947), where references to earlier papers can be found.

Internal Conversion Pairs in Carbon

C. B. Dougherty, W. F. Hornyak, T. Lauritsen, and V. K. Rasmussen
Kellogg Radiation Laboratory, California Institute of Technology, Pasadena, California
August 9, 1948

THE production of electron pairs by internal conversion of gamma-radiation in the nuclear field has been discussed by Jaeger and Hulme[1] and by Rose and Uhlenbeck.[2] The phenomenon has been studied experimentally with the 2.620-Mev radiation from ThD by several investigators.[3,4] We have observed the pairs produced by the internal conversion of the 3.11-Mev gamma-radiation produced in the reaction $C^{12}(d, p)C^{13*}$ [5] using a magnetic lens spectrometer equipped with a helical baffle system so that negative and positive electron spectra could be separately studied. Thin slabs of graphite placed inside the spectrometer were bombarded by 1.2-Mev deuterons and the momentum distribution of the electrons produced was observed for various thicknesses. In Fig. 1, curves *a* and *b* exhibit the observed negative electron spectra for target thicknesses of 57 and 12 mg/cm², respectively, measured for equal numbers of transmutations. It can be seen that the high energy peak, due to Compton electrons, increases with target (=converter) thickness as expected, while the rise below 2 Mev appears to be sensibly independent of target thickness, indicating that these electrons are associated with the number of transmutations rather than with the amount of converter.

Below 1 Mev, the curves again rise very steeply, because of the high energy tail of the Compton electrons from the

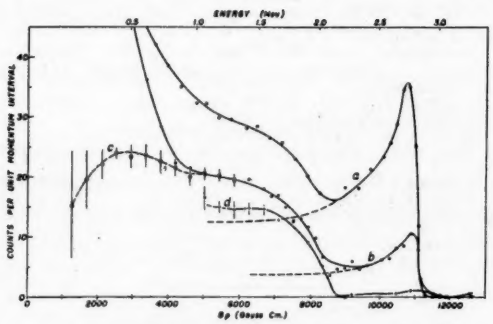

FIG. 1. Secondary electron distribution from $C^{12}+d$.

annihilation radiation from N^{13}, produced in the reaction: $C^{12}(d,n)N^{13}$. In order to eliminate the effect of these radioactive electrons, a series of runs was made in which the deuteron beam was periodically interrupted and the radioactive effect so determined was subtracted. The resulting curve, *c*, in the figure indicates the distribution so obtained with the 12-mg/cm² target. For curve *d*, taken with the same target, the spectrometer field was reversed to permit counting of positrons only, and the radioactive effect, due here to the (1.2-Mev maximum energy) positrons from N^{13}, was again separately determined and subtracted. The relatively large errors indicated for curves *c* and *d* reflect the statistical fluctuations introduced by the subtraction of the large numbers of radioactive counts. For both curves *c* and *d* the rise in the neighborhood of 2 Mev has an end point of 2.1 Mev. Thus the identification of this rise in both the electron and positron distribution curves with pair conversion of the 3.11-Mev gamma-radiation is established, while the fact that the number of pairs is independent of converter thickness indicates internal nuclear conversion. Externally created pairs would be expected to be few in number compared to the number of Compton electrons for this energy.

The general shape of the curves is in fair agreement with theoretical expectations except that the apparent preponderance of low energy negative electrons is considerably larger than can be accounted for by the effect of the Coulomb field on the internal conversion pairs. Considerations of the effect of the converter geometry indicate that some such number of low energy electrons would be expected from the Compton conversion of gamma-rays traveling parallel to the converter surface. The cross section for pair production was roughly determined by comparison with the internal conversion thorium "*X*" line[6] and by an estimate of the relative intensity of the Compton electrons; either method yields a value of the order of 10^{-3} pair per gamma-quantum.

This work was assisted by the Joint Program of the Office of Naval Research and the Atomic Energy Commission.

[1] Jaeger and Hulme, Proc. Roy. Soc. **148**, 708 (1935).
[2] M. E. Rose and G. E. Uhlenbeck, Phys. Rev. **48**, 211 (1935).
[3] Bradt, Halter, Heine, and Scherrer, Helv. Phys. Acta **19**, 431 (1946).
[4] G. D. Latyshev, Rev. Mod. Phys. **19**, 132 (1947).
[5] Bonner, Becker, Rubin, and Streib, Phys. Rev. **59**, 215A (1941).
[6] Flammesfeld, Zeits. f. Physik **114**, 227 (1939).